



# **The University of Sheffield**

## **Design and Optimisation of Power Fluidic Components for Compressible Flow Control**

A Thesis Submitted to The University of Sheffield in Partial Fulfilment of the  
Requirements for the Degree of Doctor of Philosophy

Submitted by:

**Nicolas Romero**

Department of Chemical and Biological Engineering

October 2014

Supervisors: Dr. G.H. Priestman, Dr. Jordan MacInnes

# ACKNOWLEDGEMENTS

This work is dedicated to my entire family.

***To my wife***, who endured with me the downfalls of being a student and stayed with me giving her love and support, and always encouraging me to persevere.

***To my son***, who was born during our life in Sheffield; I would like him to know that no matter what he chooses to do in his life, he has to be completely focused and work hard to achieve his dreams.

***To my parents***, Carmela and Nicolas, because they taught me the importance of responsibility and gave me the opportunities in life to succeed, as well as their unconditional love and support throughout my entire life.

***To my brothers***, Samail, Moises and Cesar, because they have been and will continue to be an essential part of my life, thanks for their support and love, especially in this occasion to my brother Moises for being with me all the time throughout my career and for all the special moments we shared.

***To my supervisors***, Dr. G.H. Priestman and Dr. Jordan MacInnes for always giving me advice in how to do things better, to see things from a different perspective and for their incredible patience and willingness to tutor me.

Last but not least, to the ***Consejo Nacional de Ciencia y Tecnología*** (CONACYT) for helping me funding my dream.

# SUMMARY

Rolls-Royce has identified several applications for Fluidic devices within their engines, including the Switched Vortex Valve, a fluidic device which has two different fluidic components joined together, providing two different states, one with low resistance to the flow and one with high resistance.

This report builds on previous work on switched vortex valves to extend their operation to compressible flow.

Further components such as Vortex Throttles and Vortex Amplifiers were analyzed and tested. The Vortex Throttle was also modelled using CFD in order to use the basic set of parameters for a more complex model of the Switched Vortex Valve and to understand the internal flow behavior within these devices.

In the Vortex Amplifiers it was found that as the supply flow pressure increased the parameter T is affected negatively and the parameter G has a slight benefit from it. A low turndown ratio would be undesired for the jet engine applications. The  $D_{ot}$  value changes are not as paramount as the diameter ratio D, but from results, a neglect of the  $D_{ot}$  effects where the values drop below 2.4 can be possible. A constant degradation of 17% between the pure throttle and the VA can be seen with different outlet bores, which can be explained by the effect of the supply flow from the plenum entering the vortex chamber degrading the vortex created by the control flow. Basic CFD model for the Vortex Throttle proved to match relatively close to the experimental data improving internal behaviour understanding and effect of tangential velocities in the vortex created.

For the SVV's an inlet angle nozzle of 5° (3°, 4° and 6° were tried) proved to be yielding the best performance in terms of stability and not impacting the control port flows to switch in comparison to the other angles tested. The control port geometry is of importance; a value of  $a_c/a_s = 2$  was found to be the value yielding the best performance without signs of instabilities. An increasing or decreasing of this value

can lead to unstable operation modes and drop in performance mainly to the pressure build up in the control port. The flow to switch from one state to the other varies from 4-6% supply flow when switching from normal state to vortex state, and 1.5-3% supply flow when switching from vortex state to normal state (for different inlet angles).

The splitter position was found to yield the best performance when  $t=3.6 \text{ mm}$ , equivalent to a value of  $a_s/a_t=0.652$  which is close to the zero entrainment point. Translation of the splitter threw allowances between the range of  $-0.2$  to  $+0.2 \text{ mm}$  in the up/down direction. It was found that as the tangential width  $t$  becomes shorter, the strength of the vortex in the vortex chamber decreases as well.

For the outlet, nozzles were used instead of diffusers given that these are easily manufactured in a laminate design. The outlet geometry it was found that smaller  $a_s/a_o$  ratios will give the best performance and turndown ratios which can relate to the same conclusion for the VA in which low values of  $D$  can yield better performances.

The SVV ring prototype showed promising results, a clear difference between low resistance and high resistance states was showed. Maintaining the required pressure in the control port manifolds proved difficult due to leaks near the edge of the manifold, thus making the affected individual components to switch from the Non-vortex to the vortex state or not being able to maintain the vortex state.

Relatively close agreement between the ring overall performance and that of the single SVV, showing that maintaining all the individual components of the ring working properly could yield the expected results. In the Normal state the agreement between an individual component of the ring and Design C was from 25% at pressure ratio of 1.5 decreasing to a difference of 11% for a pressure ratio of 3. For the vortex state a difference of 22.5% at a pressure ratio of 1.5 decreasing to a difference of almost 9% for a pressure ratio of 3.

# TABLE OF CONTENTS

Acknowledgments.....	I
Summary.....	II
Table of Contents.....	III
1. Introduction.....	1
1.1. Applications of the Switched Vortex Valves.....	2
1.2. Applications in Turbine Engines.....	2
1.2.1. Secondary Air System.....	3
1.2.1.1. Cooling.....	5
1.2.1.2. Sealing.....	6
1.2.1.3. Control of Bearing Loads.....	6
1.2.1.4. Aircraft Services.....	8
1.3. National Aerospace Technology Strategy.....	8
1.4. EFE-Environmental Friendly Engine Technology Validation Programme.....	9
1.5. Rolls-Royce Switched Vortex Valve Application.....	11
1.5.1. Scope and Introduction.....	11
1.5.2. Operational Conditions and Requirements.....	12
1.5.3. Current Architecture.....	13
1.6. Research Objectives.....	16
1.7. Thesis Layout.....	16
2. Literature Review.....	18
2.1. Components Characteristics.....	18
2.1.1. Wall-Attachment Diverter.....	19
2.1.2. Vortex Throttle.....	21
2.1.3. Vortex Amplifier.....	22
2.1.4. Matching of the Fluidic Components.....	26
2.2. Parameters and Previous Experiments of the SVV.....	28
2.2.1. Parameters of the Switched Vortex Valve.....	28
2.2.2. Previous work with Incompressible Flow in SVVs.....	29
2.2.3. Previous work with Compressible Flow in SVVs.....	35
2.3. Conclusions.....	38

3. Compressible Flow.....	40
3.1. Introduction.....	40
3.2. Switched Vortex Valve Analysis.....	40
3.3. Holes in series with compressible flow.....	43
3.4. Vortex Theory.....	47
3.5. Dynamic and Geometric Similarity.....	47
3.6. Conclusions.....	49
4. Vortex Throttle.....	51
4.1. Introduction.....	51
4.2. Experimental Procedure.....	53
4.3. Experimental Results.....	54
4.3.1.Reynolds Number.....	54
4.3.2.Pressure Drop and Diameter Ratio.....	55
4.3.3.Performance comparison, Eu number vs Re number.....	59
4.4. CFD Modelling of a Vortex Throttle.....	60
4.4.1.Introduction.....	60
4.4.2. Mathematical Formulation.....	61
4.4.2.1. Standard $\kappa - \epsilon$ .....	61
4.4.2.2. Realizable $\kappa - \epsilon$ .....	62
4.4.2.3. Reynolds Stress Model (RSM).....	63
4.4.3. Numerical Setup.....	64
4.4.4. Comparison of Experimental Results and Model Predictions.....	65
4.4.5. Discussion.....	67
4.4.6. Pressure Field.....	67
4.4.7.Flow Field.....	72
4.4.8. Effects of Mach Number.....	74
4.4.9. Effects of Turbulent Intensity.....	75
4.4.10. Pressure Drop.....	75
4.4.11. Effects of the axial outlet geometry.....	76
4.5. Discussion.....	78
4.6. Conclusions.....	80
5. Switched Vortex Valves with Compressible Flow: Experimental.....	81

5.1. Introduction.....	81
5.2. Experiments.....	82
5.2.1.Experimental Rig.....	83
5.2.2.Experimental Results.....	84
5.3. Results and Discussions.....	87
5.3.1.Leaks.....	87
5.3.2.Start up Instabilities and Inlet Nozzle Configuration.....	90
5.3.3.Control Port Width.....	93
5.3.4.Axial Outlet Diameter.....	95
5.3.5.Control Pressures and Flows.....	98
5.3.6. Splitter Position.....	102
5.4. Conclusions.....	109
6. Vortex Amplifiers.....	114
6.1. Introduction.....	114
6.2. Experimental Procedure.....	117
6.3. Experimental Results.....	118
6.4. Comparison of the VA with a VT.....	122
6.5. Possible Optimization of VA with Jet Pumps.....	125
6.5.1.Circuit Analysis.....	125
6.5.2. Design Relationship of the Jet Pump and Vortex Amplifier.....	132
6.6. Conclusions.....	133
7. Rolls-Royce Design.....	135
7.1. Introduction.....	135
7.2. Design C – Embedded Device.....	138
7.3. Manufacture and Tolerances.....	138
7.4. Switched Vortex Valve Rim.....	139
7.5. Experimental Setup.....	141
7.6. Preliminary Experimental Results.....	142
7.7. Conclusions.....	146
8. Conclusions and Recommendations for Future Work.....	148
8.1. Conclusions Overview.....	148
8.2. Switched Vortex Valves as control devices.....	149

8.3. Recommendations for Future Work.....	150
References.....	152
Nomenclature.....	155
Appendices.....	158

## INTRODUCTION

Over the past few years, fluidic devices have been considered for application in the aerospace industry, which is traditionally at the forefront of technology and it is always keen to apply known technologies and update it to match a specific working criterion, or to simply apply novel technology.

In the case of fluidic devices, the technology is updated to such a degree that it is capable to be used in this industry. In this matter, Rolls-Royce plc is involved in a project which is called the Environmental Friendly Engine or E.F.E., and is one of six different projects within the Aerospace Technology Validation Programme that is betting on fluidic devices to be designed to work in their future jet engines. This comes with a serious challenge given that most of the fluidic devices have been designed to work with incompressible flow such as water or air at really low pressures, and the conditions within the engines require that the fluidic devices work with compressible flow i.e. air at really high pressures.

Fluidic devices have been known for a very long time, most of the work involved working with water or air at low pressures. Priestman and Tippetts have been working on devices such as the Vortex Throttles, Vortex Amplifiers or more recently in the Switched Vortex Valves [33, 36].

The application of such devices in a jet engine was originally identified in 2009, and work with compressible flow started as part of the Rolls-Royce and the University of Sheffield initiative.

### **1.1 Applications of the Switched Vortex Valves.**

There are many potential uses for a switched vortex valve. There are applications for metering purposes[41], this can be achieved by making the Switched Vortex Valve to oscillate continuously by joining its control ports. The frequency of oscillation of the jet is a measurement of the flowrate. Another application is as a fluidic valve for reactor regeneration flow switching, where the flow is diverted into a channel where then it passes through a reactor[32].

Some other applications involve the use of Switched Vortex Valves in air ventilation control systems[31], as a liquid slug retarder in multiphase pipe flow[35], and more recently in the Turbine Engines and Flight Control Systems, which represent an area of potential for this type of devices[24, 44].

### **1.2 Applications in Turbine Engines.**

Many factors affect the efficiency and performance of the engine: air mass flow rates, pressure ratios, engine operating temperatures and individual component efficiencies.

Normally, an optimum pressure ratio, turbine inlet temperature and air mass flow rate are selected to obtain the required performance in the most efficient manner.

The increasing complexity of the jet engines and the extreme conditions that are present within the engines makes the use of this type of fluidic devices very useful. These fluidic control systems weigh much less than the conventional hydromechanical systems, have higher reliability due to their no-moving part design and have a quick response to changes in the properties of the fluid.

One of the applications of the Switched Vortex Valve, which is in interest of this work, is the development of a SVV suitable for the operation and control of the secondary air system within the jet engine.

### 1.2.1 Secondary Air System.

The air, which is the working fluid in a gas turbine engine, is compressed, heated, and expanded to produce most of the power, but some of this compressed air does not contribute directly to the production of thrust or shaft power, about 5% of the power supplied to the engine is used to achieve this task[24]. Instead, it is used for functions vital to the safe and efficient operation of the engine: cooling, sealing, and controlling bearing loads. This airflow is called the Secondary Air System[21] and a general arrangement and flow paths of the air system can be seen in Figure 1.1.

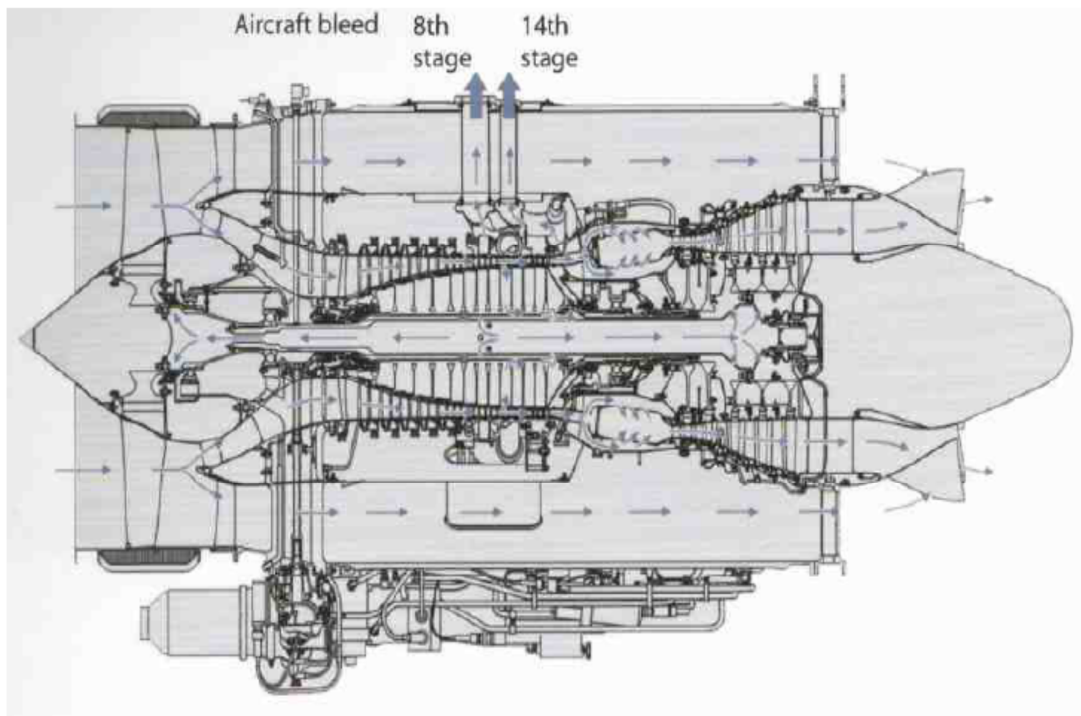


Figure 1.1. - General arrangement and flow paths of the Secondary Air System of the AE 3007 engine [21].

The air supply is divided into subsections of High pressure and Intermediate pressure, in order to fulfil different functions. This is shown in Figure 1.2.

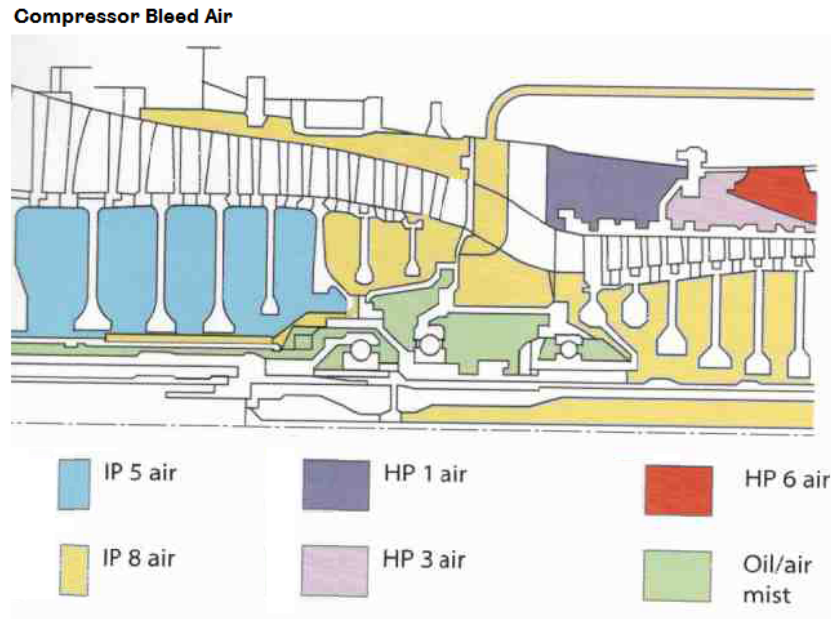


Figure 1.2. - Different subsections of the Secondary Air System [21].

The main functions of the SAS (secondary air system) are 4:

- Cooling
- Sealing
- Control of bearing loads
- Aircraft services

The switched vortex valve can be introduced in any of these engine operations, due to its valuable characteristics such as high reliability in extreme environments and instant reaction to the fluid properties. Given the different stages in a flight: Taxiing, Take-Off, Cruise and Landing, the air requirements in each of these functions are different due to the changing engine operating conditions, so in essence instead of having a mechanical device that is fixed it would be better to have a device such as the SVV that reacts instantly to the conditions present in each of those flight stages.

Using an SVV would help to minimize excessive air used by this on/off operation by only using the required amount of air for the operating conditions of the engine. The use of these fluidic devices can help to use only the required amount of air, can help control the temperature of different components in a much more efficient manner

and it can help to save weight and be more reliable than its mechanical counterparts as mentioned earlier.

Reducing this air flow by a precise amount –whether it is fluidic or mechanical control- has the potential to result in a 4 to 6% increase in power and a reduction between 3 and 5% in specific fuel consumption[12] which will transmit in massive cost savings.

### 1.2.1.1 Cooling.

Several areas of the engine require cooling to maintain safe operation.

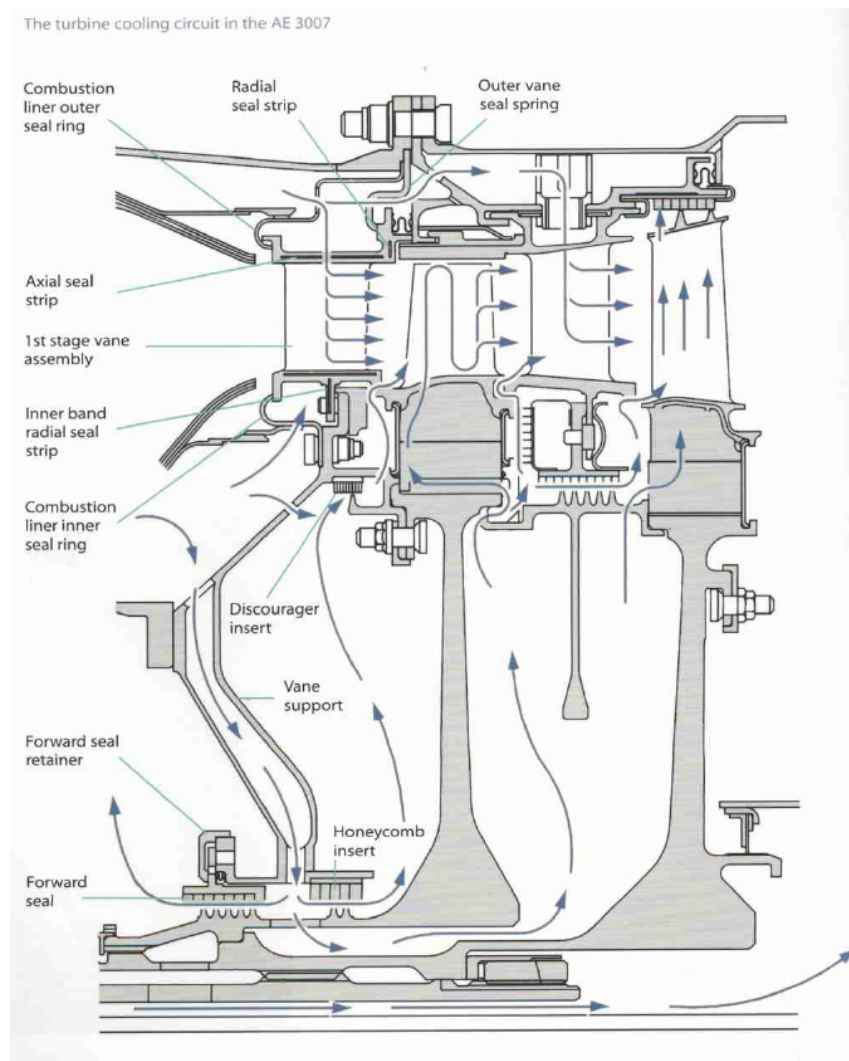


Figure 1.3. - Turbine cooling circuit of the AE 3007 engine [21].

Air extracted from the compressor discharge cools the HP and the IP turbine components. The cooling air can be over 700°C, while the mainstream gas temperature in some parts of the turbine can be up to 1,600°C. This cooling air is essential to prevent mechanical failure due to excessive thermal stresses given that the turbines are often exposed to temperatures beyond the melting point of its material. It also helps to maintain clearances between stators and rotors.

### **1.2.1.2 Sealing.**

This aims to minimise the performance penalties from air leaking overboard, across engine modules, and across turbine stages. The internal air system must provide effective sealing in order to direct cooling air to the target locations at the designed flow levels.

One important sealing function is that of preventing oil leakage. If oil gets outside the bearing chamber this may result in an engine fire; a leak into the mainstream gas path may cause aircraft cabin odour, or visible smoke. Air is used to buffer seals around bearing chambers to prevent oil leakage. This consists of a rotating part equipped with fins and a static part with a honeycomb structure. When the engine is started the rotating fins create minimum clearances by cutting into the honeycomb structure; the sealing is then done by driving air from a high pressure system to the inside of the bearing chambers via the path created by the rotating fins and the static honeycomb structure.

Another important function is the prevention of hot gas entering the cavities below the turbines; this would cause thermal stresses on the turbine disks caused by the high pressure in the turbines. Cooled air is then used for two main functions: to oppose the flow of hot gas into the cavities and to cool down the turbine disks.

### **1.2.1.3 Control of bearing loads.**

The flow of the mainstream gas exerts an axial force that acts in the forward direction of the compressor, and in the aft direction on the turbine. The shaft connecting the compressor and turbine will experience a net axial load that is the sum of the compressor and turbine loads, and the loads produced by the internal air

system acting on the discs and shafts as shown in Figure 1.4. The position of sealing elements around the compressor and turbine determine the net internal air loads and is the primary tool available to the air system designer for controlling bearing loads.

Another important factor in the resultant load is the reaction of the HP turbine. The reaction determines the gas path static pressure between the first stage nozzle guide vane and blade. This pressure can act over a large area of the disc and change net axial loads significantly. The bearing loads must be controlled to reduce the risk of overloading or unloading a thrust bearing. An unloaded bearing is more likely during engine operation, and the rolling elements can skid when unloaded causing significant heat generation leading to bearing failure.

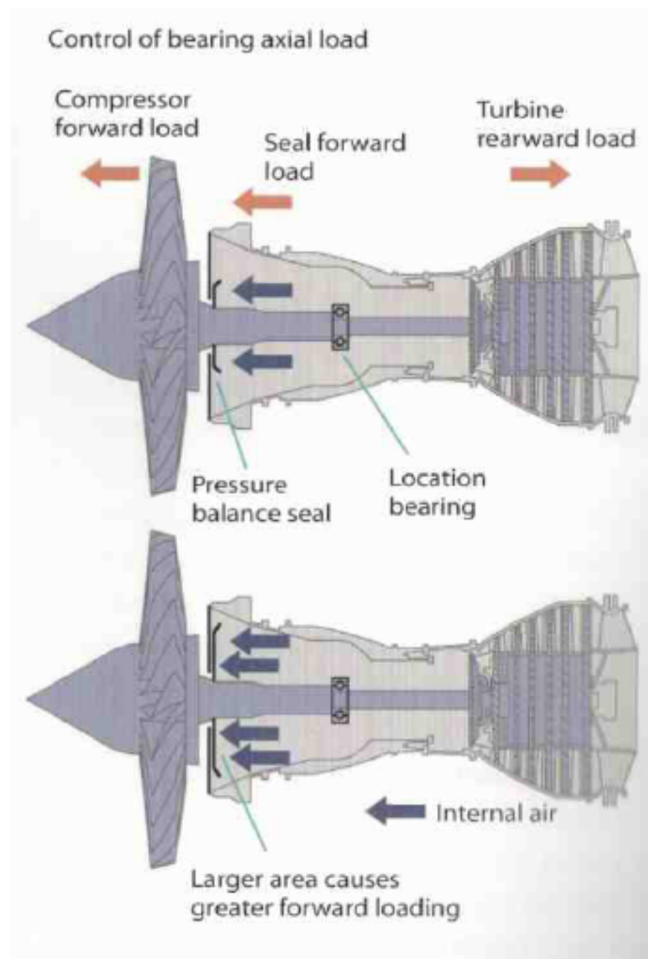


Figure 1.4. - Axial bearing load control through setting the pressure acting on disc faces [21].

#### **1.2.1.4 Aircraft Services.**

Some aircraft services require to bleed some air from the SAS to control the cabin pressurization and heating. The flow of the mainstream gas exerts an axial force that acts in the forward direction of the compressor, and in the aft direction on the turbine. The shaft connecting the compressor and turbine will experience a net axial load that is the sum of the compressor and turbine loads, and the loads produced by the internal air system acting on the discs and shafts. The position of sealing elements around the compressor and turbine determine the net internal air loads and is the primary tool available to the air system designer for controlling bearing loads.

### **1.3 National Aerospace Technology Strategy.**

The Aerospace Innovation and Growth Team Report recommended the establishment of a National Aerospace technology Strategy (NATS). The NATS is the result of an important partnership between industry, Government and academia to address UK competitiveness in aerospace technology. The objective of the strategy is to ensure that the technology generated by the UK science base flows through to industry and is embedded in the supply chain for commercial exploitation. The strategy addresses specific challenges relating to the environment, safety, security and national defence.

There are, under this strategy, the AIN (Aerospace Innovation Networks) and the ATVPs (Aerospace Technology Validation Programmes), in which this work is more interested.

These ATVPs demonstrate and integrate innovative technologies, reducing the risk in downstream product programmes. ATVPs are focused on a specific theme, identified as part of the NATS over a rolling 5-year period.

There are 6 ATVP topics in NATS:

1. - Integrated Wing: Wing optimisation, flow control and noise reduction, new materials, design and manufacturing techniques, advanced fuel and landing gear systems, 'virtual' integration and validation environment.
2. - More Electric Aircraft: Power storage, generation and control, engine systems, distribution and load management, actuators and actuation systems, environmental control system, overall integration.
3. - Environmental Friendly Engine: Aerodynamic and mechanical designs, novel high temperature materials, low emissions combustion, advanced control systems and actuators.
4. - Autonomous Systems: Security/safety, system reliability, intelligent autonomy, human factors/integrating into the environment, navigation/situational awareness, ease of operation, operations protocols.
5. - INFOAir: Secure and information sharing, protection of airspace, safe and more secure employments, test facilities for rapid investigation.
6. - Integrated Air Traffic Management Network: Autonomous decision making, reliability, safety, security, ability for deployed and remote operation, civil vs military requirements, integration.

#### **1.4 EFE – Environmental Friendly Engine Technology Validation Programme.**

With the ever increasing population rate, the globalised world and with the anticipated tripling of air traffic over the next 25 years[17], reducing the environmental impact of aviation is one of the most significant challenges facing the global aerospace sector.

There is a critical need to address the reduction of noise and polluting emissions from aircraft and engines. The UK and European aviation industry has cooperated with the Advisory Council for Aeronautics Research in Europe (ACARE) to set a series

of step-change goals for reducing carbon dioxide by 50% per passenger km, oxides of nitrogen by 80% and noise by 50%, all by 2020.

EFE is a critical part of the UK National Aerospace Technology Strategy to meet these goals and will provide the validation route for future generations of improved gas turbine systems. It will enable the pull-through of technology from the UK science and engineering base and ensure that the integrated and optimised operation of a range of new technologies is validated ahead of their introduction into production vehicles in the 2012-2015 timescale[18].

The programme is focused on the system level integration and validation of:

- Aerodynamic and mechanical designs.
- Novel high temperature materials.
- Low emissions combustion.
- Advanced control systems and actuators.

Rolls-Royce is leading a consortium of five UK aerospace companies (Goodrich, Bombardier Aerospace, Smiths Aerospace and HS Marston) and six universities (Queens Belfast, Loughborough, Oxford, Cambridge, Sheffield and Birmingham).

Rolls-Royce invests over £700 million every year on Research and Development, two-thirds of which is aimed at improving the environmental performance of its products and operations. Over £120 million of this programme is dedicated to innovative technology aimed at improving environmental performance.

The hardware donor for the EFE engine programme is the Trent 1000 engine currently in operation by Rolls-Royce; the experience gained on the EFE programme will be used in many of their next generation gas turbines. New technology may also be considered for retrofit into existing, in-service products to improve environmental performance further.

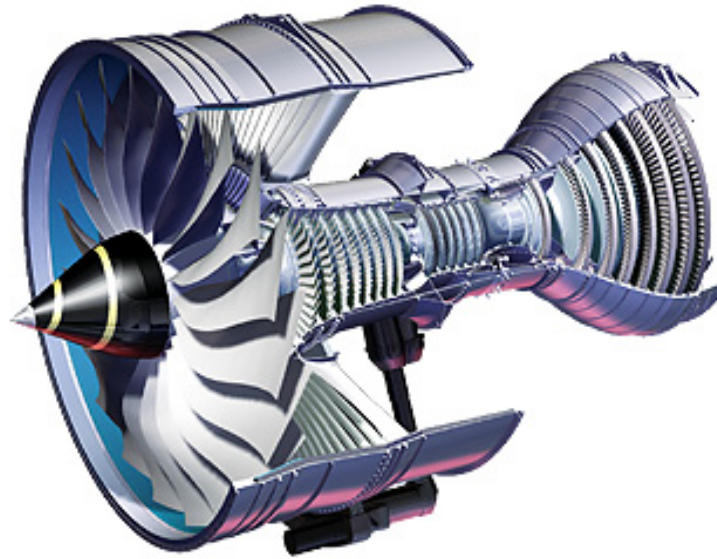


Figure 1.5. - Environmentally Friendly Engine (EFE) [21].

## **1.5 Rolls-Royce Switched Vortex Valve Application.**

The application of the Switched Vortex Valve is intended to control the flow of cooling air to the IP turbine disc and will be mounted on the HP/IP structure.

The prototype concept will be demonstrated on EFE Build Stage 4, and prior to engine test, the hardware is planned to go under rig testing at Sheffield University.

### **1.5.1 Scope and Introduction.**

The IP Turbine disc rims are subject to a continuous flow of cooling air. The use of a Switched Vortex Valve will enable a high or low flow state to be selected to suit the flight cycle stage, to prevent the ingestion of hot annulus gas into disc cavities. The disc rim overheat may result in disc burst or multiple blade failure, these potential events are hazardous and their possibility must be extremely remote.

A typical Rim Seal consists of an interchange of gas and cooling air occurring at the annulus gap, the cooling flow dilutes the ingestion of the hot annulus gas into the cavities.

The passages through which cooling air passes are designed for high cooling air flow, thus, the engine draws higher cooling air flows from the HP structure than required during the cruise phase (low cooling air flow needs), resulting in loss of costly high pressure compressed air.

The ability of the SVV to switch from high to low states and vice versa, could well provide some control of the cooling air flow rate.

Previous work involves the SVV working with incompressible flow, vortex amplifiers, vortex throttles and SVV working with compressible flow for a different application. All these will be reviewed over the course of this work.

### **1.5.2 Operational Conditions and Requirements.**

The Switched Vortex Valve will control the amount of cooling flow in the Intermediate Pressure system and will be mounted in the High Pressure Turbine or HPT cavity/Intermediate Pressure Turbine or IPT cavity boundary. The location has space limitations and the conditions in which the device will work are 301 psi on the HPT cavity and 120 psi on the IPT cavity, giving a pressure ratio of 2.51 at the maximum operational conditions found in the engine [24], those pressures being the inlet and outlet working pressures on the device. The amount of air flow required is less than 1.4 lb/s at MTO conditions.

The operating conditions in the engine are shown in the Table 1.1,

The turndown flow ratio is expected to be around 2 times the maximum flow in the low resistance state.

By changing the engine conditions during the different flight stages means that the ideal flow resistance of the device should change accordingly.

Although the temperature will be incredibly high due to the extreme operating conditions within the engine, the temperature gradient is not sufficiently high to take it into account.

Table 1.1 – Operating Conditions for the current Trent 1000 Engine.

<b>Trent 1000 Pack B (FSG49772i2)</b>					
	<b>PAMB (VENT) (psi)</b>	<b>HP3 manifold (psi)</b>	<b>Torsion Box (SUPPLY) (psi)</b>	<b>OUTPUT (psi)</b>	<b>Pressure Ratio</b>
Type Test	14.7	300	291.1	126.7	2.30
TCDS	14.7	308.2	299.8	119.2	2.52
EOR ISA+15	14.7	310.1	301.6	120	2.51
Cruise (35,000ft)	3.46	106.6	98.3	41.5	2.37
Ground Idle	14.7	33.9	33	18.3	1.80

It is very important that the materials used can withstand the extreme conditions and they are not prone to creep which is when the metals exposed to high temperatures deform or change shape and can even break due to fatigue. The turbine blades are made from a nickel-based super alloy which can withstand much higher temperatures and it is less prone to creep than titanium. So it is important that the material used is adequate to withstand the conditions.

### **1.5.3 Current Architecture.**

Figures 1.6 and 1.7 show the location in which the Switched Vortex Valve could be implemented and the space in which the rim would be installed. This location has serious space limitations so the device has to be small and compact.

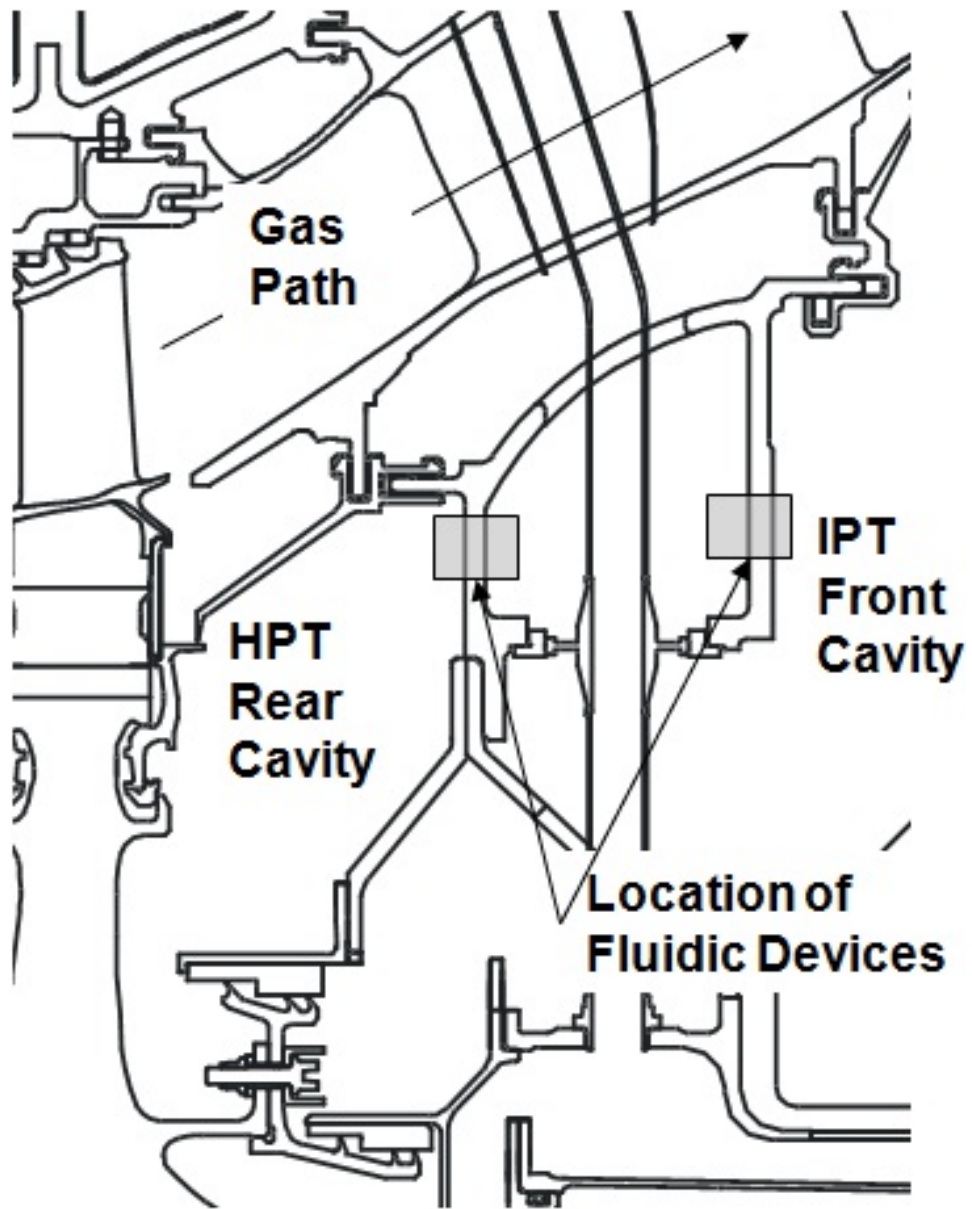


Figure 1.6. - Location of Fluidic Devices within the IP Turbine [24].

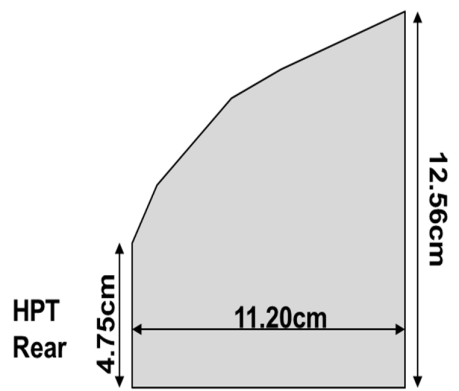
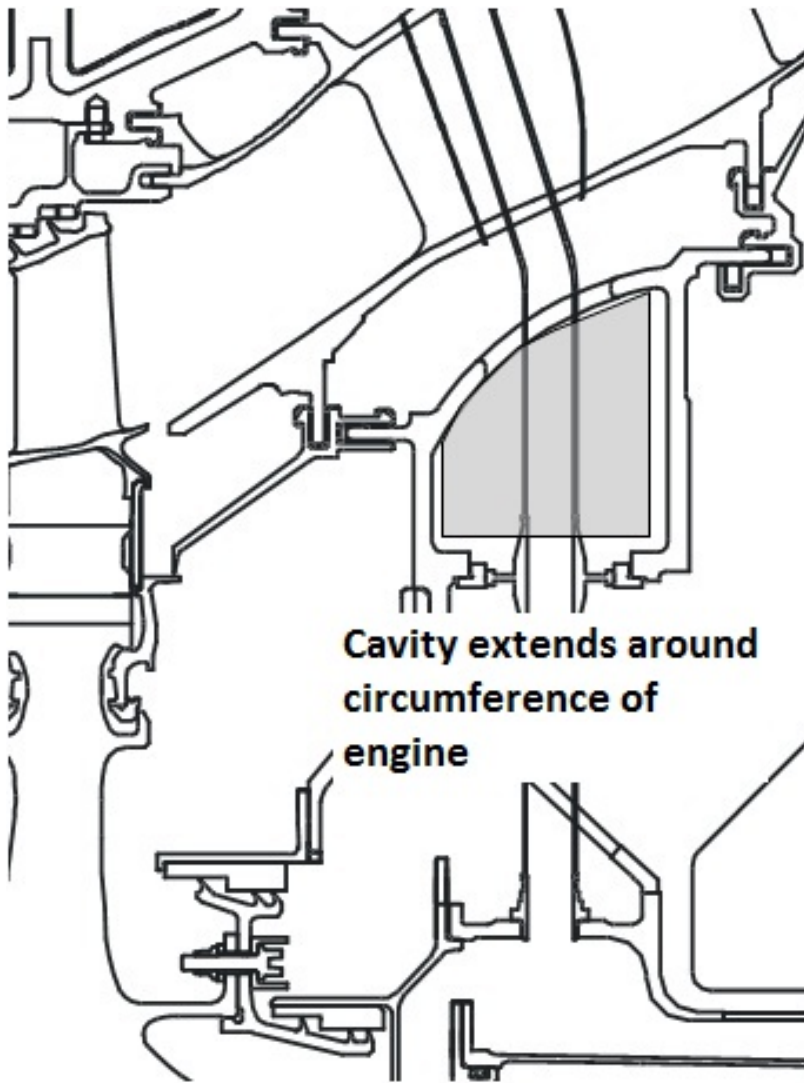


Figure 1.7. - Space envelope for the Switched Vortex Valve Rim [24].

## 1.6 Research Objectives.

A lot of work is required to be done with compressible flow, identifying some important parameters for the design of such devices to cope with the requirements that the applications need. Some of previous work on this will be presented here in order to place the foundations for understanding the operation principles of the different devices.

The main objective of this work is to optimize the Switched Vortex Valve or SW to work with compressible flow under the conditions specified by Rolls-Royce. Over the course of this work different devices will be tested with compressible flow and analyzed to try to understand the behaviour of the Switched Vortex Valve working with compressible flow.

## 1.7 Thesis Layout.

- Chapter 1, Introduction
  - o Introduces the background of the research study and its main objective.
- Chapters 2, Literature Review and Chapter 3, Compressible Flow
  - o Show the literature background and compressible flow theory, which are important to the analysis of the Switched Vortex Valve.
- Chapter 4, Vortex Throttles
  - o Shows experimental work with Vortex Throttles, its characterization and results with compressible flow.
  - o It also shows a CFD modelling with three different numerical models, the Standard  $k - \varepsilon$ , the Realizable  $k - \varepsilon$  and the Reynolds Stress Model for the prediction of such devices.
- Chapter 5, Switched Vortex Valves with Compressible Flow: Experimental
  - o Shows all the experimental work done with Switched Vortex Valves with compressible flow; it shows the analysis of the device as well as the effects of different geometries and parameters in the performance. This Chapter 5 is focused basically in the optimisation of the device to

work under the requirements needed for the application of air control in the secondary air system that Rolls-Royce specified.

- Chapter 6, Vortex Amplifiers
  - o Shows experimental work with Vortex Amplifiers and its performance comparison to that of a Vortex Throttle; it also gives the circuit analysis for a Jet Pump – Vortex Amplifier matching for future experiments and possible performance improvement.
- Chapter 7, Rolls-Royce Final Design
  - o Shows the final optimized device that will be manufactured and tested by Rolls-Royce in the E.F.E.
- Chapter 8, Conclusions and Future Work
  - o Involves the conclusions and recommendations for future work.

2

## **LITERATURE REVIEW**

### **2.1 Components Characteristics.**

The Switched Vortex Valve or SVV as in this work will be referred to (some authors may call it Coanda Switch Valve or CSV) is a fluidic device which has two different fluidic components that joined together function as a complete new device.

These two components are the Wall Attachment Diverter and the Vortex Amplifier. The first one uses the Coanda effect to divert the inlet flow to one of two of its channels. The second one uses the inherent momentum of the fluid to cause a resistance within the vortex chamber that can either let the flow pass through the vortex chamber or to stop it; that happens when the fluid enters either one of the two channels of the Wall Attachment Diverter.

If the inlet flow gets diverted towards the radial channel i.e. the channel that goes radially to the Vortex Amplifier, then there is no angular momentum within the chamber thus creating barely any resistance to the flow of the fluid through the chamber.

In the other case, if the fluid gets diverted to the tangential channel i.e. the channel that goes tangentially to the Vortex Amplifier, then there is an angular momentum inherent in the own fluid creating a vortex within the chamber, this vortex creates a

high resistance i.e. a static pressure gradient across the vortex, to the flow of the fluid.

These two states are known as the Normal or Low Resistance state and Vortex or High Resistance state (flow entering radially and flow entering tangentially respectively), and they can be switched by slightly opening the desired control port.

### 2.1.1 Wall-Attachment Diverter.

This is the fluidic component which gives the Switched Vortex Valve the ability to divert the flow as shown in Figure 2.1. Many have addressed this fluidic device and its particular applications [5, 7, 41]

It relies upon the interaction between the fluid jet issued from the main nozzle and a solid sidewall. This interaction is commonly known as the Coanda effect. The Coanda effect works when the entrainment of the fluid is restricted by the presence of the wall resulting in a reduction in local pressure i.e. a low pressure system right next to one of the control ports entrance. This low pressure system forces the fluid jet to attach itself to its contiguous channel.

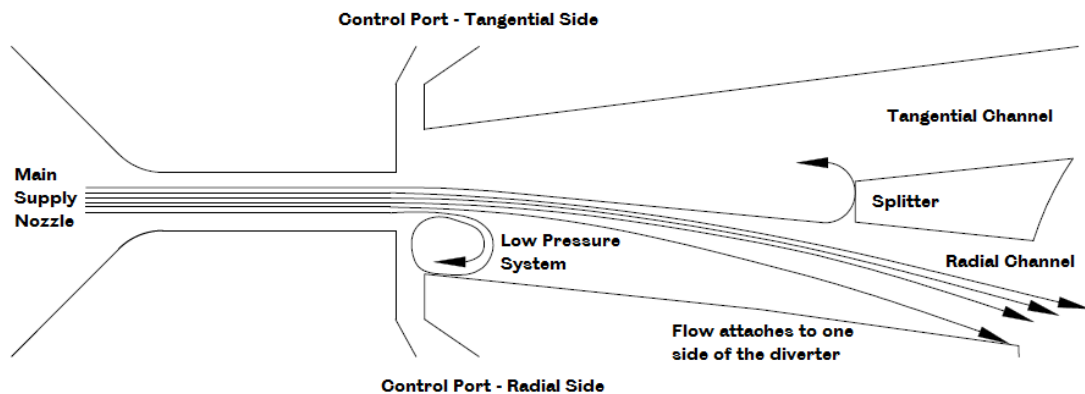


Figure 2.1. - Wall-Attachment Diverter.

The symmetry of the two sidewalls in the Wall Attachment Diverter does not produce a cancelling of wall effects so a stable central flow is avoided and the supply flow only attaches to either one of the side walls and is diverted to the adjacent outlet. The outlet adjacent to where the jet is attached is marked as the active outlet and the

other as passive. For the low resistance state, the active channel is the radial channel and in this work this is how it is going to be called. For the high resistance state the active channel is the tangential channel and in this work this is how it is going to be called.

If the diverter is discharging from the radial channel directly into atmosphere with both outlet channels left fully opened and the control ports closed, fluid from the tangential channel outlet is entrained and discharged together with the supply flow via the radial channel outlet. However, when the load on the radial channel outlet is increased to permit less flow through the channel, spillover will occur with some supply flow discharged through the tangential channel outlet. If this procedure is continued, either the flow out from the radial channel is totally stopped or the jet switches into the other channel.

The principle geometric variables of the Wall Attachment Diverter are normally measured in terms of the nozzle width  $d$  and can be seen in Figure 2.2. The wall setback  $b$  is very important for the switching; smaller  $b$  require smaller control pressure and flow for switching, however, when  $b$  is very small ( $< 0.2d$ ) the device becomes oversensitive to small geometrical or flow changes, hence usually  $0.2d < b < 1d$ .

The flow rate and pressure required to switch the Wall Attachment Diverter is usually of the order of 10% of the supply flow and pressure.

The shape and the position of the splitter offer great variety. If the diverter is to discharge freely with no restriction of its output channel then a rounded or sharpened tipped splitter is simple and adequate. As the output channel is increasingly restricted, increasing flow must spill over the splitter. When operating with both outlets restricted, it is possible to have load switching in the device, i.e. flow changes occurring in the outlets to cause switching, then a cusped [34, 31, 7] or a flat splitter can help to maintain stability. A normal value for the splitter distance  $s$ , is to be between  $5d$  and  $10d$ , having the latter a 40% recovery of the supply pressure in the output channel when the flow there equals the flow from the nozzle, and operating with one control port closed.

As decreasing the splitter distance, the restriction of the output channels increases, and when increasing the splitter distance the restriction decreases.

The important dimension parameters for a good performance diverter are [41]:

- Width of the control channel,  $c = 0.8$  times the nozzle width
- Splitter distance from the nozzle,  $s = 8$  times the nozzle width
- Setback,  $D = 2.5$  times the nozzle width
- Wall angle,  $\theta = 12^\circ$

### 2.1.2 Vortex Throttle.

The Vortex Throttle is a no-moving-part fluidic device which main objective is often to maximize pressure loss for a given minimum flow area. It contains a cylindrical chamber and a tangential control port. The operation of such devices is based on a high loss of energy associated with the swirling fluid as it passes through the device. The Vortex Throttle is shown in Figure 2.3.

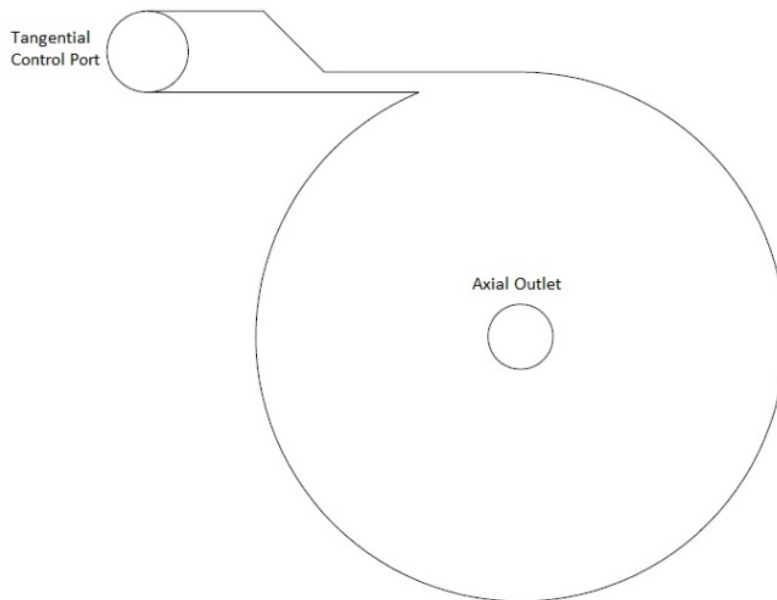


Figure 2.3. - Vortex Throttle.

The Vortex Throttle is the basic design to other vortex devices such as the Vortex Amplifier.

The performance of the Vortex Throttle is often expressed in terms of an Euler number  $Eu$ , defined as

$$Eu = \frac{\Delta P}{0.5\rho v^2}$$

in which the fluid density and velocity used in the above equation are both based on flow at the tangential port.

Priestman [20] studied the effects in performance of changes in geometry for compressible subsonic flow and for incompressible non-cavitating flow, and could be regarded as being the same when measured in terms of conditions at the tangential port.

The maximum values of Euler number found for squared-edged throttles were about 66. According to Priestman, to maximize the performance the axial port should have a parallel length of at least twice its diameter.

Priestman says that the optimum diameter ratio,  $d_c/d_o$ , was about 6 but varying this in the range 5 to 8 had only relatively small effect.

### **2.1.3 Vortex Amplifier.**

The fluidic component which provides the high or low resistance to the flow in the Switched Vortex Valve is the Vortex Amplifier or VA as shown in Figure 2.4 and Figure 2.5.

The Vortex Amplifier contains a thin cylindrical chamber and its operation is based on the same principle as the vortex throttle.

The feature which differentiates a Vortex Amplifier from the Vortex Throttle is that a Vortex Amplifier has a radial inlet port which is designed so that no angular momentum is transmitted to the flow entering the chamber.

The main supply flow enters the vortex chamber radially and a small tangential flow is used as control flow to generate a vortex. The strength of the vortex is determined by the amount of control flow fed into the device. The tangential flow is forced into the chamber from a higher pressure than the supply flow. With no control flow, the

resistance to flow is minimum. When control flow is introduced, a vortex is generated and a pressure gradient across the chamber is produced thus increasing the resistance to the flow. A high amount of control flow can stop or reverse the supply flow.

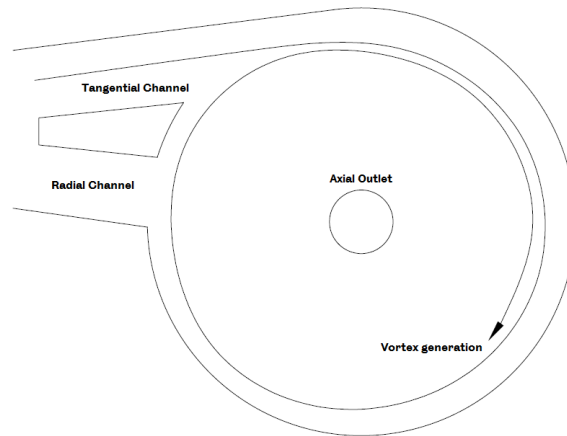


Figure 2.4. - Vortex Amplifier – Vortex State (High Resistance).

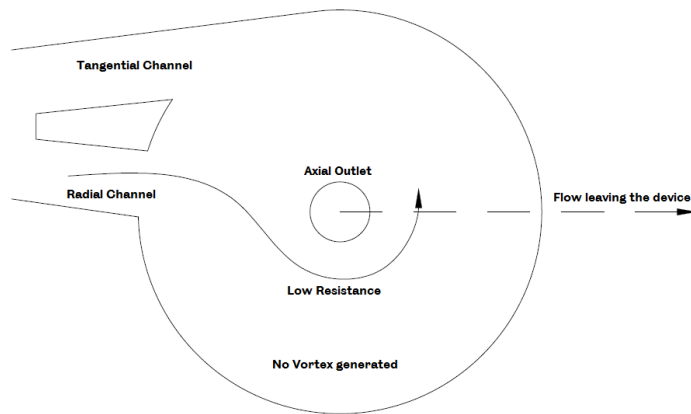


Figure 2.5. - Vortex Amplifier – Normal State (Low Resistance).

Some of the important parameters are these:

- a) Size of the outlet hole.
- b) Cross-sectional area of control jet.
- c) Chamber height.

- d) Chamber diameter.
- e) Diffusing or non-diffusing outlet.

Some of these parameters are described by the following ratios,

$$D = \frac{\text{chamber diameter}}{\text{outlet hole diameter}}$$

$$A_c = \frac{\text{cross - sectional area of control jet}}{\text{area of outlet hole}}$$

$$H = \frac{\text{chamber height}}{\text{outlet hole diameter}}$$

The operation of the Vortex Amplifier can be described by the following variables,

Supply variables:

$$p_s - p_o : \text{supply pressure} - \text{outlet pressure}$$

$$q_s : \text{supply flow to the radial inlet}$$

Control variables

$$p_c - p_o : \text{control pressure} - \text{outlet pressure}$$

$$q_c : \text{control flow}$$

In some applications it can be appropriate to use other variables, such as

$$p_c - p_s : \text{control to supply pressure}$$

$$q_o : \text{outflow}$$

These variables are related by the fact that the sum of the correctly directed pressure differences is zero and

$$q_o = q_c + q_s$$

For compressible flow, one needs to consider the mass flows for the above variables.

The characterization results from maintaining a constant supply pressure ( $p_s - p_o$ ) and recording  $q_s$  as a function of the control pressure ( $p_c - p_o$ ) or flow.

Two useful gain parameters are defined in terms of the ratios of flows and pressures in the high and low resistance states of the Vortex Amplifiers. The parameters are the turndown ratio or  $T$  and the control pressure ratio or  $G$ . The two defining states are referred to as the low resistance state when  $q_c$  is zero, and the high resistance state when  $q_s$  is zero.

The gain parameters  $T$  and  $G$  are defined by

$$T = \frac{q_s \text{ in the low resistance state}}{q_c \text{ in the high resistance state}}$$

$$G = \frac{(p_c - p_o) \text{ in the high resistance state}}{p_s - p_o}$$

Both determined with  $p_s - p_o$  constant.

$T$  is a measure of flow gain and  $G$  is an inverse measure of pressure gain, so in general it is beneficial if  $T$  is large and  $G$  is small [5].

A lower limit for  $G$  is unity, because in the high resistance state,  $p_c$  must be at least equal to  $p_s$  in order to force the control flow into the Vortex Amplifier.

The main design feature which determines the relative values of  $T$  and  $G$  for a basic design of Vortex Amplifiers is the control jet area. A small jet area gives a large control momentum flux for a given control flow which produces a strong vortex and a high flow gain, but it also requires a high control pressure which lead to a high value of  $G$ . Hence, over a certain range, increased  $T$  can be obtained at the expense of increasing  $G$ .

Another performance parameter of the Vortex Amplifier is the parameter  $X$ , which is  $E_c = (p_c - p_o)/(p_s - p_o)$  in the low resistance state,

As an example Figure 2.6 shows the performance and design of a Vortex Amplifier determined by Wormley [45], who presented the results operating with air at supply

pressures of about 0.2 bar, and shows the turndown ratio and control pressure ratio as functions of the design of the Vortex Amplifier which is given by the inverse of  $D$ .

From Wormley's chart, it can be deduced that the turndown ratio becomes greater as the chamber/outlet diameter ratio is made smaller, as well as having smaller control port area or  $A_c$  but incurring in greater values of  $G$ .

Another important feature in the Vortex Amplifiers is the use of diffusing outlets. These type of outlets were investigated [30, 27].

The resistance produced by the outlet can be reduced for subsonic flow by making it in the form of a small angle conical diffuser. An outlet of this type can carry between two and three times the flow that would pass through a nozzle with an equal throat and pressure drop.

In a Vortex Amplifier this greatly improves the performance by reducing even more the resistance in the low resistance state. This benefit, however, is greatly influenced by the need of a subsonic flow which sets severe constraints on when the diffuser can recover pressure.

#### **2.1.4 Matching of the Fluidic Components.**

Wang's work [41] shows in great detail how to match the two main fluidic components that create the Switched Vortex Valve: the Wall-Attachment Diverter and the Vortex Amplifier.

The technique aids the design process by allowing some choice in the performance of the combinations of elements by scaling the size of one or both constituent parts.

The results of matching the two fluidic elements can be presented to show the actual performance of the combined device [41]. Wang found that for a combination of a good performance wall attachment diverter and a VA the predicted turndown ratio is close to 1.382.

Wang implies that the matching technique is enhanced by the possibility of choosing the relative scale of the elements to meet any particular requirement.

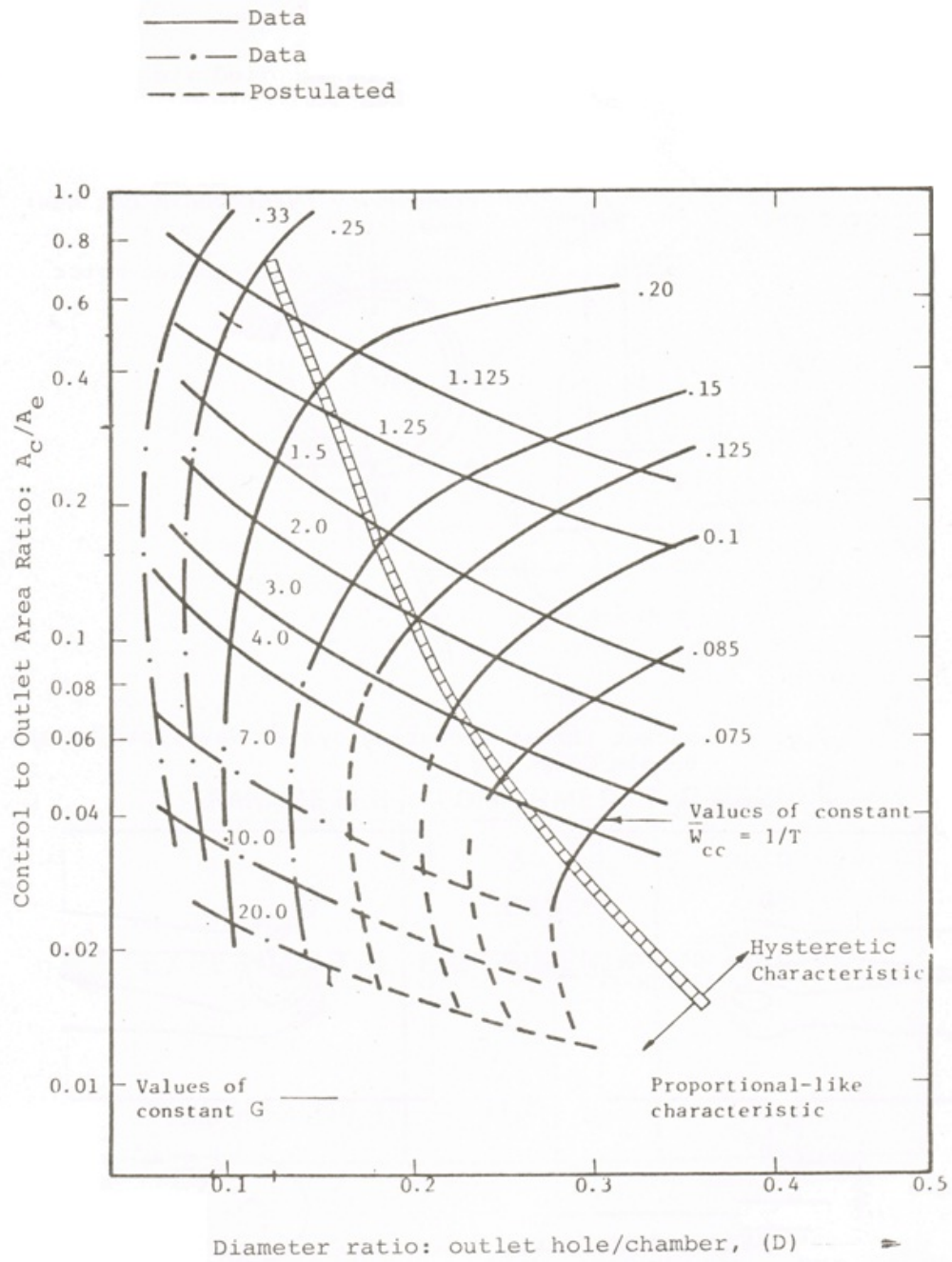


Figure 2.6.-Wormley's chart for single outlet Vortex Amplifiers [45].

## 2.2 Parameters and Previous Experiments of the SVV.

### 2.2.1 Parameters of the Switched Vortex Valve.

It is important to identify some of the important characteristics of the Switched Vortex Valve. To optimise the device there has been some work[26] involving changes in geometry to improve the performance.

Some of the parameters that are of importance in the device are the following:

- Area ratio  $a_s/a_t$ , where  $a_s$  is the inlet nozzle cross sectional area, and  $a_t$  is the tangential channel cross sectional area.
- Area ratio  $a_s/a_o$ , where  $a_o$  is the axial outlet cross sectional area.
- Diameter ratio  $d_c/d_o$ , where  $d_c$  is the diameter of the vortex chamber, and  $d_o$  is the axial outlet diameter.
- Height ratio  $H$ , is the ratio between the height  $h_d$  of the device and the inlet nozzle width.

$h_d$  = height of the device

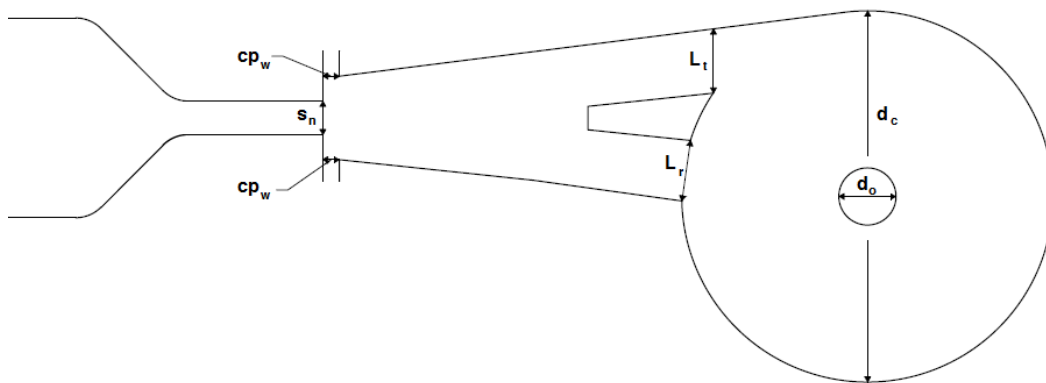


Figure 2.7. - Geometry parameters of a SVV.

In Figure 2.7 the length  $s_n$  is the width of the inlet nozzle or supply nozzle,  $cp_w$  is the width of the control ports,  $L_t$  is the width of the tangential channel,  $L_r$  is the width of

the radial channel,  $d_c$  is the diameter of the vortex chamber, and  $d_o$  is the diameter of the axial outlet. In order to get the respective areas the parameter  $h_d$  which is the height of the device has to be used.

There are some other parameters that could improve the performance of the device but there are not enough data to establish this. Some of these parameters are the inlet nozzle configuration, the control port entrance width, the height of the device, and some other configurations.

In this work, some of these parameters will be explored and tested.

### 2.2.2 Previous work with Incompressible Flow in Switched Vortex Valves.

In the studies on the optimisation of the SVV performance made by RuhGoh[26], it is shown that it is better that the SVV be regarded as a single integrated unit, this because it was observed that the performance characteristics of the combined device were yielding poor performance.

After treating the SVV as a single integrated unit, the final performance predicting equation for predicting  $E$  is shown below:

$$E = \frac{c_{sv} + (a_s/a_o)^2 + (a_s/a_t)^2 [(\alpha\psi d_c/d_o)^2 + 1 - 2\alpha^2]}{c_{sn} + c_{cn}(a_s/a_o)^2} \quad \text{Eq. (2.1)}$$

Where the numerator represents the High resistance state operation, the denominator represents the Low resistance state operation,  $\alpha$  is a velocity recovery factor which relates a chamber peripheral velocity to the theoretical inlet velocity and  $\psi$  is the overall circulation factor. Those two factors,  $\alpha$  and  $\psi$  were incorporated from a mathematical model of a vortex throttle determined by Priestman[20].

For fluidic operations, it is desirable to increase the performance turndown ratio  $E$ , but in this work the turndown ratio will be specified as  $T_f$ .

An ideal value for this ratio is infinity, but this would require the main flow in the high resistance state to be zero, which is fundamentally not possible. To date there is lack of detailed information about optimisation data which maximizes  $E$ . So the work

made by Ruh Goh aimed to achieve the maximum resistance ratio possible by a systematic variation of the design of several features of the device.

Based from the equation, it is evident that the design dimensions which have significant effect on performance are the ratios  $a_s/a_o$ ,  $d_c/d_o$  and  $a_s/a_t$ . The device used, can be seen in Figure 2.8.

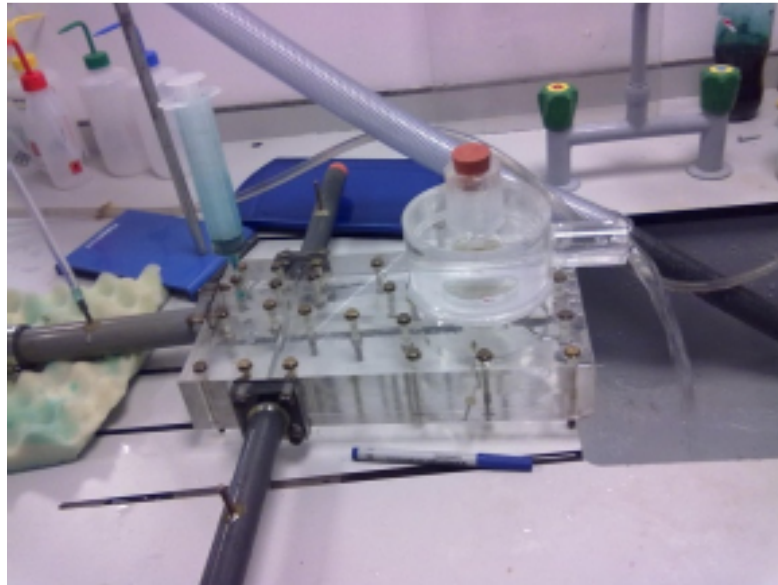


Figure 2.8. - Ruh Goh's Switched Vortex Valve in operation with water at small pressures.

Assumptions on the case of incompressible flow were made to simplify the analysis of the device, so the results for air made by Ruh Goh are not directly applicable to compressible flow, and therefore there is a deviation from the final performance predicting equation at high Reynolds number, although the pressures at which Ruh Goh's worked were too small, the maximum pressure used in the supply for compressible flow (air) was 3.5 psig.

The preliminary experiments enabled the detailed geometry of the radial and tangential channel to be optimised. This included the elimination of flow instabilities in the low resistance state by simply profiling the radial channel on a suitable way, a problem that was solved before by the use of a de-swirl vane within the camber which eliminates the angular momentum of the flow, thus, eliminating any swirl.

The other parameters that were varied enabled the empirical constant in the model to be confirmed. Both the model and the experiments confirmed that for a SVV with a single nozzle-type outlet, a good performance corresponded to an  $E$ -value of about 16.

The SVV performance is also dependent on the Reynolds number and high performance can be achieved in the ranges of 20,000 Re to 40,000 Re for the size of device used in Ruh Goh's work, as it is shown in Figure 2.9.

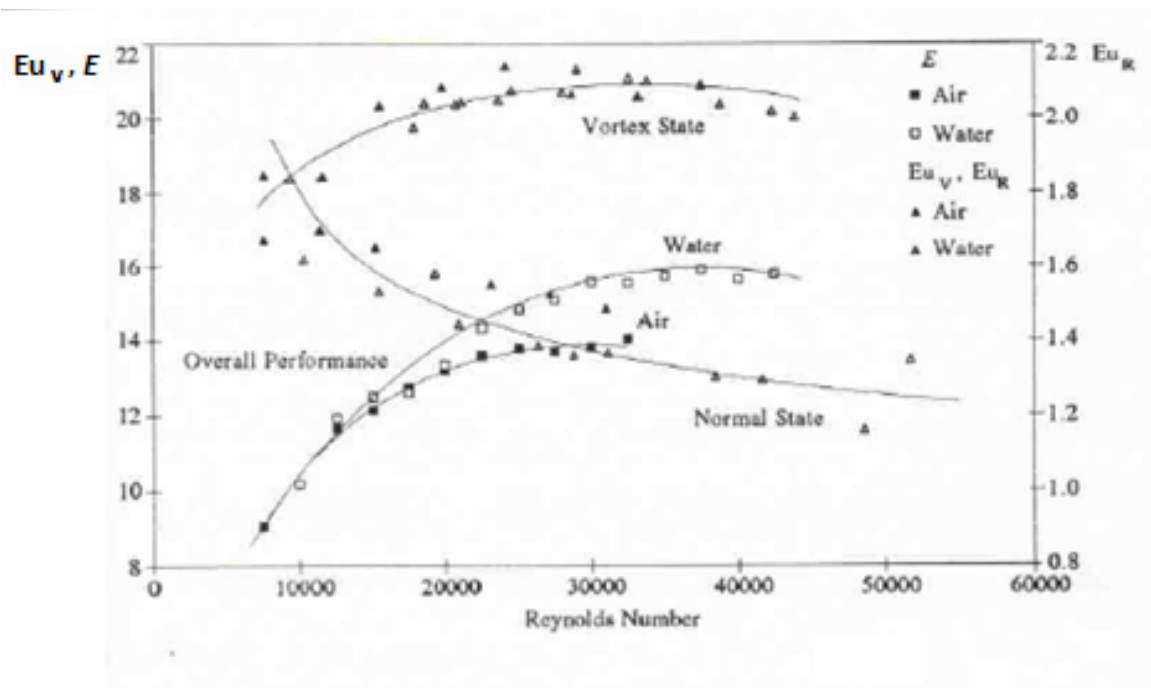


Figure 2.9. - Reynolds Number Effect on SVV Performance [26].

According to the analysis from Ruh Goh, the best performance of the device at a Reynolds number of 30,000 is achieved with a value of unity for the height  $H$ . These optimum values are shown from Figure 2.10 to Figure 2.12.

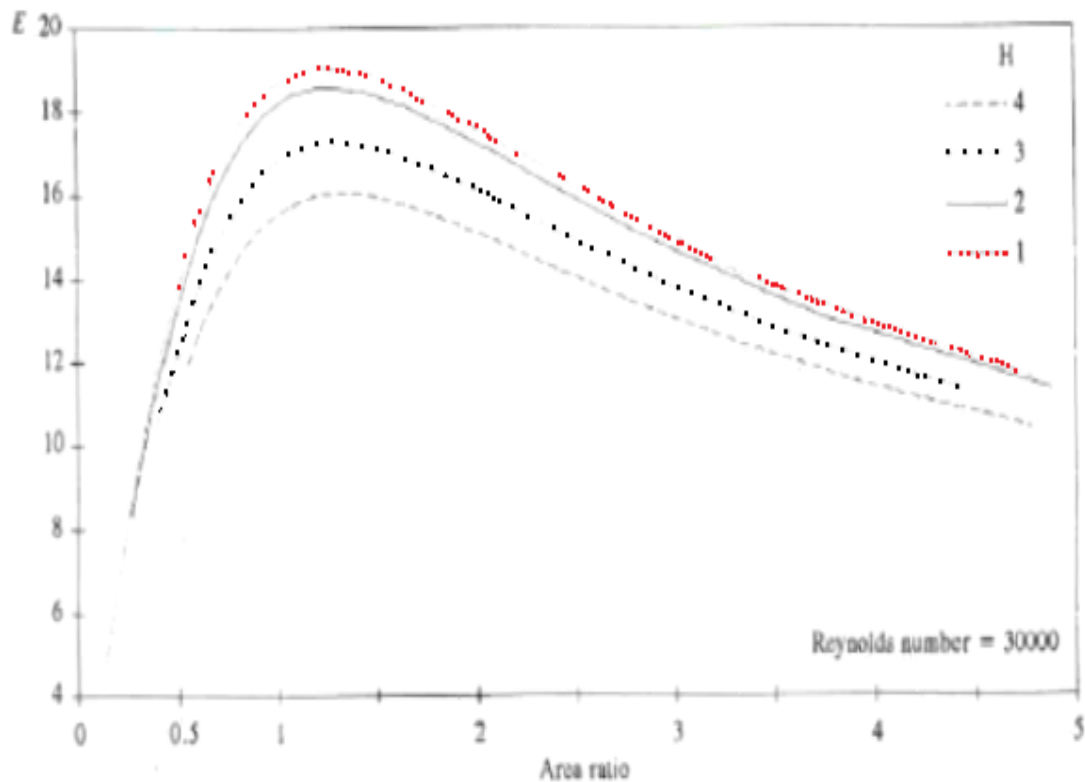


Figure 2.10. - Variation of  $E$  with  $a_s/a_o$  [26]

The optimum  $a_s/a_o$  ratio is predicted to be between the values of 1 to 1.5, for the non-dimensional height  $H$  of 2 and unity. This can be seen in Figure 2.10.

For the  $d_c/d_o$  ratio, the optimum value is to be between the values of 6.5 to 8.5 for a non-dimensional height  $H$  of 2 and between values of 10 to 12 for a value of unity of  $H$  as shown in Figure 2.11.

For the variation of  $E$  as a function of  $H$  at  $Re = 30,000$  with  $a_s/a_o$  constant at unity; at as  $H$  is reduced the performance increases and miximises at approximately at  $H = 1$  and a further decrease in  $H$  will result in a decrease in performance. At very small values of  $H$  the performance increases.

The area ratio  $a_s/a_t$  was set constant at 0.54, this is close to the value of 0.6 found by Tippetts[34] which is the maximum ratio where there is no spillover into the radial

channel in the vortex state, thus close to the zero entrainment operation point. This value of 0.54 corresponds to  $\theta=6^\circ$ .

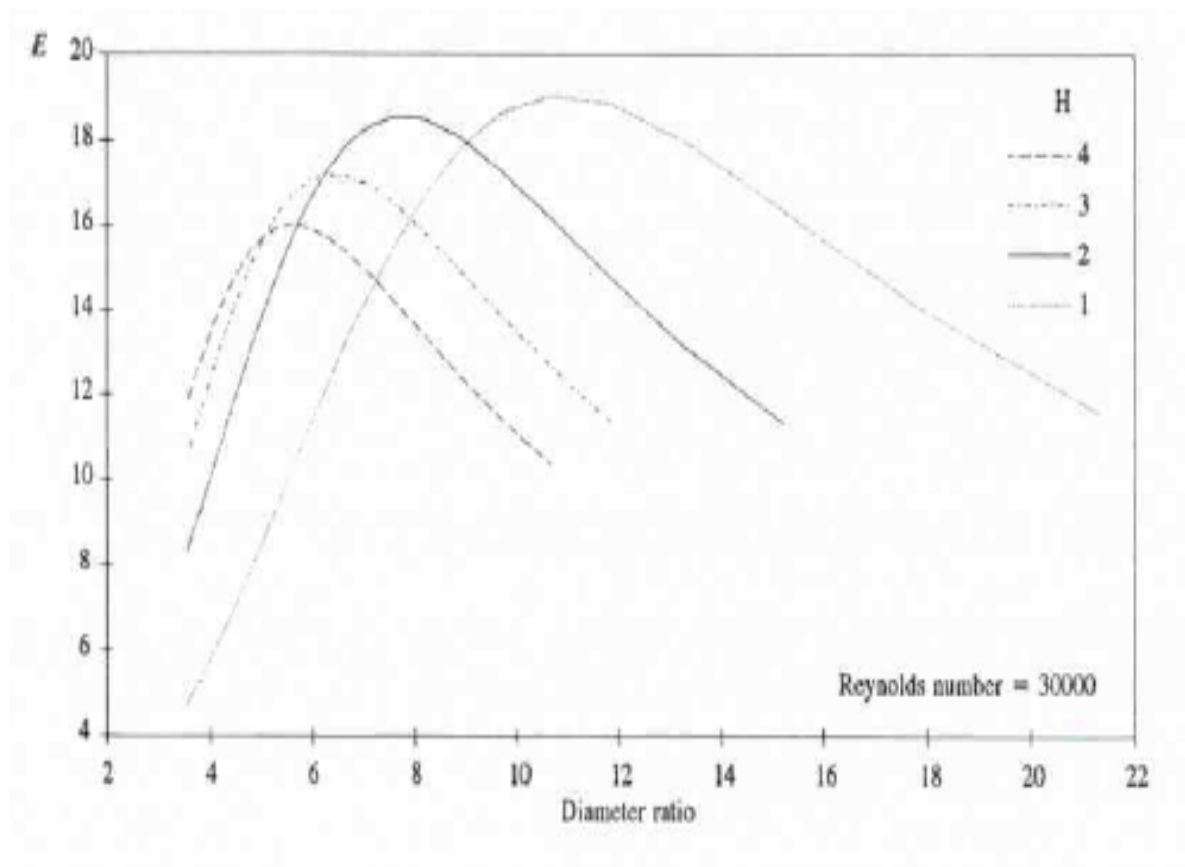


Figure 2.11. - Variation of  $E$  with  $d_c/d_o$  [26].

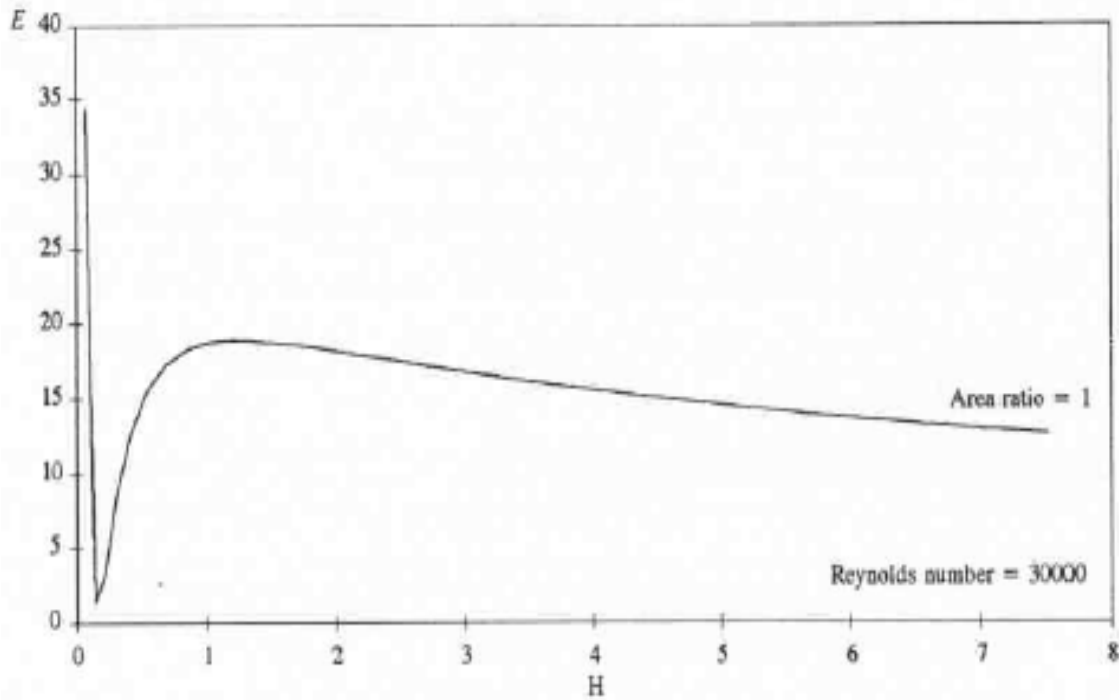


Figure 2.12. - Variation of  $E$  with  $H$  [26].

Table 2.1 shows the geometry used by Ruh Goh in her work. According to the incompressible work for the Switched Vortex Valves, the best performance is achieved with the ratios shown in Table 2.2.

Table 2.1.- Geometry of the SVV used by Ruh Goh for incompressible flow.

Inlet nozzle	
Outlet diameter	15.9, 18.95 mm
Splitter angle (Tangential side) $\theta$	6°
Splitter angle (Radial side) $\alpha$	12°
Height	19.6 mm

Table 2.2. - Geometry ratios yielding the best performance for incompressible flow.

H (height/supply width)	1
$a_s/a_o$ (inlet supply area/outlet area)	1.5
$d_c/d_o$ (chamber diameter/outlet diameter)	11

### 2.2.3 Previous work with Compressible Flow in Switched Vortex Valves.

Early work on Switched Vortex Valves working with compressible flow [36] concentrated on a burst duct protection application which was one of many identified as being promising for a fluidic solution (as shown in the previous Chapter).

The first experiments had shown that the Switched Vortex Valves had useful turndown performance (between 2 and 3, depending on the exact operating conditions).

The experiments were using outlet diffusers or “venturis” with throat bores between 5 and 6 mm. Figure 2.13 and 2.14 presents the flow data as a function of the pressure ratio  $P_s/P_d$ .

The representation of the performance of the Switched Vortex Valve will be explained in detail in Chapter 5.

Experiments with changing single nozzle outlet diameter are shown in Figure 2.15, in which shows the performance of the Switched Vortex Valve with different outlet nozzle diameters (5, 6, 7, 8 and 9 mm), the performance is shown with the discharge coefficient as a function of the pressure ratio  $P_s/P_d$ .

From Figures 2.13 to 2.15, it is clear that a full sensitivity analysis of the performance had not been done; most of the work was to fulfil the operation requirements of the specific application being considered and make the device to work under those conditions.

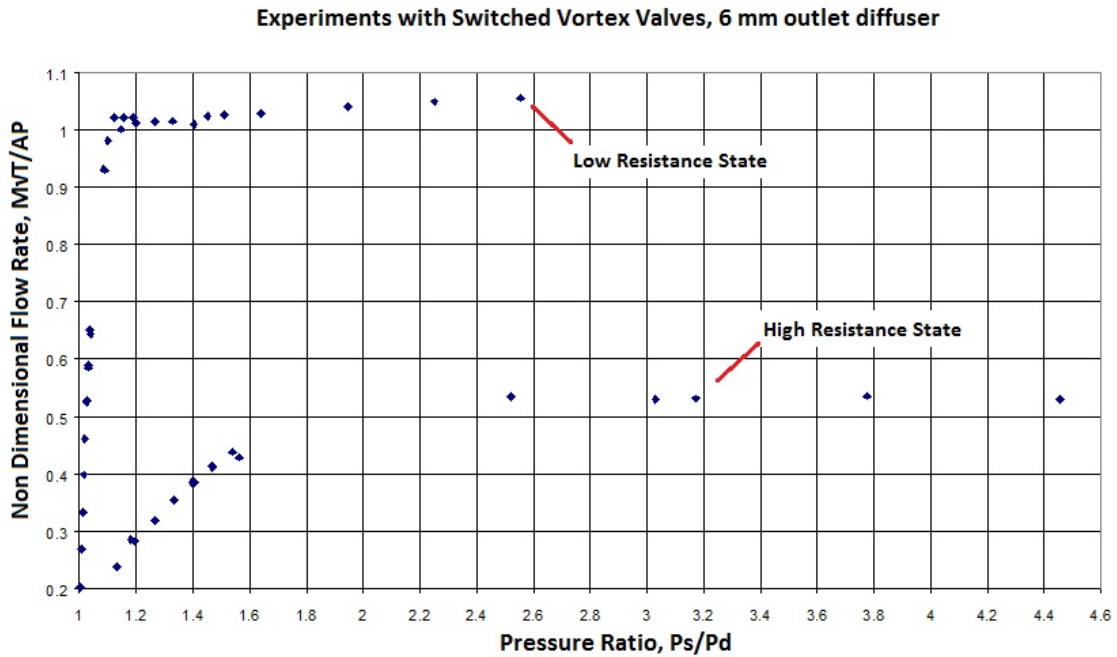


Figure 2.13. -Initial Experiments with Compressible Flow for the Burst Duct Protection Application, 6 mm bore outlet diffuser. Presentation of the performance in terms of the non dimensional flow parameter  $M\sqrt{T}/AP$  [36].

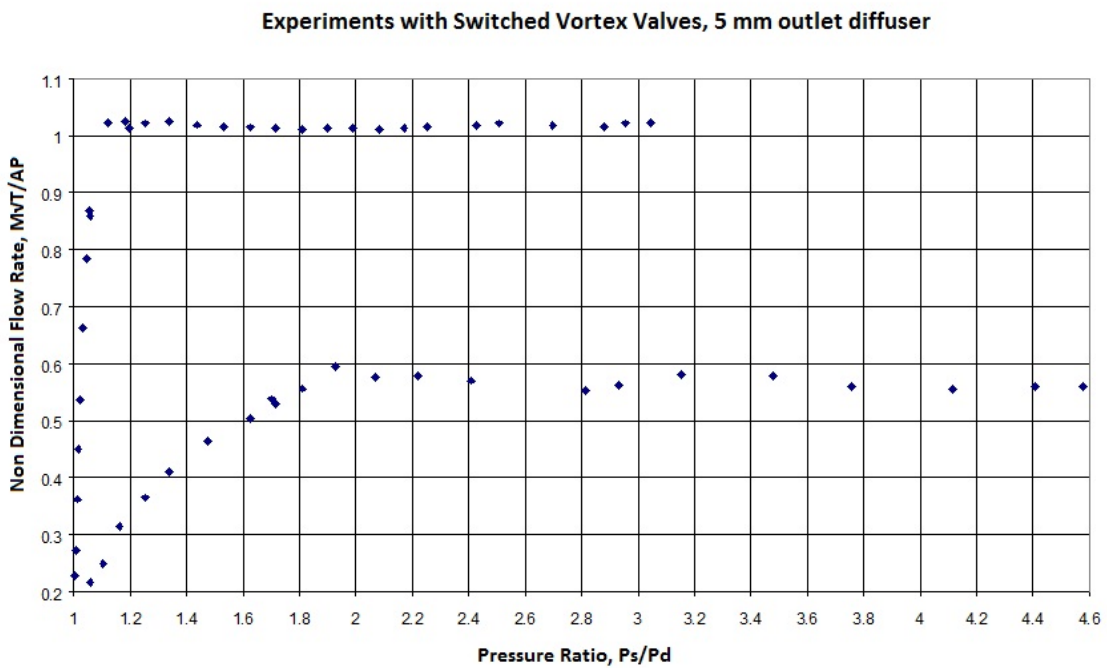


Figure 2.14. - Initial Experiments with Compressible Flow, 5 mm bore outlet diffuser [36].

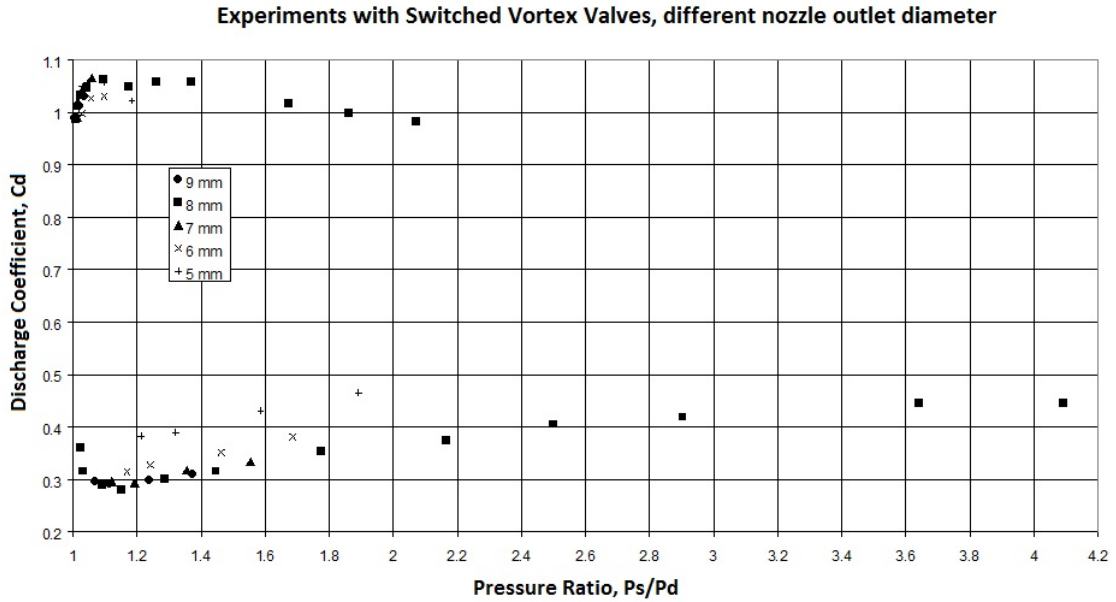


Figure 2.15. - Initial Experiments with Compressible Flow, Different nozzle outlet diameter [36].

Table 2.3 shows the geometry of the Switched Vortex Valve used on previous work with compressible flow.

Table 2.3.- Geometry of the SVV used by Tippetts and Priestman [36] for compressible flow.

Inlet nozzle	4.7 mm
Outlet diameter	5, 6, 7, 8 mm
Vortex Chamber diameter	52 mm
Height	11.7 mm
Control Port width	4.7, 2.35 mm
Splitter angle (Tangential side) $\theta$	6°
Splitter angle (Radial side) $\alpha$	12°

### **2.3 Conclusions.**

Although the Switched Vortex Valves have been around for quite a considerable time, most of the analysis has been done with incompressible fluids and little with multiphase flow. Tippetts and Priestman [36] made some initial experiments regarding a different type of application, also within the Rolls-Royce initiative. The experiments presented a good start point for the optimisation of the Switched Vortex Valves.

It is clear that there is a broad range of applications in which the fluidic devices can be used. Specifically the device used for the burst duct application could be suitable for the problem in hand given that it works with compressible flow and it achieves the pressure ratio needed. As well, from the vortex amplifier literature it can be deduced that the performance of this devices can be greatly improved when the vortex chamber diameter is reduced, thus indicating that by making the device smaller could imply a better performance hence solving both space availability issues and performance issues.

It can be seen from the experimental results and device geometry used it can be seen that the performance it is suitable for the requirements needed for this research. For the compressible flow experiments, the pressure ratio of 2.5 is achieved but the larger device means that it will not fit in the location specified in the engine. So the main thing is to scale down the device as mentioned above, bring the geometry to fit into the space limits while maintaining the performance shown in those experiments, which is mainly implied by the reduction of the vortex chamber diameter.

This work will try first to understand the behaviour of the Switched Vortex Valve by analyzing its different components separately, with emphasis in the Vortex Amplifier. Then the switched vortex valve will be analysed to make sure that the scaled down configuration will work under the engine conditions. The scaled down device will have to show that the pressure ratios are achieved, that the new geometry will fit into the space available and that the overall performance and stability is not endangered by the smaller configuration and extreme conditions, all these with supplying the necessary flow according to the different conditions within the engine.

This work will analyse as well the impact that the splitter and the control ports flow have with the stability and performance of the device given that very little or no work has been done regarding these.

For this work, it is intended to use the set of equations and parameters for performance taking into account the compressibility factors. There will be exploratory experiments to see if some of the parameters within the geometry affect the performance of the device.

The conditions present in the jet engines are quite challenging and the Switched Vortex Valve has to cope with extreme conditions and be capable to work under the set of requirements Rolls-Royce need so this optimisation will be based on the requirements of Rolls-Royce for the particular application of Rim Sealing flow modulation and the final design will be included for testing in the prototype engine that Rolls-Royce is designing.

The experiments will include:

- Performance on different pressure ratios (compressible mass flow rates vs PR).
- Inlet geometries.
- Control Port widths and flows.
- Splitter position (rotational and transitional)
- Vortex Amplifier outlet geometry.

Details of these experiments will be shown in Chapter5.

### **3**

## **COMPRESSIBLE FLOW**

### **3.1 Introduction.**

The work with incompressible flow in which the idealization of constant density was used has been outlined in Chapter 2. The methodology to analyse the compressible flow theory is typical of standard literature and will not be extended in this work.

This Chapter will outline and analyse the compressible flow theory in order to get a more comprehensive and detailed idea of how to apply the theory to the future analysis of the Switched Vortex Valves.

The methodology is based on the literature by Streeter and Wylie[46].

### **3.2 Switched Vortex Valve Analysis.**

To give a full understanding of how the switched vortex valve can be analysed, an overall analysis to the system has to be made and developed.

One of the main purposes of the experiments is to relate the Pressure Ratio and the outlet mass flow rate. These two parameters can be linked with the occurrence of choking, which is defined as the maximum mass flow rate as a function of the absolute pressure ratio across the device..

Reducing the pressure downstream helps the fluid to flow from upstream to downstream of the system at a rate which increases with the pressure drop downstream until the velocity at some point in the system achieves the local sonic velocity.

When the local velocity reaches the sonic velocity at this point, then a choked condition forms, therefore any reductions to the downstream pressure will have no effect on conditions upstream as the fluid information cannot travel upstream. However, this further downstream pressure reductions will increase the pressure ratio. This ratio between the pressure at the choked point in the system to the upstream pressure is known as the critical pressure ratio.

In a conventional De Laval nozzle (isentropic flow), the critical pressure ratio is given by:

$$\frac{p^*}{p_0} = \left( \frac{2}{\gamma + 1} \right)^{\gamma/(\gamma-1)} = 0.528 \quad \text{Eq. (3.1)}$$

In which  $\gamma = 1.4$  for air and  $p^*$  is the critical pressure and  $p_0$  the upstream pressure of the system.

With the isentropic idealisation, the friction effects can be negligible due to the short lengths and the heat transfer can also be neglected given that the changes that a particle suffers are sufficiently low that the gradients of velocity and temperature maintain low.

The mass flow rate for isentropic flow can be expressed as

$$\dot{m} = \rho_0 (\gamma RT_0)^{0.5} A \left\{ \frac{2}{\gamma - 1} \left( \frac{p}{p_0} \right)^{2/\gamma} \left[ 1 - \left( \frac{p}{p_0} \right)^{\gamma-1/\gamma} \right] \right\}^{0.5} \quad \text{Eq. (3.2)}$$

This can be written in terms of the stagnation pressure using  $\rho_0 = p_0/RT_0$  as

$$\dot{m} = \frac{p_0 A}{\sqrt{RT_0}} \left\{ \frac{2}{\gamma - 1} \left( \frac{p}{p_0} \right)^{2/\gamma} \left[ 1 - \left( \frac{p}{p_0} \right)^{\gamma-1/\gamma} \right] \right\}^{0.5} \quad \text{Eq. (3.3)}$$

So isentropic compressible flow rate can be expressed in terms of a non-dimensional mass flow rate

$$\psi = \frac{\dot{m}\sqrt{RT_0}}{p_0 A} \quad \text{Eq. (3.4)}$$

This function depends only on  $\gamma$  and the pressure ratio

$$\psi = f(\gamma, p/p_0) = \left\{ \frac{2}{\gamma-1} \left( \frac{p}{p_0} \right)^{2/\gamma} \left[ 1 - \left( \frac{p}{p_0} \right)^{\gamma-1/\gamma} \right] \right\}^{0.5} \quad \text{Eq. (3.5)}$$

For choked flow, that is when the velocity becomes sonic at the throat

$$\psi^* = \gamma^{0.5} \left( \frac{2}{\gamma-1} \right)^{\frac{\gamma+1}{2(\gamma-1)}} \quad \text{Eq. (3.6)}$$

Non-isentropic flow becomes more involved as a result of frictional effects including shock wave formation.

A simple case is that of a nozzle followed by a duct of constant area, as shown in Fig. 3.1.

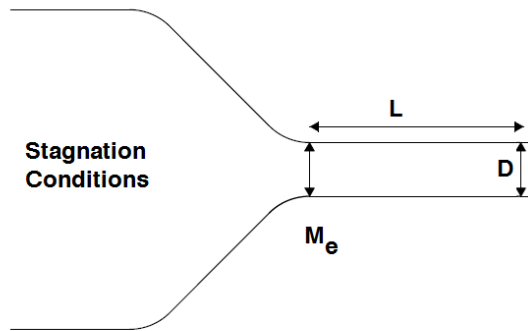


Figure 3.1. - Nozzle followed by a duct.

The case for which the flow is choked at the duct outlet results in

$$\psi = \frac{\dot{m}\sqrt{RT_0}}{p_0 A} = \left( \frac{p}{p_0} \right)^{\frac{\gamma+1}{2\gamma}} \gamma^{0.5} M_e \left\{ \frac{1}{M_e} \left[ \frac{\gamma+1}{2+(\gamma-1)M_e^2} \right]^{0.5} \right\}^{\frac{\gamma+1}{2\gamma}} \quad \text{Eq. (3.7)}$$

Where  $M_e$  is determined from the geometry of the duct and the average Moody friction factor  $\tilde{f}$  in the duct flow

$$\frac{\tilde{f}L}{D} = \frac{1-M_e^2}{\gamma M_e^2} + \frac{\gamma+1}{2\gamma} \ln \left[ \frac{(\gamma+1)M_e^2}{2+(\gamma+1)M_e^2} \right] \quad \text{Eq. (3.8)}$$

Again  $\psi(\gamma, P/p_0)$  for fixed  $L, D, \tilde{f}$ .

### 3.3 Holes in series with compressible flow.

Given that the switched vortex valve has essentially two holes, an inlet nozzle and an outlet, it can be analyzed as a device with two-holes in series.

To specify the area used in the analysis of a two-hole device, the effective geometrical “ideal square-law area” is used, and it states that the effective area or  $A_{eff}$  between two holes is defined as the cross-section that would have the same resistance coefficient in incompressible flow to that of the two restrictions in series without the influence of a vortex. This effective area is given by

$$A_{eff} = \frac{A_s A_o}{\sqrt{A_s^2 + A_o^2}}$$

where  $A_s$  is the area in the inlet nozzle and  $A_o$  is the area of the outlet of the switched vortex valve respectively.

The usefulness of the square-law area becomes handy to analyze the two holes working in series as a hole with the same effective area working with incompressible flow.

The calculations for compressible flow use the isentropic idealization to calculate the flow rate through a series of nozzles; Figure 7.1 shows the circuit analysis.

The mass flow rate for section A denoted by  $\alpha$ , in which  $P_x$  is changing from the maximum constant pressure in the system,  $P_s$ , to the minimum value which is  $P_o$ , in this case to simplify the analysis to be the atmospheric pressure. This is done accordingly to the conditions for each set of pressure ratios ( $P_o/P_x$ ), using the isentropic equations for the corresponding conditions (subcritical or critical).

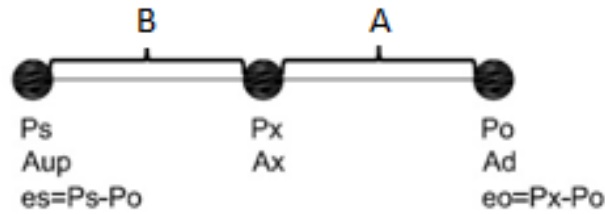


Figure 7.1. - Two-holes in series circuit analysis.

The mass flow rate for section B denoted by  $\beta$ , is calculated in a similar way,  $P_x$  will change from the maximum constant value of  $P_s$  to the minimum value of  $P_o$  and the pressure ratio will change in respect to  $P_x/P_s$ ; in the calculation for section B, it is assumed that  $A_x = 1 \text{ mm}^2$  to simplify the analysis.

The mass flow rates for both sections in the entire analysis have to be calculated using the downstream density which can be said to be constant at the outlet of the device, this to ensure that the two-hole analysis can be compared properly to the incompressible flow analysis.

With the values of  $\alpha$  and  $\beta$ ,  $A_{up}$  can be calculated by

$$A_{up} = \frac{\alpha}{\beta}$$

This area  $A_{up}$  can be used to show the area ratio output as supply/outlet area ratio or *SOAR* which is equivalent to

$$SOAR = \frac{A_{up}}{A_d}$$

This *SOAR* parameter will change accordingly to the range of pressure ratios, having the higher *SOAR* value at the higher pressure ratio achieved for section a.

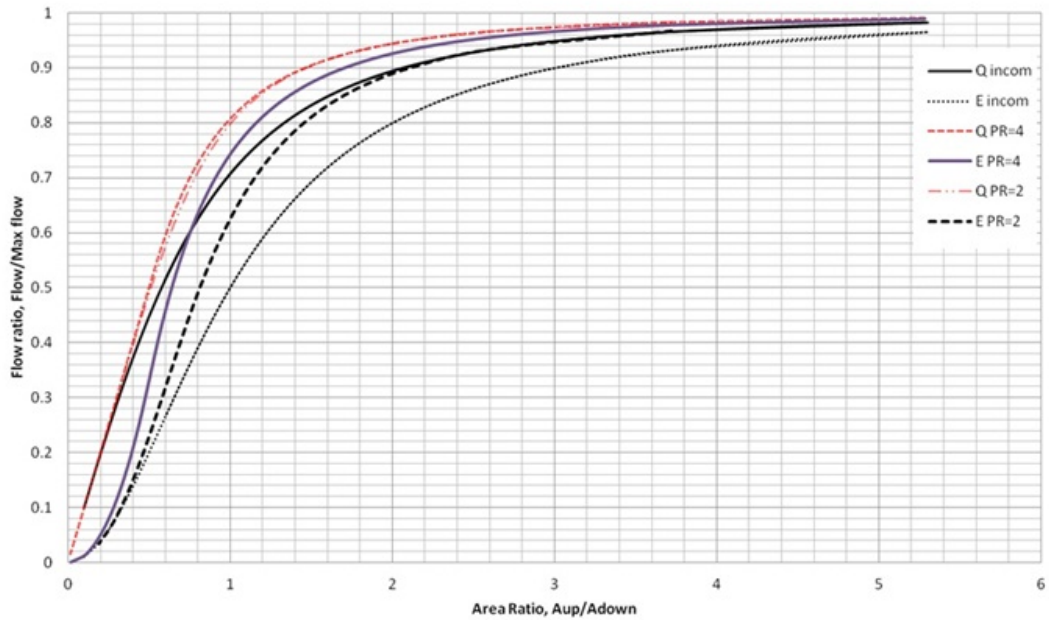
The flow rate ratio will be expressed as the flow rate values of section a divided by the maximum flow rate of that section, which will be at the highest value of  $P_x$ ,

$$Q_r = \frac{\alpha_n}{\alpha_{max}}$$

The  $SOAR$  and  $Q_r$  values can be used to compare the behaviour of the compressible flow through two-holes at a particular overall pressure ratio  $P_s/P_o$  as that of incompressible flow. Figure 7.2(a) shows the change of the flow rate ratio as a function of the area ratio  $A_{up}/A_d$  for both incompressible flow and compressible flow at different values of overall pressure ratios  $P_s/P_o$ . It is of interest to state that the compressible flow rate ratio curves at different overall pressure ratios will converge at an overall pressure ratio value of 2.628. This analysis then can be used to compare the compressible flow theory to that of the incompressible flow assuming flow through two-holes with a constant effective area of  $A_{eff}$ . Figure 7.2(b) shows the flow rate ratio between incompressible flow to compressible flow through the same constant effective area, and it can be seen that the square-law is correct to within 3% of the incompressible flow up to the overall pressure ratio of 2.628; beyond this point, the square-law fails to converge the incompressible and compressible flow theories due to the compressibility effects.

This analysis confirms that the  $A_{eff}$  parameter can be used to analyse the SVV as a two-hole device and it can be compared to the incompressible flow theory up to an overall pressure ratio of 2.628, so it can then be used in the non-dimensional parameter  $\psi$  to calculate the isentropic mass flow rate through the device.

**Flow ratio, Flow/Max Flow, Incompressible and Compressible flow at different PR**



**Flow ratio Incompressible/Compressible with same effective area**

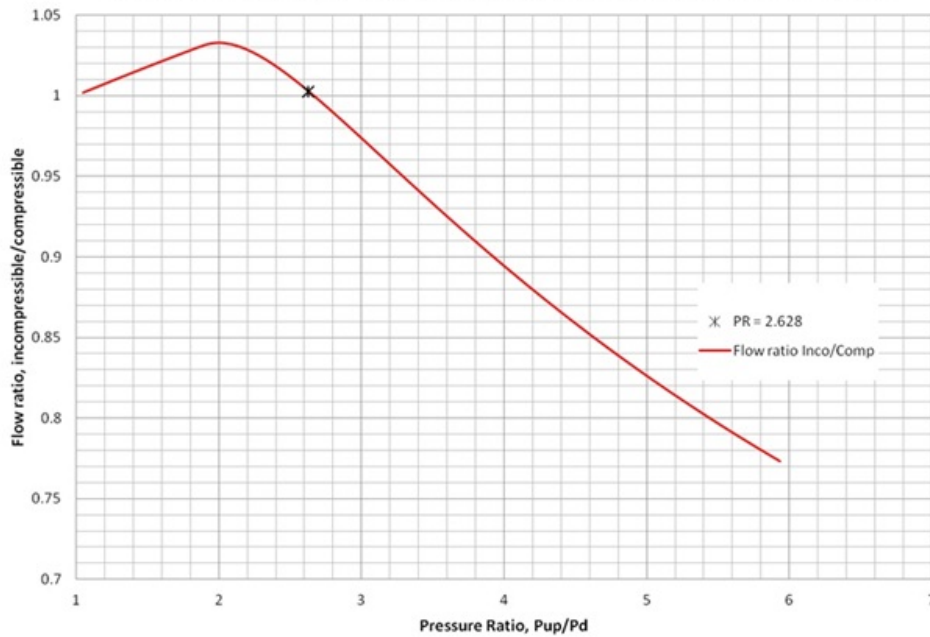


Figure 7.2. - (a) Flow rate curves of incompressible flow and compressible flow at different overall pressure ratios and different area ratio  $A_{up}/A_d$ . (b) Flow rate between incompressible flow and compressible flow at the same constant effective area.

### 3.4 Vortex Theory.

A lot of analysis has been made for compressible vortex flow, either analytical or numerical [42] but the mathematical models for circular flows can be based on a combination of forced vortex, free vortex and sink flows. A confined vortex flow is assumed to be a forced vortex existing within the chamber exit radius in which the fluid rotates as a solid body, driven by a surrounding free vortex.

The radial pressure gradient is given by

$$\frac{\partial p}{\partial r} = \rho \frac{u_{\theta}^2}{r} \quad \text{Eq. (3.9)}$$

where  $u_{\theta}$  is the tangential velocity component at radius  $r$ . The maximum tangential velocity occurs at the point of transition from the free to the forced vortex known as “Rankine vortex”.

The free vortex flow in the vortex chamber can be represented for a viscous and variable density flow by the Navier-Stokes equation of motion:

$$\rho \frac{DU}{Dt} = \rho g - \bar{V} p + \mu \bar{V}^2 U + \frac{1}{3} \mu \bar{V} (\bar{V} U) \quad \text{Eq. (3.10)}$$

If this equation is represented in cylindrical coordinates,  $r, \theta, z$  and the assumption that the flow is frictionless and steady is made, then it reduces to

$$u_r \frac{\partial u_r}{\partial r} - \frac{u_{\theta}^2}{r} = -\frac{1}{\rho} \frac{\partial p}{\partial r} \quad \text{Eq. (3.11)}$$

from which the tangential velocity in the vortex may be found if the distribution of density  $\rho$ , radial velocity  $u_r$  and static pressure  $p$  are known.

### 3.5 Dynamic and Geometric Similarity.

In fluid dynamics it is always desirable to find the relation between the flow patterns around geometrically similar bodies. That is, to deduce the results for a full-scale body from the test model. The problem is to determine the conditions under which

the forms of flows around geometrically similar bodies are themselves geometrically similar. Such similarity of flow is known as dynamic similarity[19].

In this particular work, we will be testing some devices that should be able to be scaled down and have the same performances as the test devices. So, the dynamic similarity is highly important.

The dynamic similarity may be attained if the different kinds of forces acting at every point of similar positions in the two flow fields on volume elements at this points have the same ratio. There are some non-dimensional parameters which characterize the dynamic similarity of the important forces for a given problem may be obtained from the fundamental equations. Here are the most important dimensionless parameters:

- a) Mach number  $M$ . This is a measure of the compressibility of the fluid due to a high flow speed and is defined as

$$\text{MachNumber} = M = \frac{\text{velocity}}{\text{speed of sound}} = \frac{V}{v_s} = \frac{V}{(\gamma RT)^{0.5}}$$

Where,  $\gamma$  is the ratio of specific heats,  $R$  is the gas constant and  $T$  is the static temperature.

For a very small Mach number, the variation of density, i.e., the compressibility effect, due to the variation of velocity of the flow field is negligible and the fluid may be considered to be incompressible. For large Mach numbers, the effect of compressibility must be considered. The Mach number indicates the importance of inertia to thermal forces; that is, the ratio of the fluid mean motion relative to its molecular activity.

- b) Reynolds Number  $Re$ . This is the most important parameter for the fluid dynamics of a viscous fluid and is defined as follows:

$$\text{ReynoldsNumber} = Re = \frac{\rho VD}{\mu} = \frac{VD}{\nu} = \frac{mD}{A\mu}$$

where  $\mu$  is the coefficient of viscosity, and  $\nu = \frac{\mu}{\rho}$  is the coefficient of kinematic viscosity,  $A$  is the area where the flow is passing, and  $m$  is the mass flow. The

Reynolds number is a measure of the ratio of inertial force to viscous force. When the Reynolds number of a system is small, the viscous force is predominant and the effect of viscosity is important in the whole field. When the Reynolds number is large, the inertial force is predominant and the effect of viscosity is important only in the narrow boundary-layer region near the solid boundary or in any other region of large variation in velocity.

To attain the dynamic similarity between a prototype and a scaled model, these two parameters have to be matched in every point of both of the flow fields.

The geometric similarity is attained when all the ratios between the geometry of the prototype and the scaled model are kept the same. Of course, according to the Reynolds number, if the area of the channel in which the flow is passing through is changed, the Reynolds number will change too. In this case, due to the high velocities and Reynolds numbers that are present in the devices, the viscous effects can be negligible for the study of this type of devices. Therefore, by matching the Mach number and maintaining a high Reynolds number in the prototype and the scaled model, the dynamic similarity could be attained.

### **3.6 Conclusions.**

The compressible flow theory and the isentropic idealization can be used to the analysis of the Switched Vortex Valves.

It is clear with this analysis that the compressibility effects are clearly stated and as will be shown later in this work it is a good way to represent the behaviour of the Switched Vortex Valve in which the compressibility effects will be clearly visible.

The pressure ratio is of importance given that the pressure in the engine are high and cannot be recreated in the laboratory without expensive equipment and exhaustive safety features, thus the pressure ratio becomes a fundamental

parameter in which the device can be tested at the same pressure ratios as in the engine with relatively low pressures.

The specific analysis for the Switched Vortex Valve working with compressible flow will be detailed in Chapter 5 and will use some equations detailed in this Chapter.

## 4

### VORTEX THROTTLE

#### 4.1 Introduction.

For a Vortex Throttle, the flow entering the device through the tangential port sets up a vortex and establishes a large pressure drop across the device. The flow in vortex throttles can be classified as confined vortex flows. The performance of these devices is largely dominated by the confined turbulent vortex due to the tangentially entering fluid.

The experiments with the Vortex Throttle will focus on the performance and effect of the axial outlet diameter, changing the geometry ratio between the vortex chamber and the axial outlet and on the Reynolds effects on the vortex strength.

A series of generic tests were done on Reynolds effects on the vortex strength. Over a certain range of Reynolds number, the discharge coefficient drops due to the strengthening of the vortex, however, the interest in this work is at higher values of  $Re$ .

The objective is to find what could be expected to be the best possible throttling performance for a Switched Vortex Valve. For a Vortex Amplifier, which will be detailed in Chapter 6, it seems unlikely that a practical Vortex Amplifier could surpass the performance of a Vortex Throttle because the supply flow entry must

always cause some degradation of the vortex flow. So the data obtained could represent the upper performance limit for Vortex Amplifiers.

The basic throttle is shown in Figure 4.1, pressure drop and flow were measured for the Vortex Throttle with various sizes of outlets and tangential ports (fitting some inserts). Results were processed in terms of the diameter ratio  $D$  (chamber diameter/outlet hole diameter) and outlet/tangential nozzle area ratio or  $D_{ot}$ . Performance factors were derived from a theoretical pressure at the periphery of the vortex chamber  $P_p$ , total pressure drop and theoretical pressure drop through the outlet and tangential port with non swirling flow. From this, several Vortex Amplifier performance related parameters can be calculated, and will be detailed again in Chapter 6 but only mentioned here:

- a) Theoretical turndown ratio (Theoretical non swirling flow/experimental flow at same pressure ratio)
- b) Theoretical G.
- c) Vortex strength merit M (Total pressure drop divided by theoretical non-swirling flow pressure drop through the tangential nozzle and the outlet nozzle)

The M factor is indicative of diodicity because the two pressure drops relate to the vortex and the non-vortex throughflow.

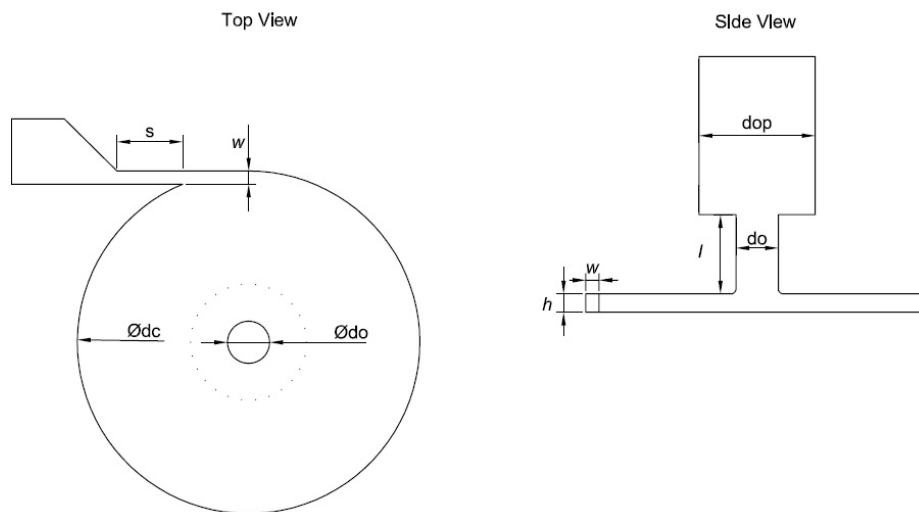


Figure 4.1. - Basic design of Vortex Throttle.

From Priestman and Yang [47] it has been found that the pressure drop across the vortex throttles occurs through the axial throttling port by the dissipation of the high tangential velocity.

From Vatistas [39] it is found that stronger vortices will be produced by increasing the diameter ratio and/or Reynolds number, resulting in a higher tangential velocity and hence a higher pressure drop.

For the purpose of this work, it is considered that two main geometry parameters will have a high impact on the performance of the vortex amplifier, the first being the diameter ratio, and the second one being the outlet to tangential inlet ratio ( $D_{ot}$ ).

Changes in the outlet bore and inlet area were planned in order to find a peak performance range in which the vortex amplifier can work at its best within these configurations.

## **4.2 Experimental Procedure.**

To test the Vortex Throttle, the rig consists of one inlet and one outlet, upstream and downstream of the device respectively.

The inlet part of the device consists of a supply of pressurized air connected to a calibrated rotameter and this connected to the tangential control port of the device.

The outlet part of the device consists of a rotameter connected to the outlet of the device.

Both, inlet and outlet have pressure gauges to measure the static pressure at any given time.

The rig is shown in Figure 4.2

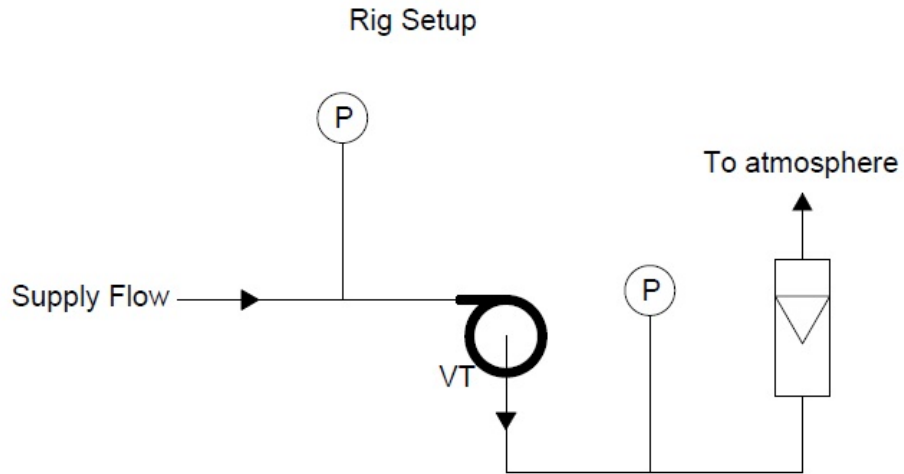


Figure 4.2. - Experimental Setup for the Vortex Throttle.

### 4.3 Experimental Results.

#### 4.3.1 Reynolds Number.

For the throttle data, the Reynolds number was notionally based on the tangential or control nozzle flow and calculated using the vortex chamber height.

Figure 4.3 shows some data for the M factor for the maximum control port width (18.8 mm) and for three outlet nozzle bores.

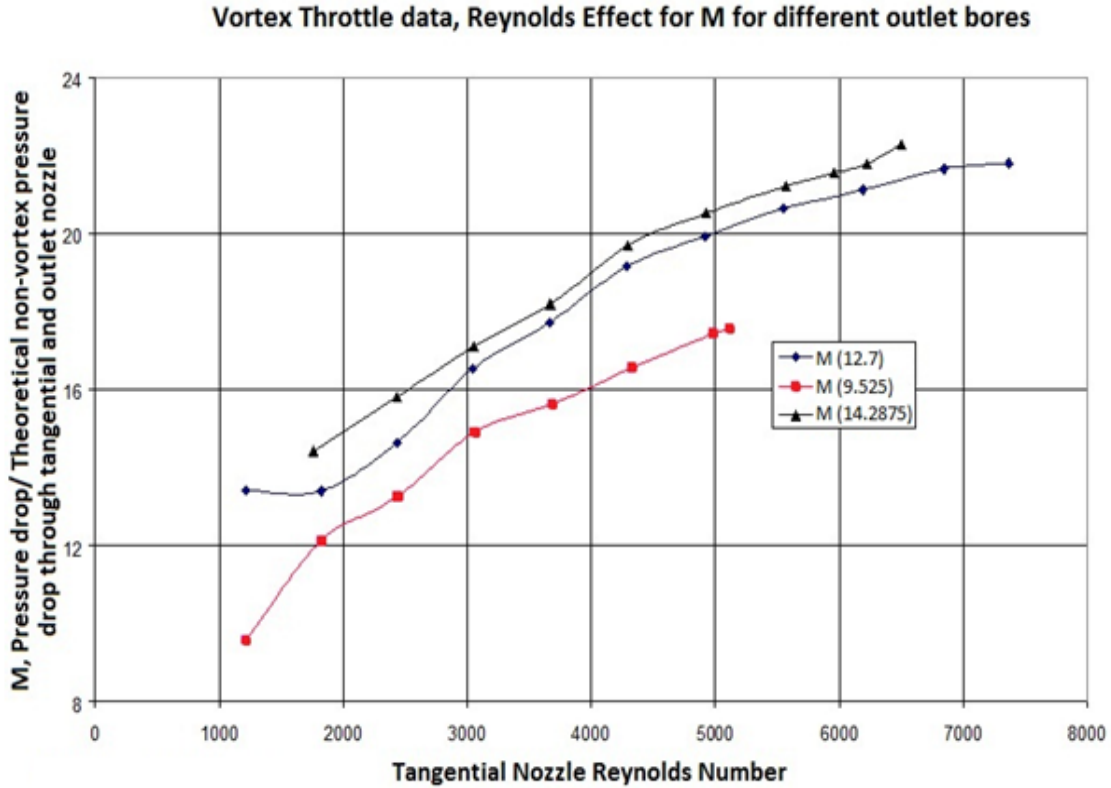


Figure 4.3. - Vortex Throttle data, Reynolds Effect for M for different outlet bores.

#### 4.3.2 Pressure Drop and Diameter Ratio.

The results show the flow rate as a function of the pressure drop across the device. For a Vortex Throttle, it is expected that as the flow rate increases the pressure drop also increases in a similar way to the flow rate; this behaviour is shown in Figure 4.4.

It is also clear that as the outlet diameter or bore increases, the flow rate through the device does also, this is due to the increased area in which the flow can pass through. The increased outlet area helps the device to dissipate the turbulent kinetic energy by dissipating the tangential velocity. So it can be said that the pressure drop increases as the tangential flow and velocity increases, and the outlet diameter will have an effect in the flow rate permitted through the device, increasing as the pressure drop does.

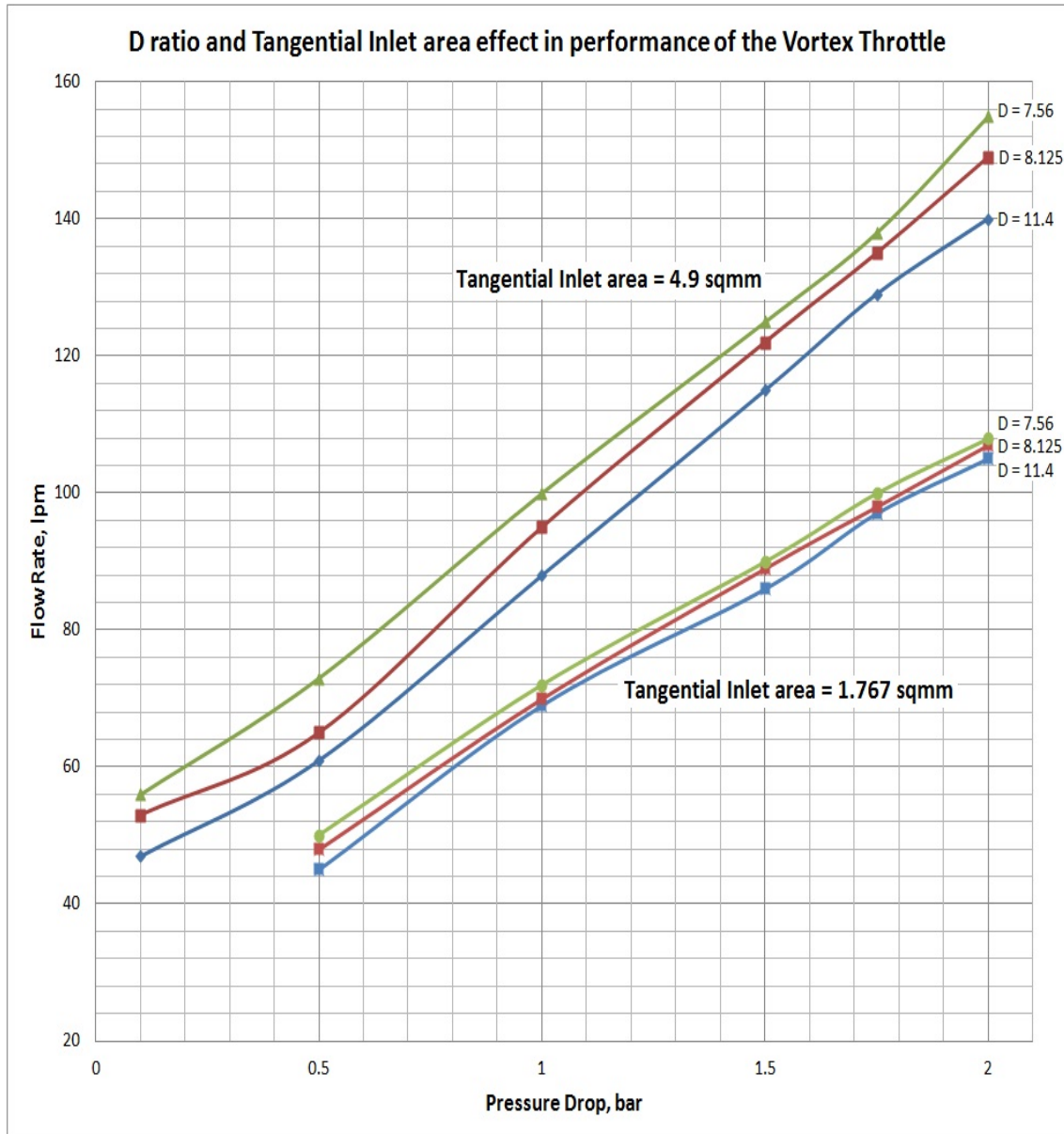


Figure 4.4. - D ratio ( $d_c/d_o$ ) and Tangential Inlet Area Effect in Performance of the Vortex Throttle.

From previous experiments [33] different data was gathered with a 25 mm diameter vortex chamber Vortex Throttle, and different outlet diameters were tested and comparing Figure 4.4 and 4.5 similar behaviour can be seen as increasing the outlet diameter of the device.

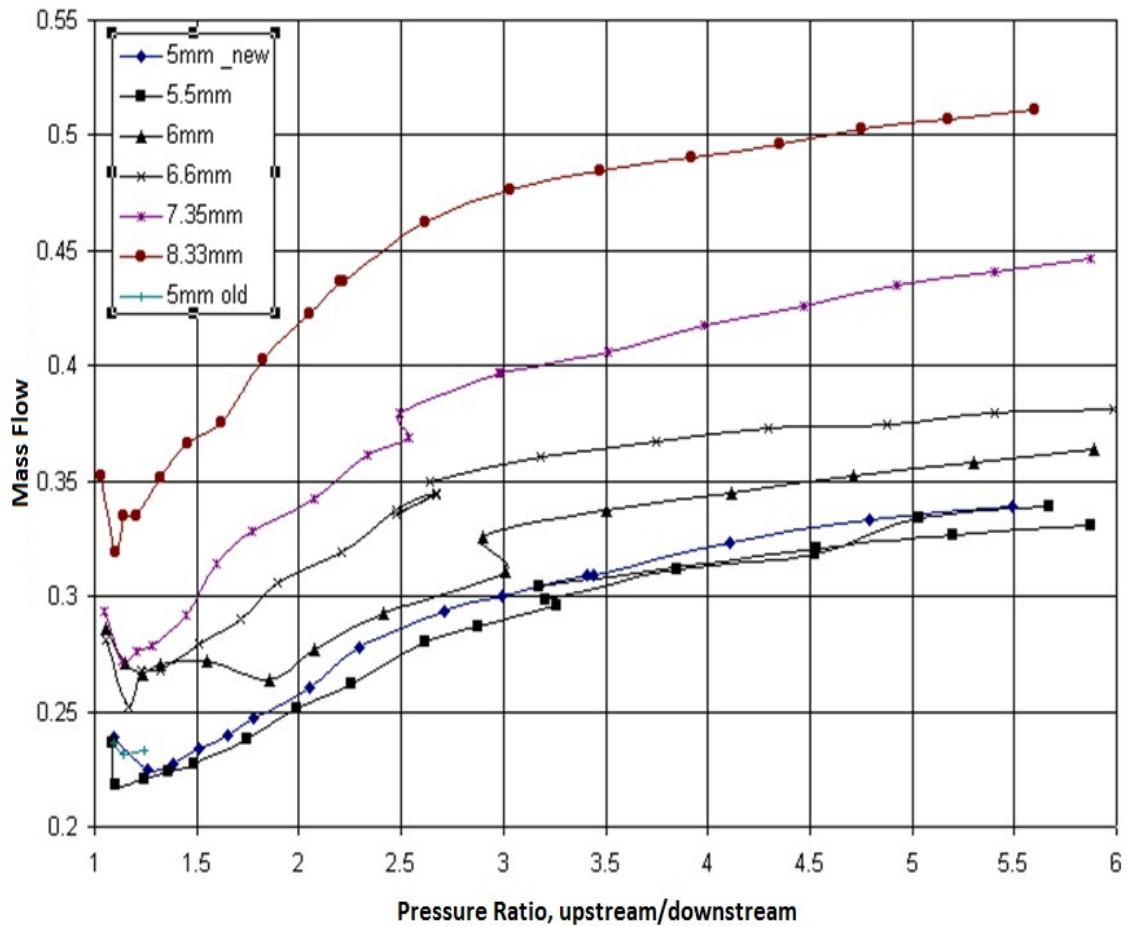


Figure 4.5. - Performance of a 25 mm vortex chamber Vortex Throttle.

Some other selected results are present in Table 4.1, which shows various characterising ratios for design and performance for a range of outlet sizes and tangential port sizes.  $D$  ratio and outlet/tangential area ratio characterise these. The data is organised in terms of ascending turndown ratio.

From Figure 4.6 it can be seen that high turndown ratio values tend to be associated with smaller diameter ratios. It can be seen also that the highest diodicity factor occurs with the outlet/tangential area ratio being almost 1.

Table 4.1. - Vortex Throttle, selected results sorted by the Turndown Ratio, T.

<b>D</b>	$D_{ot}$	<b>T</b>	<b>M</b>	<b>Re</b>
20.2	0.5	3.2	7.9	9707
20.0	0.4	3.3	8.6	7974
13.3	0.6	4.8	17.6	5114
13.2	0.9	5.2	12.2	12045
13.2	1.1	5.2	10.1	14699
10.0	1.0	6.8	22.3	6502
10.1	1.6	7.0	10.9	13922
10.1	1.9	7.2	9.5	17041
8.9	1.4	7.3	14.1	12906
8.9	1.4	7.7	21.8	7370
8.8	2.0	7.9	9.5	13744
8.8	2.5	8.2	8.2	19525
7.1	3.3	10.2	7.5	20012
6.4	4.0	11.6	6.5	19846
5.8	4.9	11.7	4.8	19544
5.8	5.9	12.1	3.8	21342

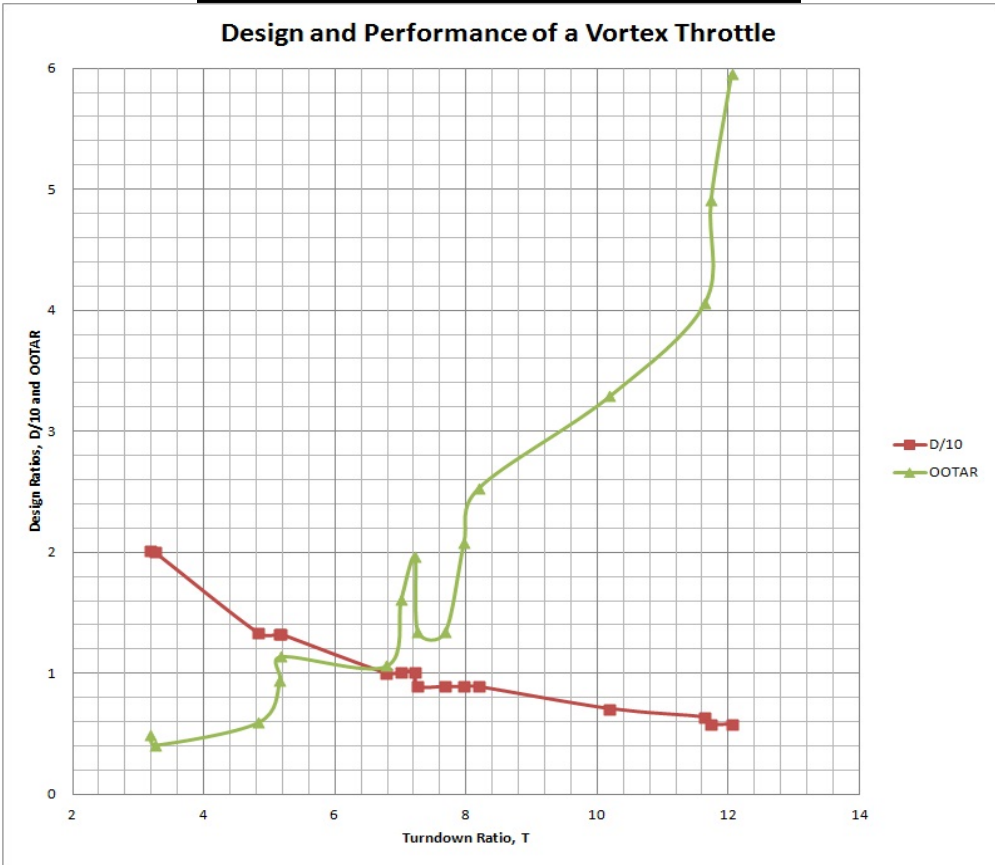


Figure 4.6. -Selected Results of D/10 and  $D_{ot}$  Parameters as functions of Turndown Ratio, T.

### 4.3.3 Performance comparison, Euler number vs. Reynolds number.

As mentioned in Chapter 2, the performance of the Vortex Throttle is often represented by the Euler number calculated on the fluid density and velocity at the tangential port.

Figure 4.7 shows the variation of Eu with Re for new data obtained using the same geometry as in Priestman's work and compared with some selected results for air [20] with the geometry of used in the experiments shown in Table 4.2.

Table 4.2. - Details of throttle dimensions tested in Priestman's study.

<i>dc</i>	<i>h</i>	<i>w</i>	<i>do</i>	<i>l</i>
102	13.12	10.05	12.75	13
76	13.12	10.2	12.85	13

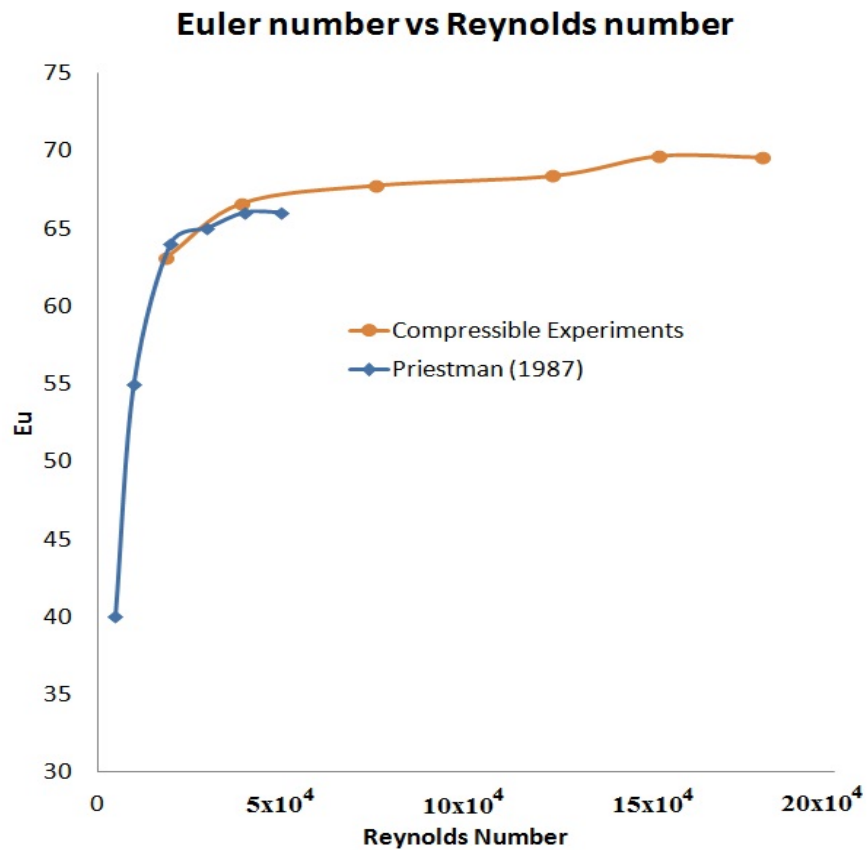


Figure 4.7. – Variation of Eu with Re comparison between current data and Priestman's [20].

From Figure 4.7, it can be seen that the results from the compressible flow yield slightly better performance, increasing as the tangential velocity increases. Here it can be seen that the Eu numbers reached were almost identical to the maximum values of 66 found by Priestman.

This is as expected, given that increasing the tangential velocity will increase the pressure drop across the device, thus increasing the performance. A CFD model can be useful to give better understanding as it can give insight into the behaviour of the internal flow within the vortex throttle and it can give basic parameters and understanding of the use of different models to start a CFD model for a full SVV.

It is of great importance to have the actual fluidic device manufactured to test the real performance of it, but the CFD can give accurate results without the need of spending in manufacture. The CFD model can be tweaked and fine tuned until the desired performance is achieved and then manufacture a live test piece to correlate experimental data vs modelling.

#### **4.4 CFD Modelling of a Vortex Throttle.**

##### **4.4.1 Introduction**

The analytical analysis of vortex throttle is complex, due to the complicated flow fields present in the devices, unknown boundary conditions and high non-linearity of the Navier-Stokes equations. However, closed-form solutions for vortex flows can be obtained by numerical methods used in computational fluid dynamics.

For strongly swirling incompressible turbulent flow, the most difficult problem to deal with is the turbulence modelling. Several models can be used to tackle this problem, such as the standard  $\kappa - \varepsilon$  model, the Reynolds Stress Model or RSM, and the Shear Stress Transport or SST  $\kappa - \omega$  model[3]. Work with incompressible fluids and compressible fluids at low pressures with different models has been made, and there is barely any difference between one model to another[47], in this case the standard  $\kappa - \varepsilon$ , the realizable  $\kappa - \varepsilon$ , and the RSM will be used in the present study.

The study will be done with compressible flow, although the velocities in the device are not expected to exceed the Mach number. The purpose of this study is to provide further internal flow modelling of the vortex throttles through which better understanding of the complicated flow fields can be achieved.

#### 4.4.2 Mathematical Formulation

As mentioned above, the equations employed to describe the flow field in the vortex throttles are the time-averaged Navier-Stokes equations and the continuity equation in the cylindrical coordinate system. The Navier-Stokes equations introduce six unknowns, called Reynolds stresses; a turbulence model is required to approximate these unknowns. The general equations can be found in any work regarding CFD theory, so most of them are not shown here.

##### 4.4.2.1 Standard $\kappa - \varepsilon$ .

The standard  $\kappa - \varepsilon$  model is one of the most common turbulence models[28]. It is a two equation model, so it includes two extra transport equations to represent the turbulent properties of the flow. This allows to account for effects like convection and diffusion of turbulent energy.

The first transported variable is turbulent kinetic energy,  $\kappa$  which determines the energy in the turbulence. The second transported variable in this case is the turbulent dissipation,  $\varepsilon$  which determines the scale of the turbulence.

The transport equations for  $k$  and  $\varepsilon$  are as follows

$$\begin{aligned} \frac{\partial}{\partial x}(\rho U k) + \frac{1}{r} \frac{\partial}{\partial r}(r \rho V k) \\ = \frac{\partial}{\partial x} \left\{ \left( \mu + \frac{\mu_t}{Pr_k} \right) \frac{\partial k}{\partial x} \right\} + \frac{1}{r} \frac{\partial}{\partial r} \left\{ r \left( \mu + \frac{\mu_t}{Pr_k} \right) \frac{\partial k}{\partial r} \right\} + G_k - \rho \varepsilon \end{aligned} \quad \text{Eq. (4.1)}$$

$$\begin{aligned} \frac{\partial}{\partial x}(\rho U \varepsilon) + \frac{1}{r} \frac{\partial}{\partial r}(r \rho V \varepsilon) \\ = \frac{\partial}{\partial x} \left\{ \left( \mu + \frac{\mu_t}{Pr_\varepsilon} \right) \frac{\partial \varepsilon}{\partial x} \right\} + \frac{1}{r} \frac{\partial}{\partial r} \left\{ r \left( \mu + \frac{\mu_t}{Pr_\varepsilon} \right) \frac{\partial \varepsilon}{\partial r} \right\} \\ + \frac{\varepsilon}{k} (C_{\varepsilon 1} G_k - C_{\varepsilon 2} \rho \varepsilon) \end{aligned} \quad \text{Eq. (4.2)}$$

$$G_k = \mu_t \left[ 2 \left\{ \left( \frac{\partial U}{\partial x} \right)^2 + \left( \frac{\partial V}{\partial r} \right)^2 + \left( \frac{V}{r} \right)^2 \right\} + \left( \frac{\partial U}{\partial r} + \frac{\partial V}{\partial x} \right)^2 + \left( \frac{\partial W}{\partial x} \right)^2 + \left\{ r \frac{\partial}{\partial r} \left( \frac{W}{r} \right) \right\}^2 \right] \quad \text{Eq. (4.3)}$$

where  $G_k$  represents the generation of turbulent kinetic energy that arises due to mean velocity gradients.

$C_{\varepsilon 1}$ ,  $C_{\varepsilon 2}$  and  $C_\mu$  are constants that have been determined experimentally and are taken to have the following values,

$$C_{\varepsilon 1} = 1.44, C_{\varepsilon 2} = 1.92, C_\mu = 0.09$$

$Pr_k$  and  $Pr_\varepsilon$  are turbulent Prandtl numbers for the turbulent kinetic energy and its dissipation rate. These have also been derived experimentally and are defined as follows,

$$Pr_k = 1.0, Pr_\varepsilon = 1.3$$

#### 4.4.2.2 Realizable $\kappa - \varepsilon$ .

The Realizable model features two main differences from the standard  $\kappa - \varepsilon$  model. It uses a new equation for the turbulent viscosity and the dissipation rate transport equation has been derived from the equation for the transport of the mean-square vorticity fluctuation. The form of the eddy viscosity (turbulent) equations is based on the realizability constraints; the positivity of normal Reynolds stresses and Schwarz' inequality for turbulent shear stresses, i.e. certain mathematical constraints on the normal stresses are satisfied.

This is not satisfied by the standard  $\kappa - \varepsilon$  model which makes the realizable model more precise than the standard  $\kappa - \varepsilon$  model at predicting flows such as separated flows and flows with complex secondary flow features.

In terms of changes, the transport equations become:

$$\frac{\partial}{\partial t} (\rho k) + \frac{\partial}{\partial x_j} (\rho k u_j) = \frac{\partial}{\partial x_j} \left\{ \left( \mu + \frac{\mu_t}{\sigma_k} \right) \frac{\partial k}{\partial x_j} \right\} + G_k + G_b - \rho \varepsilon - Y_M + S_k \quad \text{Eq. (4.4)}$$

$$\frac{\partial}{\partial t} (\rho \varepsilon) + \frac{\partial}{\partial x_j} (\rho \varepsilon u_j) = \frac{\partial}{\partial x_j} \left\{ \left( \mu + \frac{\mu_t}{\sigma_\varepsilon} \right) \frac{\partial \varepsilon}{\partial x_j} \right\} + \rho C_1 S \varepsilon - \rho C_2 \frac{\varepsilon^2}{k + \sqrt{v \varepsilon}} + C_{\varepsilon 1} \frac{\varepsilon}{k} C_{\varepsilon 3} G_b + S_\varepsilon \quad \text{Eq. (4.5)}$$

where  $G_k$  represents the generation of turbulent kinetic energy that arises due to mean velocity gradients,  $G_b$  is generation of turbulent kinetic energy that arises due to buoyancy, and  $Y_M$  represents the fluctuating dilation in compressible turbulence that contributes to the overall dissipation rate.  $S_k$  and  $S_\varepsilon$  are source terms defined by the user.

The constants  $C_{\varepsilon 1}$ ,  $C_2$ ,  $\sigma_k$ , and  $\sigma_\varepsilon$  have been determined by Shih [29] and are defined as follows,

$$C_{\varepsilon 1} = 1.44, C_2 = 1.9, \sigma_k = 1.0, \sigma_\varepsilon = 1.2$$

#### 4.4.2.3 Reynolds Stress Model (RSM).

The RSM closes the Reynolds-averaged Navier-Stokes equations by solving transport equations for the Reynolds stresses, together with an equation for the dissipation rate. This means that five additional transport equations are required in 2D flows and seven additional transport equations must be solved in 3D.

For this model, the Reynolds stresses are directly computed by their transport equations, and the isotropic eddy viscosity assumption (Boussinesq hypothesis) is no longer used:

$$\begin{aligned} \frac{\partial}{\partial x_k} (\rho u_k \overline{u'_i u'_j}) &= \frac{\partial}{\partial x_k} \left( \frac{\mu_t}{\sigma_k} \frac{\partial \overline{u'_i u'_j}}{\partial x_k} \right) + \frac{\partial}{\partial x_k} \left\{ \mu \frac{\partial}{\partial x_k} (\overline{u'_i u'_j}) \right\} - \rho \left( \overline{u'_i u'_j} \frac{\partial u_j}{\partial x_k} + \overline{u'_i u'_j} \frac{\partial u_i}{\partial x_k} \right) \\ &+ \Phi_{ij} - \frac{2}{3} \delta_{ij} \rho \varepsilon \end{aligned} \quad \text{Eq. (4.6)}$$

where the term on the left hand side of equation 5.14 represents the convection, the terms on the right hand side represent the turbulent diffusion as proposed by Lien and Leschziner [14], molecular diffusion, stress production, pressure strain, and the dissipation, respectively.

Since the Reynolds stress model accounts for the effects of streamline curvature, swirl, rotation, and rapid changes in strain rate in a more rigorous manner than the two equation models, it has greater potential to give accurate predictions for

complex flows. However, the fidelity of RSM predictions is still limited by the closure assumptions employed to model various terms in the exact transport equations for the Reynolds stresses. The modelling of the pressure strain and dissipation rate terms is particularly challenging, and often considered to be responsible for compromising the accuracy of RSM predictions. The use of RSM is greatly implemented in cyclone flows, high swirling flows, rotating flow passages and stress-induced secondary flows in ducts.

#### 4.4.3 Numerical Setup

The software used is ANSYS 13.0, which has the Design Modeller software, the Meshing software and the FLUENT package built in.

For the mesh, the size function used was 'Proximity and Curvature' which helps to increase the number of cells close to the walls, tangential port and specially where the axial outlet meets the vortex chamber, with an active assembly of the initial size seed, medium smoothing to lower the computational power needed. The total number of mesh elements is 273,058 with 58,194 nodes.

In this study the pressure in the inlet and the outlet are known, the no-slip condition is applied at the solid walls, which means that the velocity of the fluid at the wall should be the same as that of the wall, and given the walls in this study are fixed, the velocities at the walls are specified to be zero.

Boundary conditions are specified in order to solve the finite difference equations.

The turbulence intensity and turbulence length are the input values to derive the turbulence dissipation rate  $\varepsilon$ . The turbulence intensity can be estimated from the following formula derived from an empirical correlation for pipe flows [38]

$$I = \frac{u'}{V_{avg}} = 0.16(\text{Re}_o)^{-1/8} \quad \text{Eq. (4.7)}$$

The turbulence length scale  $l$  is a physical quantity related to the size of the large eddies that contain the energy in turbulent flows. An approximate relationship between  $l$  and the physical size of the vortex chamber diameter  $D_c$  is

$$l = 0.07D_c \quad \text{Eq. (4.8)}$$

The relationship between the turbulent kinetic energy  $k$  and turbulence intensity  $I$  is

$$k = \frac{3}{2}(V_{avg}I)^2 \quad \text{Eq. (4.9)}$$

where  $V_{avg}$  is the average axial velocity. The turbulence dissipation rate  $\varepsilon$  can be determined as

$$\varepsilon = C_\mu^{3/4} \frac{k^{3/2}}{l} \quad \text{Eq. (4.10)}$$

The values of the Reynolds stresses explicitly at the inlet are given by

$$\overline{u'_i u'_j} = 0 \text{ and } \overline{u'_i{}^2} = \frac{2}{3}k \quad \text{Eq. (4.11)}$$

#### 4.4.4 Comparison of Experimental Results and Models Predictions

The problem is considered to be a compressible, steady and turbulent swirling flow. In this case, the model is for a flow in 3D.

The computational domain is shown in Figure 4.8.

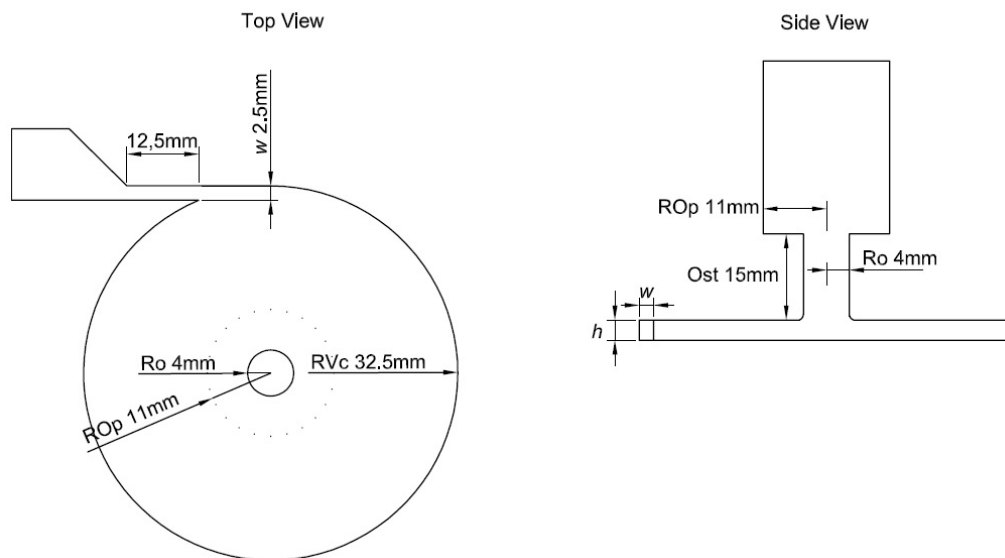


Figure 4.8. - Computational Domain.

Figure 4.9 compares the experimental data with the models predictions of flow rate for a specified pressure drop. It can be seen that the model prediction for the realizable and the standard  $\kappa - \epsilon$  models are not as good as the prediction for the Reynolds stress model, specially at really low and high pressure drops (10,000 Pa and 150,000 Pa) but are more closely matching the experimental result at intermediate pressure drops (50,000 Pa and 100,000 Pa).

The Reynolds stress model follows a similar behaviour as the experimental one, and although the other two equations models present this behaviour, their predictions deviate from the experiment results specially when the velocity increases (high compressibility effects).

The measured flow rate is slightly greater than all the models prediction. This could be due to the wall shear stresses in determining the flow rate in the models; in the absence of internal wall friction, the strength of the vortex would increase, however, in practice wall friction forces limit this effect.

The results shown in Figure 4.9, indicates that the best computational model to predict this type of device is the Reynolds stress model, however, other types of model can be studied if given the computational power required for such a complex analysis.

This statement agrees with literature in that the RSM gives predictions slightly closer to the experimental data than other models [48]

For compressible flows with high velocities, the Reynolds number does not have a significant effect given that at high velocities the viscous forces could be negligible. However, Figure 4.10 shows the streamlines predicted at different Reynolds number for the Reynolds stress model.

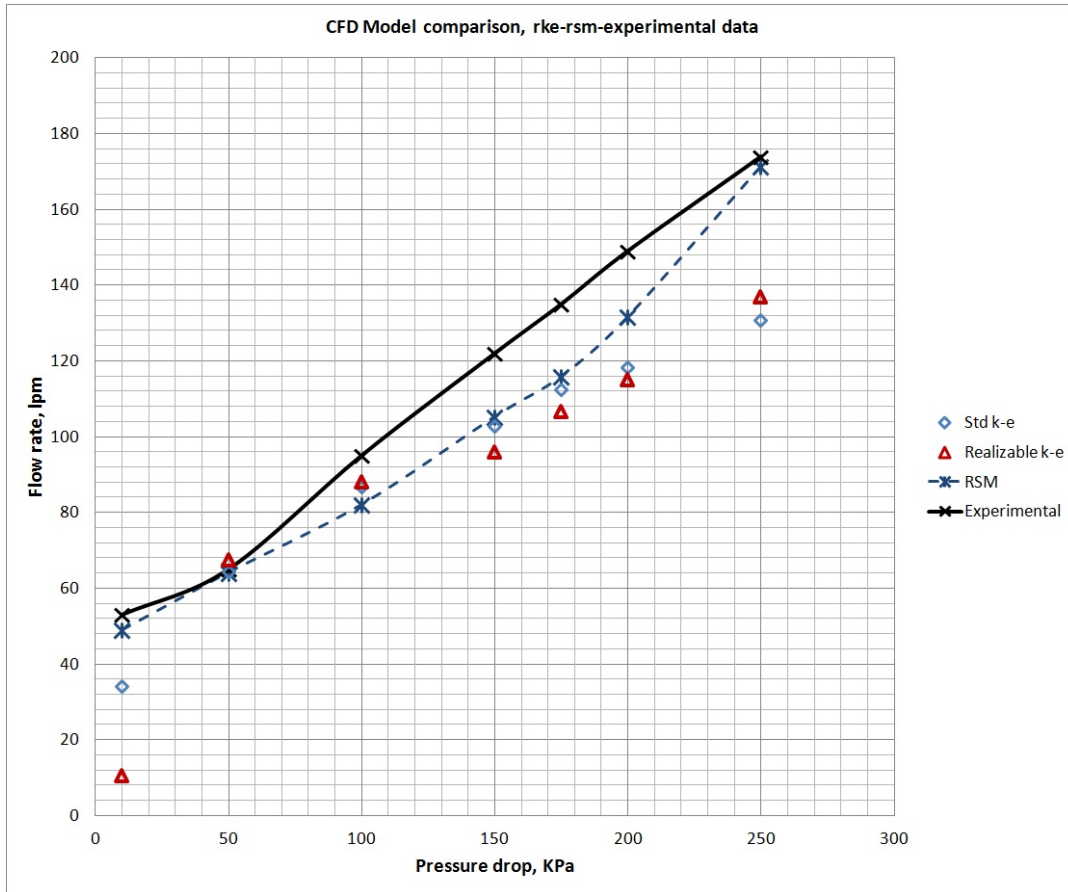


Figure 4.9. - Comparison between Experimental data and predictions of the CFD models, showing the flow rate as a function of the pressure drop.

#### 4.4.5 Discussion

Given the results, the following work will only focus on the Reynolds stress model, however, some results may be compared to the other two equations models.

#### 4.4.6 Pressure Field

Figures 4.11 to 4.13 show the pressure profile in the vortex throttle predicted by the Reynolds stress model for a specific plane. It can be seen that a low pressure zone occurs around the axis of the vortex chamber as a result of centrifugal force. This is the cause of a central recirculation zone in the axial port.

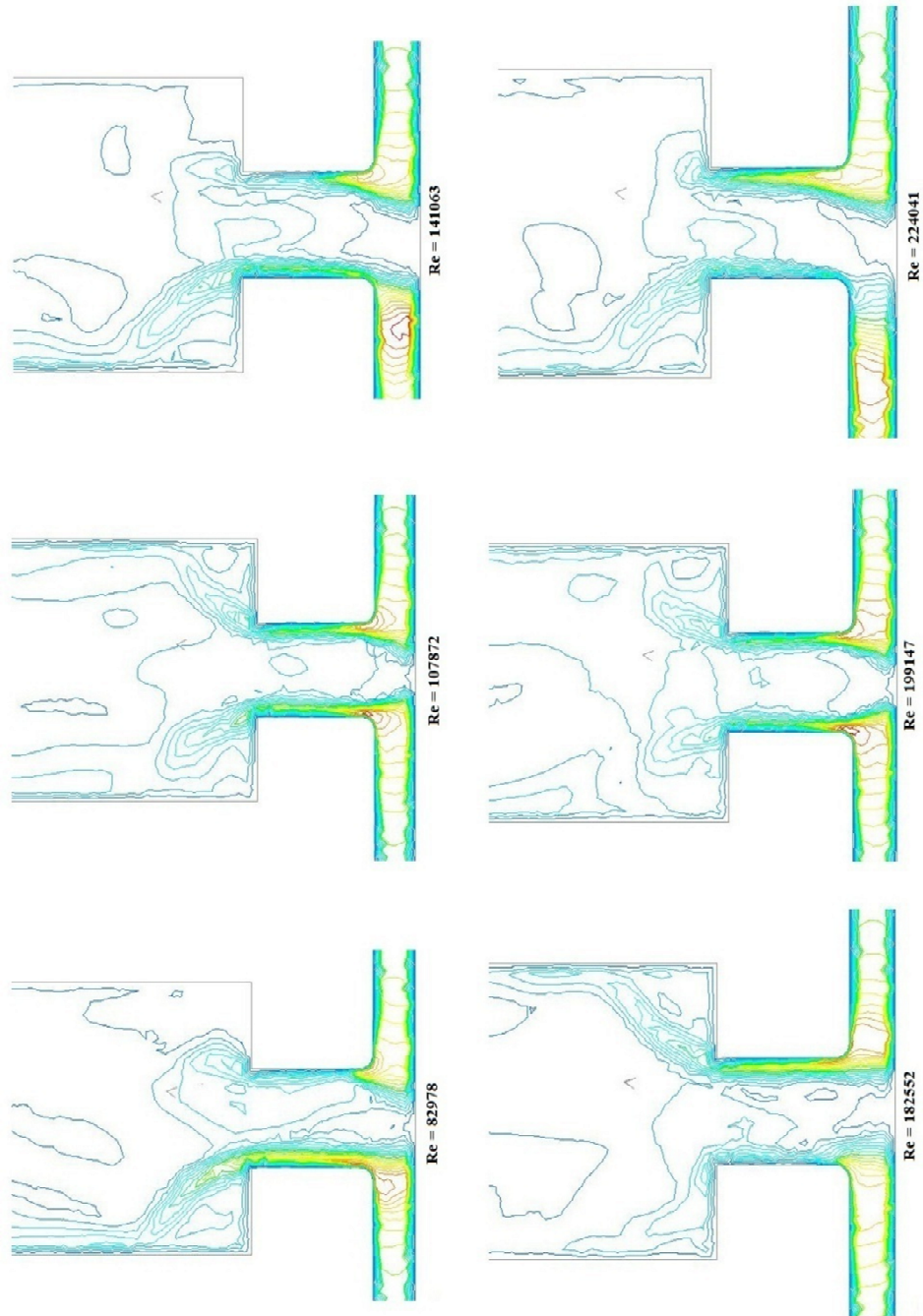


Figure 4.10 – Streamlines predicted at different Reynolds numbers.

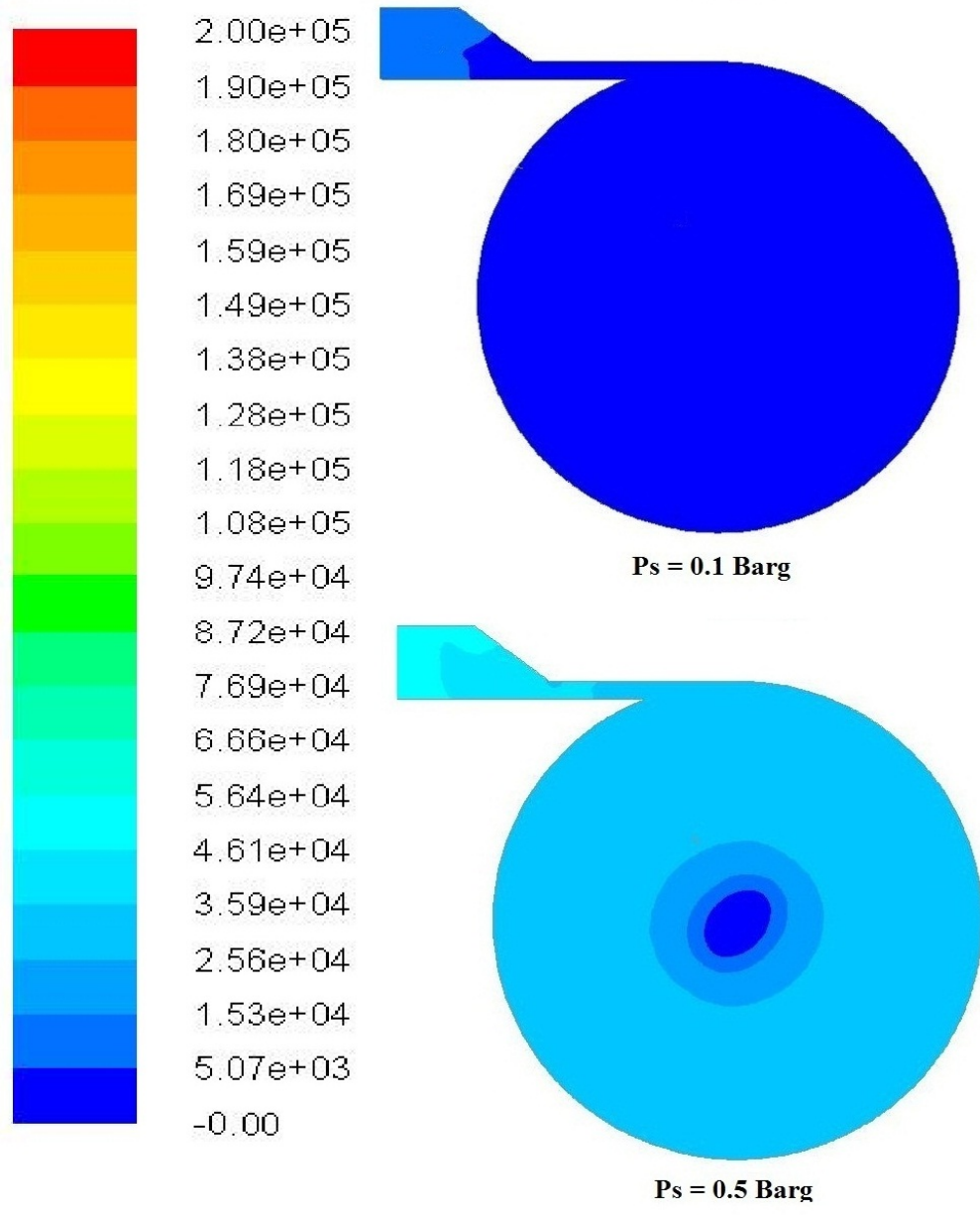


Figure 4.11. - Pressure across the vortex throttle at different inlet pressures and a scale from 0 to 50 KPa (Pressure scale in Pa).

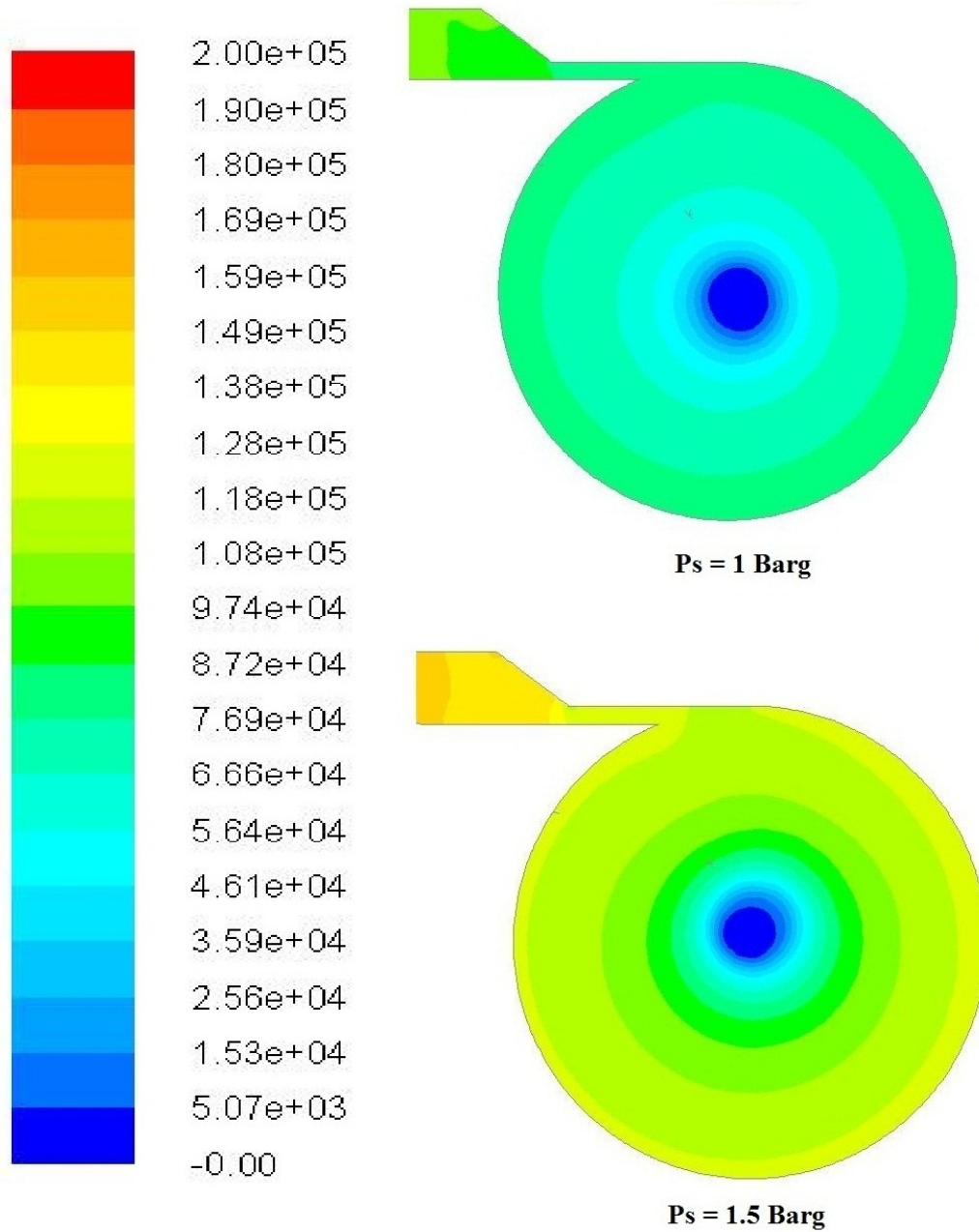


Figure 4.12. - Pressure across the vortex throttle at different inlet pressures and a scale from 0 to 200 Kpa (Pressure scale in Pa).

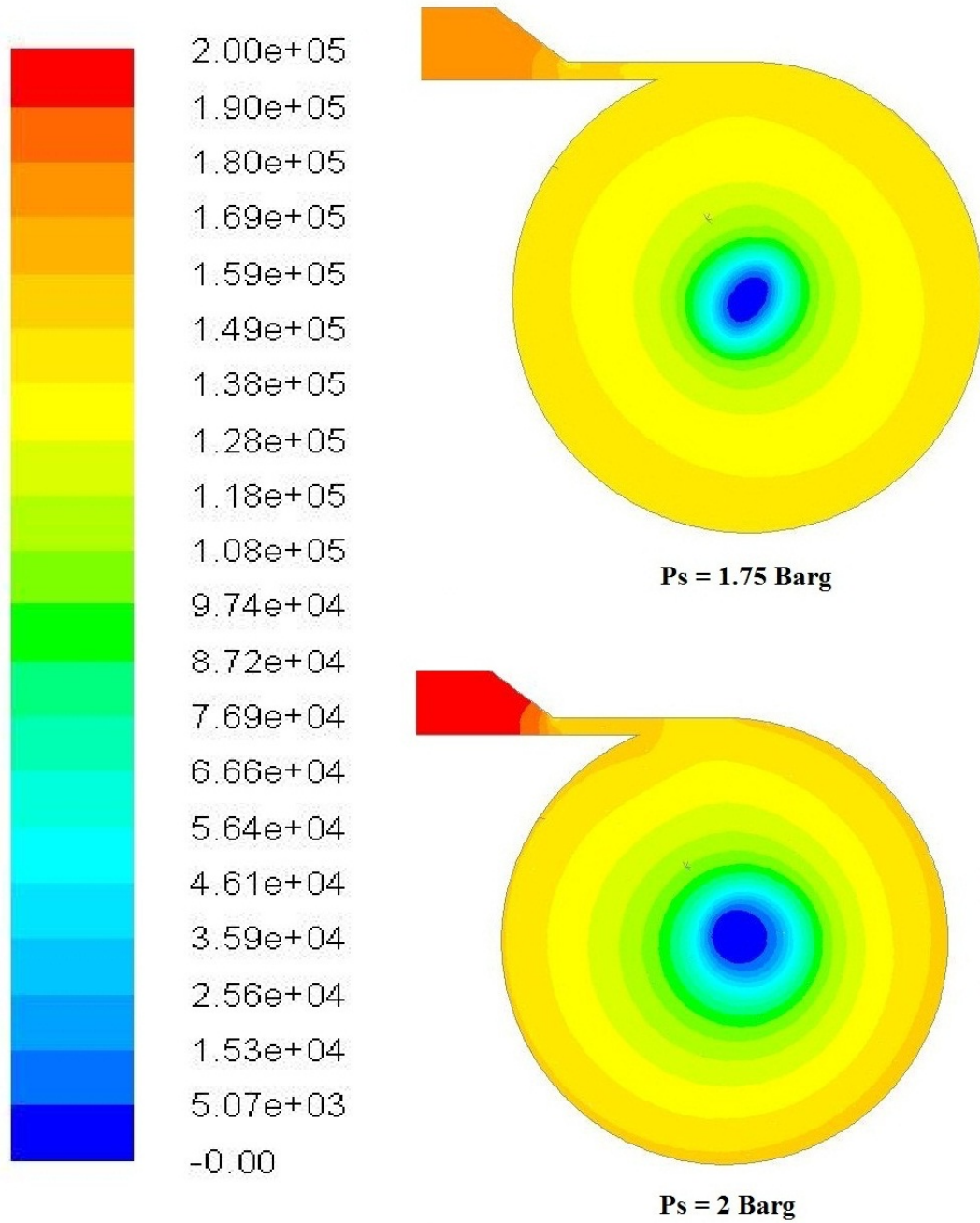


Figure 4.13. - Pressure across the vortex throttle at different inlet pressures and a scale from 0 to 200 Kpa (Pressure scale in Pa).

#### 4.4.7 Flow Field

Figure 4.14 shows the streamlines and velocities prediction in the axial port, showing the two recirculation zones mentioned before.

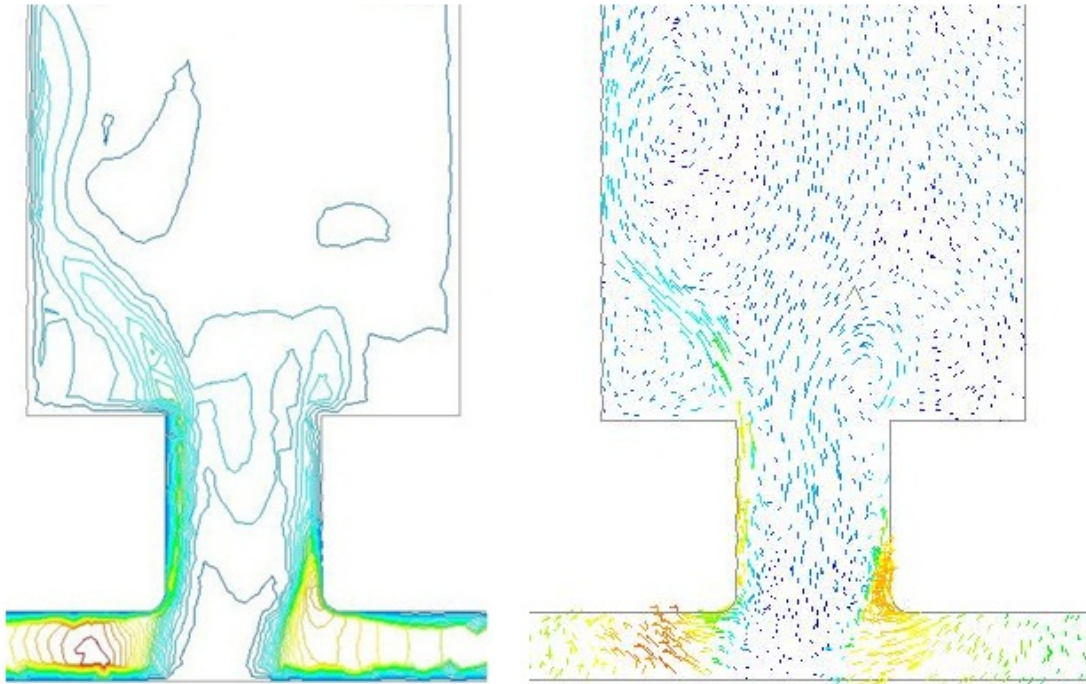


Figure 4.14. - Streamlines and Velocity vectors at the axial port of the Vortex Chamber at a Reynolds number of 141163.

The model predicts recirculation zones in the axial port, due to the centrifugal force created in the vortex chamber.

Comparing Figure 4.12 and Figure 4.14 it can be seen that as the tangential velocity increases, the pressure drop across the vortex throttle also increases. Figures 4.15 to 4.17 show the scaled flow field at different inlet pressures.

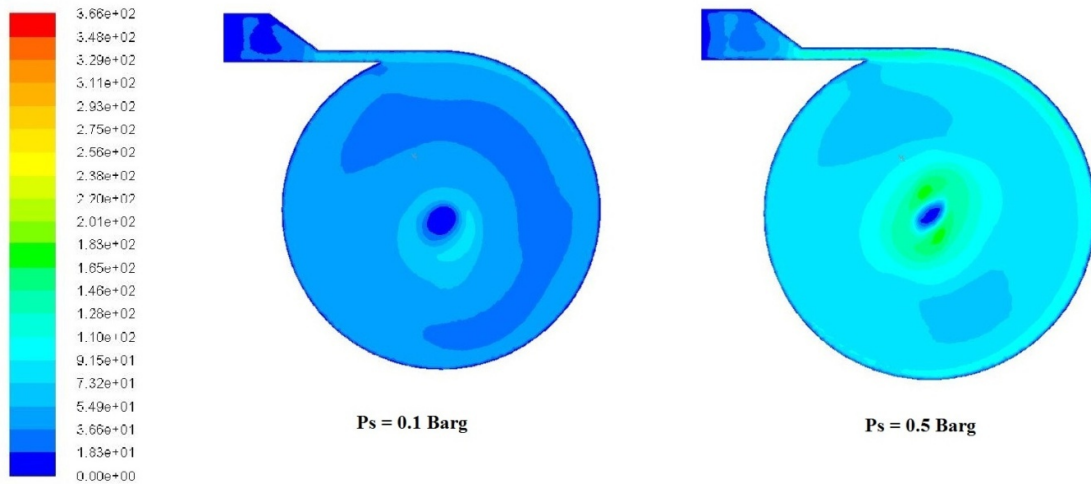


Figure 4.15. – Flow field at inlet pressures of 0.1 Barg and 0.5 Barg and a scale from 0 to 366 m/s.

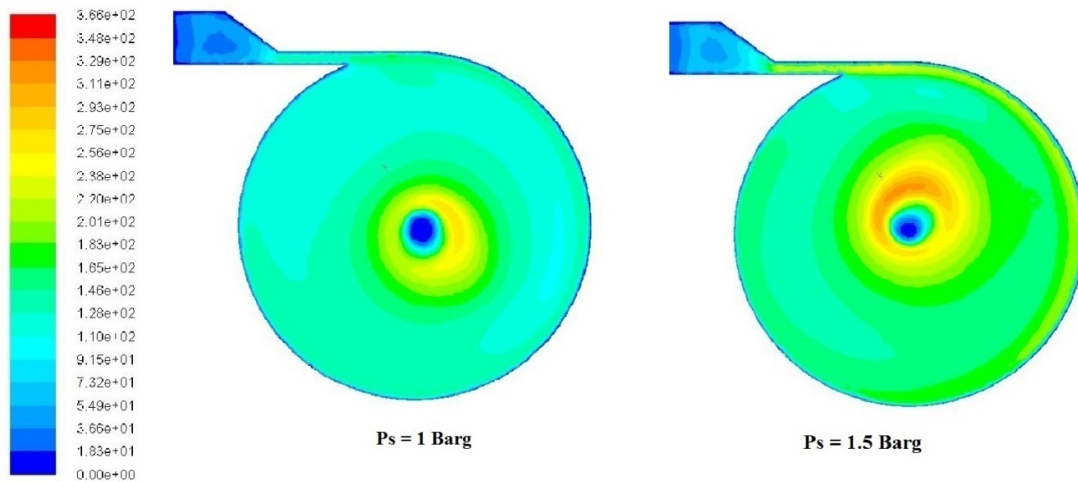


Figure 4.16. – Flow field at inlet pressures of 1 Barg and 1.5 Barg and a scale from 0 to 366 m/s.

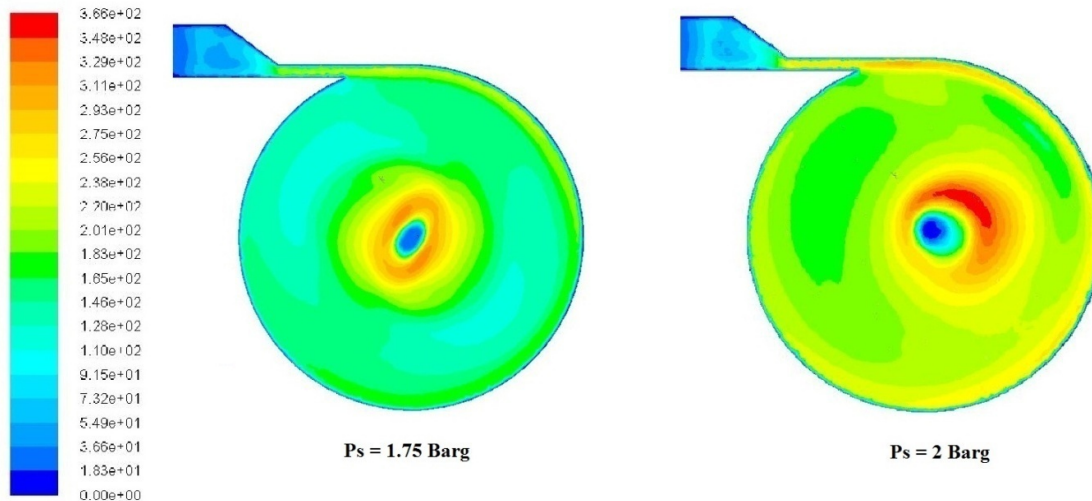


Figure 4.17. – Flow field at inlet pressures of 1.75 Barg and 2 Barg and a scale from 0 to 366 m/s.

#### 4.4.8 Effects of Mach Number

Given that the velocities in the device are very high, the Reynolds number - which describes the ratio of inertial forces to viscous forces-, can be neglected. The Mach number, which defines the compressibility effects on a compressible flow, is a better parameter to use.

At low Mach numbers (0.3 Ma) the compressibility effects are less significant and the fluid behaves as an incompressible flow. In this case we can see that below  $Ma = 1$ , the model can predict the flow rate through the Vortex Throttle at a given pressure drop, as seen in Figure 4.18. When the Ma number increases, the compressibility effects and the flow behaviour are so complex that the standard  $\kappa - \varepsilon$  model and the realizable  $\kappa - \varepsilon$  models deviate from experimental results and fail to properly simulate this type of conditions but the Reynolds stress model appears to have a better match to the experimental trend line behaviour. This is because at high Ma numbers, shock waves might appear in the system, and while there are other models such as Large Eddy Simulation model or LES that can predict these shock waves, the standard  $\kappa - \varepsilon$  and the realizable  $\kappa - \varepsilon$  models cannot predict the correct shock-amplifications of turbulence kinetic energy and dissipation rate [16].

Pressures above 2 bar (gauge) were tried in this study but as the pressure increased, the flow velocity also increased, so the model used here is not ideal for the purposes of flow velocities above the  $Ma = 1$  as the predictions clearly deviate from the experimental data as seen previously.

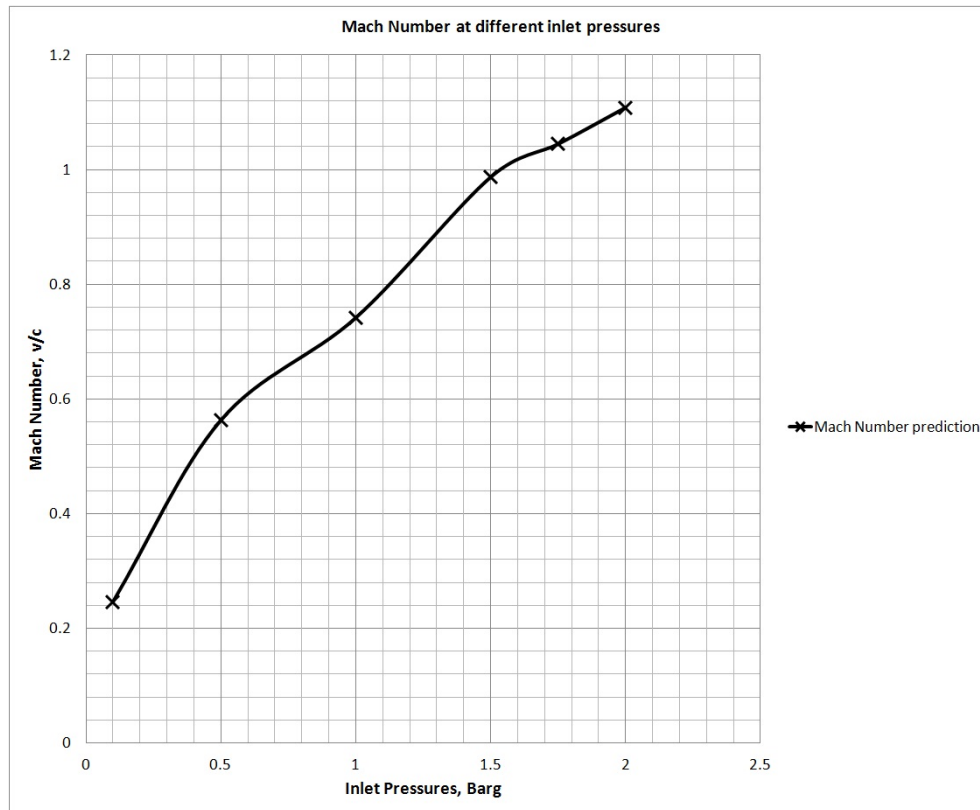


Figure 4.18. - Mach Number prediction at the different inlet pressures.

#### 4.4.9 Effects of Turbulent Intensity

The default value of 10 per cent for the turbulent intensity is assumed. However, different values of turbulent intensity were adopted to assess its effect. Values from 1 to 30 per cent have been adopted. However, these changes did not have any effect on the overall predictions of any of the models used.

#### 4.4.10 Pressure Drop

The pressure drop across the vortex chamber differs from that in pipe flow, due to the mechanism of swirl flow which depends mainly on intensity of tangential velocity[38].

This may be verified by Figure 4.19, in which it is shown that the turbulent kinetic energy is dissipated in the axial port mainly by dissipating the high tangential velocity.

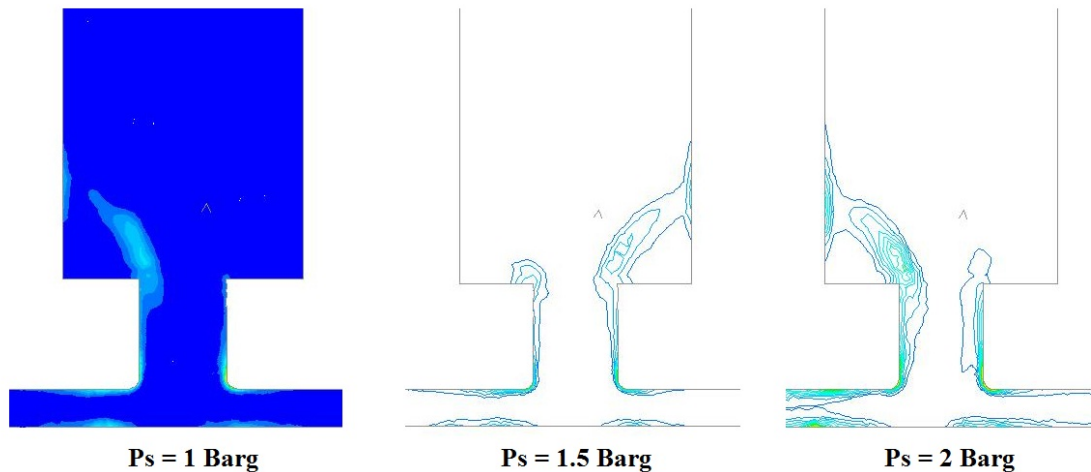


Figure 4.19. - Contours of Turbulent kinetic energy dissipation rate predicted at  $Re = 161100$ .

According to Jawarneh[9], at higher Reynolds numbers the core size of the vortex expand and this will increase the pressure drop. With the increase of the tangential velocity and Reynolds number, the pressure drop increases as clearly seen in Figures 4.11 to 4.13, where the pressure drop increases as the tangential velocity increases.

#### 4.4.11 Effects of the axial outlet geometry.

Two different types of outlet geometries were used; the first one is the one presented earlier as the computational domain geometry, and a second one which main difference is the outlet section.

In this case, different outlet straight sections were used, while the outlet was venting straight to atmosphere, as shown in Figure 4.20.

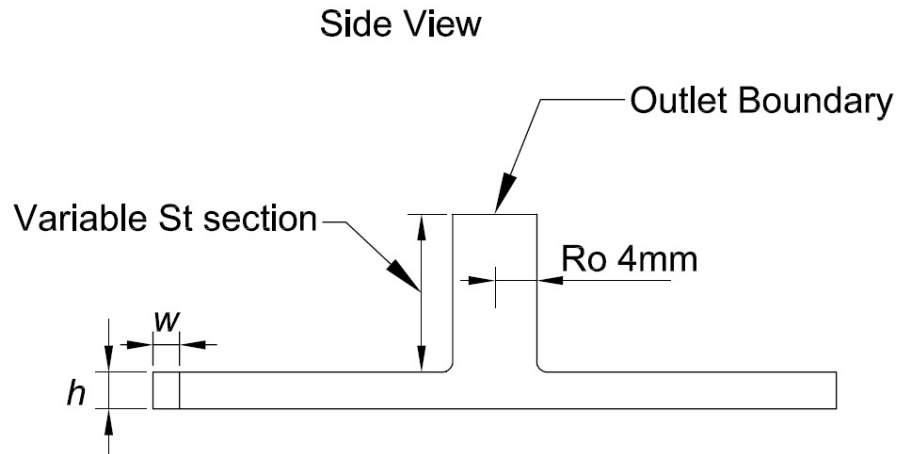


Figure 4.20. - Vortex Throttle computational domain for the variable straight outlet section.

At first it was thought that modelling the outlet as if it was connected to an infinite diameter pipe would affect the predictions of the model, but the model did not show any major difference between the two different geometries as shown in Figure 4.21. The turbulence dissipation rate is mainly seen in the axial outlet, the straight outlet gives a smoother dissipation of turbulence whereas the other geometry tends to dissipate the turbulence further above creating another recirculation zone as shown in Figure 4.14.

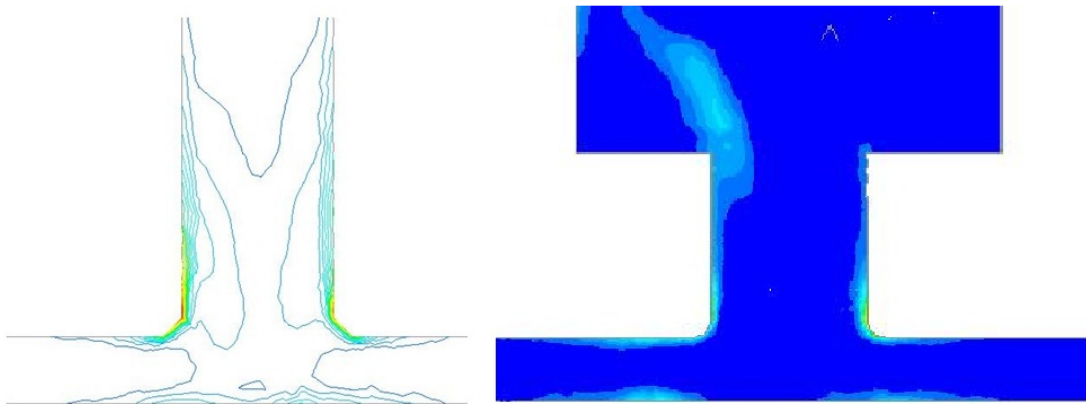


Figure 4.21. – Turbulence dissipation rate with different outlets at the same inlet pressure of 1 Barg.

#### 4.5 Discussion.

The results for the Vortex Throttle will be useful in identifying the upper limits of a Vortex Amplifier of the same geometrical characteristics. It is clear that the diameter ratio is an important parameter determining the performance of the Vortex Throttle as well as the Tangential inlet area, which will determine the amount of flow that will go through the device at a determined pressure.

From the results it can be seen that the  $D_{ot}$  value yields good turndown ratios from the value of 1 and improving slightly as it reaches the value of 2, from this value of  $D_{ot} = 2$  the turndown ratio increases up to the region between the values of 4 and 6 in which the turndown ratio does not improve any further.

There is a significant effect on the turndown ratio as the D ratio decreases, i.e. when the outlet diameter is getting bigger, this due to the fact that the air is having an easier path to the exit, for this case the best turndown ratio range is yielded at a D value between 5 and 7 without compromising too much the flow rate passing through, this agrees on the findings of Priestman [20]; the opposite can be said when the D ratio increases, there is a tendency to decrease the turndown ratio from the range between  $D = 10$  to 20.

So, for the special needs of a Switched Vortex Valve a good vortex chamber/outlet diameter ratio value should be between 5 and 7 and the  $D_{ot}$  value between 1 and 4.

An unorthodox approach was used to model a CFD model of the Vortex Throttle. Usually, as mentioned above, the CFD model is the starting point to manufacture a test piece, this because the CFD model can predict accurately the performance of the device, but given the complexity of the device and the need for a basic set of parameters to be used for an even more complex device such as the SVV it was logical to use the experimental data and try to match the CFD performance to the real one by using different turbulence model and select the one that yielded the closest predictions to the actual performance.

The two different  $\kappa - \varepsilon$  models were used to simulate numerically highly swirling confined compressible flow in vortex throttles, and the predictions were a bit more

deviated than the ones offered by the Reynolds stress model. Although it gives a better prediction at high pressure drops, the Reynolds stress model consumes a lot more computer power given the higher complexity inherent in calculate the 7 different equations.

The effects of Reynolds number and pressure drop have been analyzed.

Although there are several models that can simulate turbulent flow, the two  $\kappa - \varepsilon$  models have shown good agreement with the experimental data at intermediate pressure drops (50,000 Pa to 100,000 Pa), but deviate to predict the flow at low and high pressure drops (10,000 Pa and above 150,000 Pa, region in which the flow chokes) this due to the inability of the model to predict the shock amplifications of turbulence kinetic energy and dissipation rate of a shock wave.

As for the Reynolds stress model, the predictions are within 15% accuracy to the experimental data, which can be regarded as good agreement, but a different model such as the Large Eddy Simulation model might simulate that type of even higher swirling turbulent flows with much more accuracy than the Reynolds stress model, or even change the different default values to improve the Reynolds stress model to give more accurate predictions even at intermediate pressure drops.

The Reynolds number does not have a great effect in the prediction of the model; this because the flow is highly turbulent and the velocities are incredibly high, making the effects of the viscous forces to be negligible.

The range of turbulent intensities did not influence the predictions of the model.

The pressure drop across the vortex depends on dissipating the tangential velocity through the axial port, so increasing the tangential velocity in the vortex chamber produces a higher pressure drop. Therefore it is of great importance the design of the axial outlet port; a well design axial port could dissipate better the tangential velocity, producing an even higher pressure drop.

#### 4.6 Conclusions.

The vortex throttles are of significant importance to the performance when the device is part of a switched vortex valve. From the results it should be expected that for a switched vortex valve having a D ratio between the values of 5 and 7 and low  $D_{ot}$  values between 1 and 4 should yield good turndown ratios. It shall be noted as well that perhaps the turndown ratios and overall performance of the switched vortex valves would not be as good as the individual vortex throttles this due to the overall effect that a Wall Attachment diverter dynamic behaviour would have over the vortex throttle.

ANSYS Fluent CFD was used to model an already tested Vortex Throttle, this will help to model the performance of a Vortex Throttle and as said above determine the upper limits of performance for Vortex Amplifiers, by doing this a lot of testing time will be reduced just to a simple CFD model to predict its performance. The model will also help to understand the inner behaviour of the flow and the pressure field of the device, and how the outlet geometry affects the performance of it.

The model in this work could be used to predict the performance of a vortex throttle using compressible flow approaching the critical conditions for choked flow, and for design purposes.

CFD modelling could be further improved and taken to more complex devices; it has been shown that the model which gives closer results to experimental data is the RSM model. With this fact, the CFD model could be improved by sorting out the particulars of the numerical method in order to account for the complex behaviour of the switched vortex valves.

It could also be used to predict the behaviour of the devices working at extremely high pressures such as the ones present in the jet engine, thus maintaining the same pressure ratios as those used in the laboratory at low pressures and obtain comparable data. The University of Surrey will be using this vortex model as base scenario for its simulations. They will use their coanda switch simulation and this model to create a general SVV arrangement in the future.

## **SWITCHED VORTEX VALVES WITH COMPRESSIBLE FLOW: Experimental**

### **5.1 Introduction.**

Work with incompressible flow in fluidic devices has been made for many years [26, 41, 31, 20] and although sometimes the devices were working with compressible fluids such as air, the compressibility effects were neglected as the pressures in the experiments were not increased to a point where these would affect the result.

In recent years, the aerospace industry has been pointing towards this type of devices to increase the reliability and performance of its engines [24, 44]; given that a fluidic device uses fluid phenomena such as the Coanda effect and vortex resistance to function as a valve without the mechanical bits that imply more complexity.

In this application the switched vortex valves have to work in an environment of high pressure and high temperatures, and the current performance analysis has not been designed to tackle this.

As mentioned in Chapter 2 the previous approach was to neglect the compressibility effects when working with a compressible fluid and consider different parameters to reflect the performance of the device.

The objective of this work is to apply the compressible flow theory so that it can reflect the performance of the device in a way that the compressibility effects are

shown. The theoretical background for compressible flow was analyzed and outlined in Chapter 3.

Initial results of the performance of the switched vortex valve when working with compressible flow are presented here and the results are compared with the theoretical model for compressible flow. Future work will focus on the optimisation of the switched vortex valve when working with compressible flow.

It is worth to mention that the switched vortex valve is a laminate device, i.e. it is conformed by three different plates or laminates (Appendix A):

- Top laminate: Integrates the top boundary of the device along with the inlet, control ports and outlet bores in order to connect the required fittings.
- Middle laminate: Integrates the geometry layout of the device as well as its boundaries.
- Bottom laminate: Integrates the bottom boundary of the device; it also serves as the base for the splitter.

This laminate design is useful in placing such devices in a flat ring in order to suit specific purposes, such as having several identical devices working in parallel as it will be shown in Chapter 7.

## **5.2 Experiments.**

For the experiments, a bistable Switched Vortex Valve was used, Figure 5.1 shows the general geometry used in the experiments, the outlet of the device first was tested with the diffuser type of outlet.

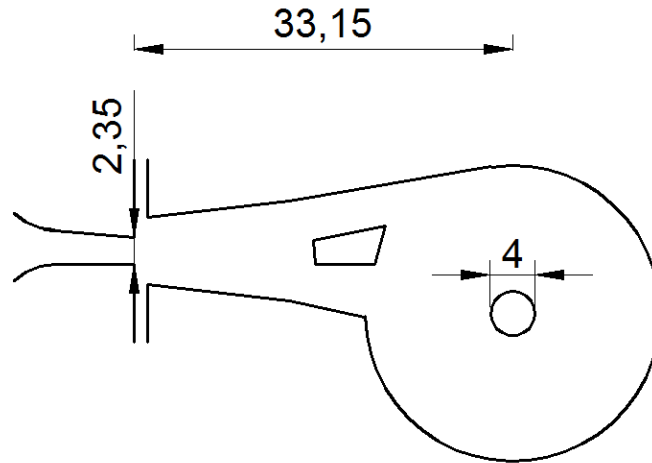


Figure 5.1 - Geometry design of the Switched Vortex Valve.

### 5.2.1 Experimental Rig.

The experimental rig consists in three parts, an upstream and a downstream part and the test device, Figure 5.2. For the upstream part a supply of compressed air is connected to the inlet of the switched vortex valve.

The compressor used was rated to supply compressed air at 7 bar. The outlet of the compressor was connected to a pressure regulator by a 1" heavy duty flexible hose that could withstand the pressure of the system.

The hose was connected directly to a manual pressure regulator with a pressure display gauge with a condensate trap to allow any fluid condensation to be trapped and not flow through the system. The outlet of the hose was attached to stainless steel threaded fittings to be able to properly attach the hose to the pressure regulator. This stainless steel threaded attachment was secured by jubilee rings to the hose. The threaded connections were sealed with PTFE sealant tape.

The outlet of the pressure regulator was then connected to a 3/4" hose fixed with jubilee rings via a stainless steel threaded connection and sealed with PTFE sealant tape. Before the connection to the test device, an instrument pressure gauge was installed, this tapping could be switched from a low rated gauge between 0-14 psi, to a medium rated gauge between 0-2 bar and a high rated gauge between 0-5 bar.

This ¾" hose was then connected to the inlet of the test device and secured by jubilee rings and sealant tape as needed.

The outlet of the test device then was connected to a 1" hose secured by jubilee rings, which then was connected to a PVC pipe system that distributed the flow through two different rotameters, one rated for 200-1000 lpm and a smaller one rated for 50-500 lpm. The flow could be manually switched between the two rotameters via a manual valve in the PVC piping system. Both rotameters' outlet were installed with a muffler to minimize the noise of the rig. This outlet system had a pressure gauge installed.

For the control ports of the test device, small hoses with manual valves were connected to the control port pipes and secured with rings, although the test device being a bistable device has its two control ports closed but these are used in order to manually switch the device from the low resistance to the high resistance state or vice versa.

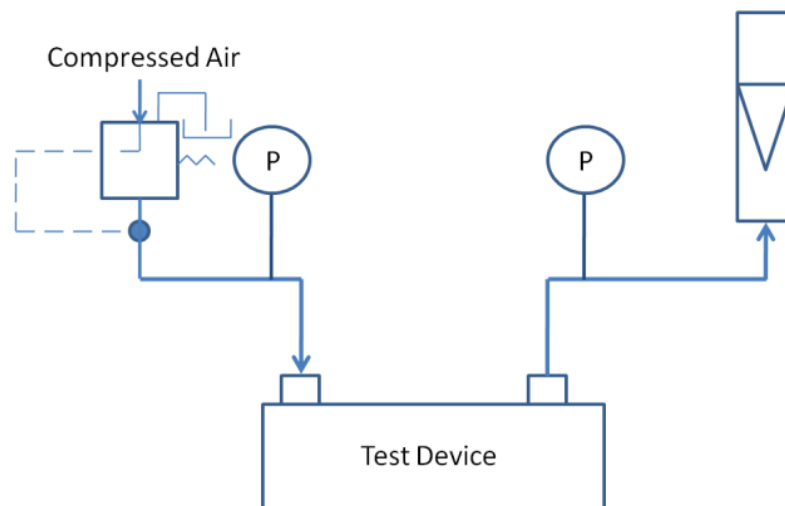


Figure 5.2. - Rig schematic.

### 5.2.2 Experimental Results.

The results from the experiments represent the outlet flow rate as a function of the pressure ratio between the inlet and the outlet of the device. Appendix B shows the experimental data for this work.

In this work, the pressure ratio was inversed so the critical conditions appear when the pressure ratio between the inlet and the outlet reaches a value of 1.894.

Given that the isentropic flow through a nozzle is dependent on  $\gamma$  and the pressure ratio when no critical conditions are present, and only dependant on  $\gamma$  when critical conditions appear, then the experimental performance curves should present at least a similar behaviour to that of the isentropic theory, although the performance of the device can be expected to be slightly different to the theoretical model, because the stagnation conditions in the inlet nozzle are assumed to be the same conditions of the upstream part of the rig.

Figure 5.3 shows the general experimental behaviour of the flow within the Switched Vortex Valve and the comparison with the theoretical model. The low resistance performance state isentropic theoretical line is calculated as if the flow was passing through a nozzle of same area as the effective area of the device; for the isentropic theoretical line in the high resistance state, it is assumed that the flow turndown ratio -which is the ratio of flow between the low and high resistance states at the same pressure ratio between the inlet and the outlet- in the device, is about two, this only for demonstrative purposes.

From Figure 5.3, it also can be identified that the critical conditions appear once the pressure ratio  $P_s/P_o$  reaches the above mentioned value of 1.894. The low resistance state performance and the high resistance state performance are depicted by the upper and the lower performance curves respectively.

Figure 5.4 shows the behaviour of the switched vortex valve as an ideal choked orifice. In this case, the value is above 1 due to the higher flow rate through the device that the switched vortex valve is behaving as an ideal choked orifice with an area of  $A_{eff}$ . It shows that for low pressure ratios the measured flow is higher than the ideal one because of the use of a diffuser.

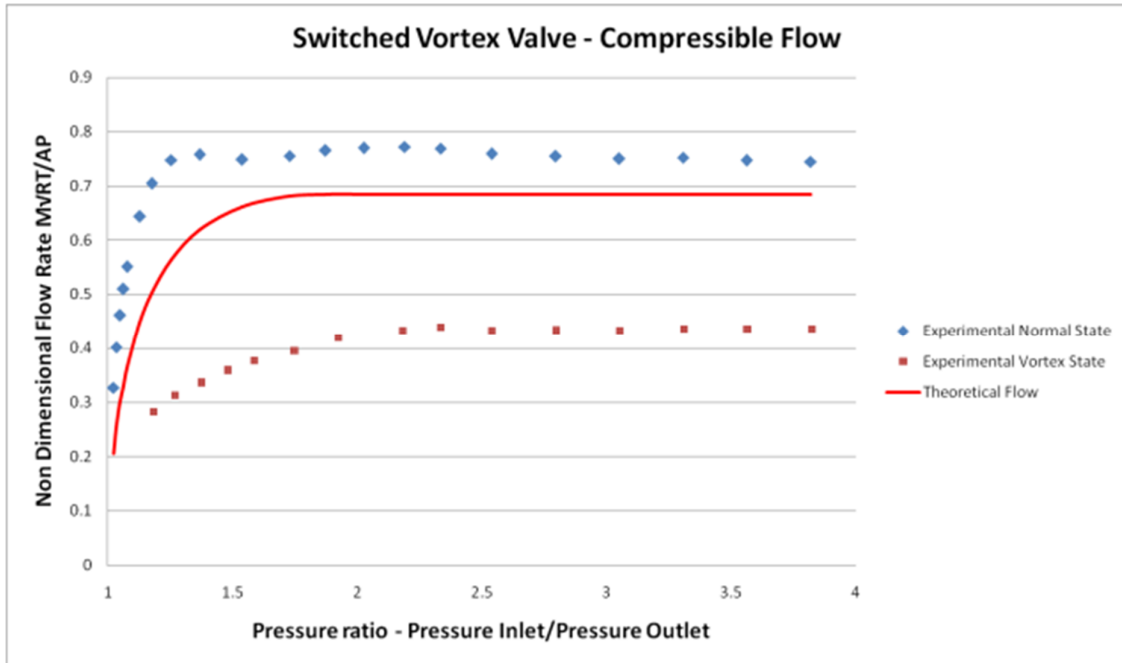


Figure 5.3. - Performance of the switched vortex valve in both states and comparison with the theoretical isentropic flow rate.

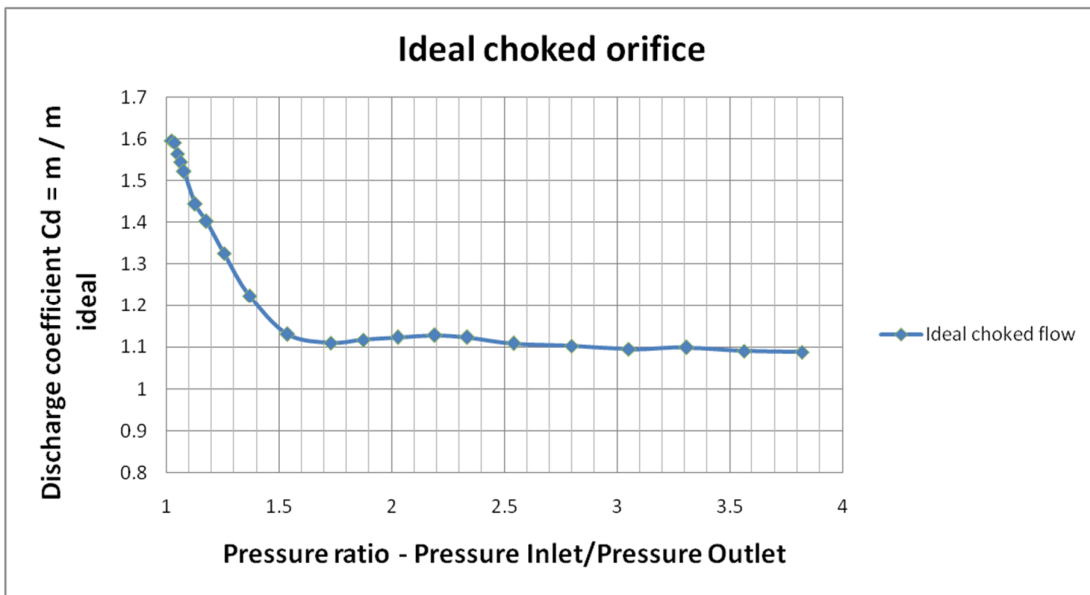


Figure 5.4. – Behaviour of the switched vortex valve as a choked orifice.

### 5.3 Results and Discussions.

In this work, two different Switched Vortex Valves were used, Figure 5.5 shows the two different types, one type will be called Design B (DB) and the other one will be called Design C (DC ), dimensions for the two different design are shown in the Appendix A.

The DC design was manufactured in an effort to reduce the size of the device in order to be suitable for the needs of Rolls-Royce; it was scaled from the DB design which was slightly different design to one that Priestman and Tippetts designed for the application of a burst duct in the jet engine [36 ] which proved to be efficient under extreme conditions.

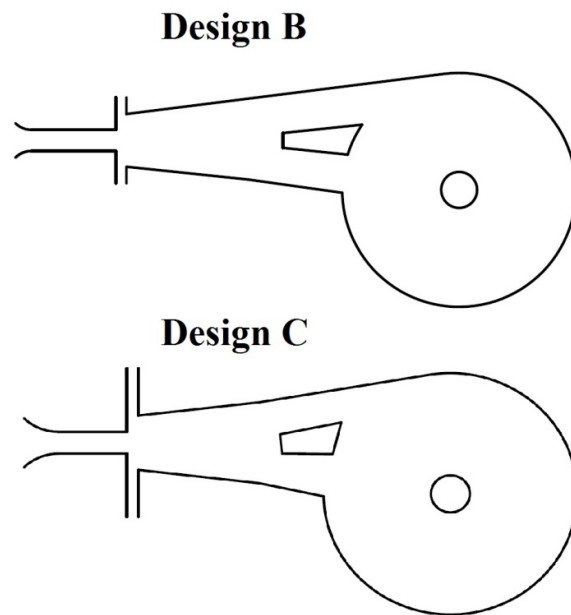


Figure 5.5. - Different Switched Vortex Valve designs.

#### 5.3.1 Leaks.

According to the compressible flow theory, the DC design was scaled down so that all the properties in the design DB were matched, so in theory the performance comparison between the two designs was supposed to be in agreement to each

other. Unfortunately as shown in Figure 5.6 this was not the case and serious differences were identified.

Although the low resistance states and the high resistance states presented a slightly dissimilar behaviour in both designs, the most noticeable difference was that the pressure ratio at which the two designs changed from one state to the other, was significantly higher in the DB design (2.28) than the one shown by the DC design (1.3).

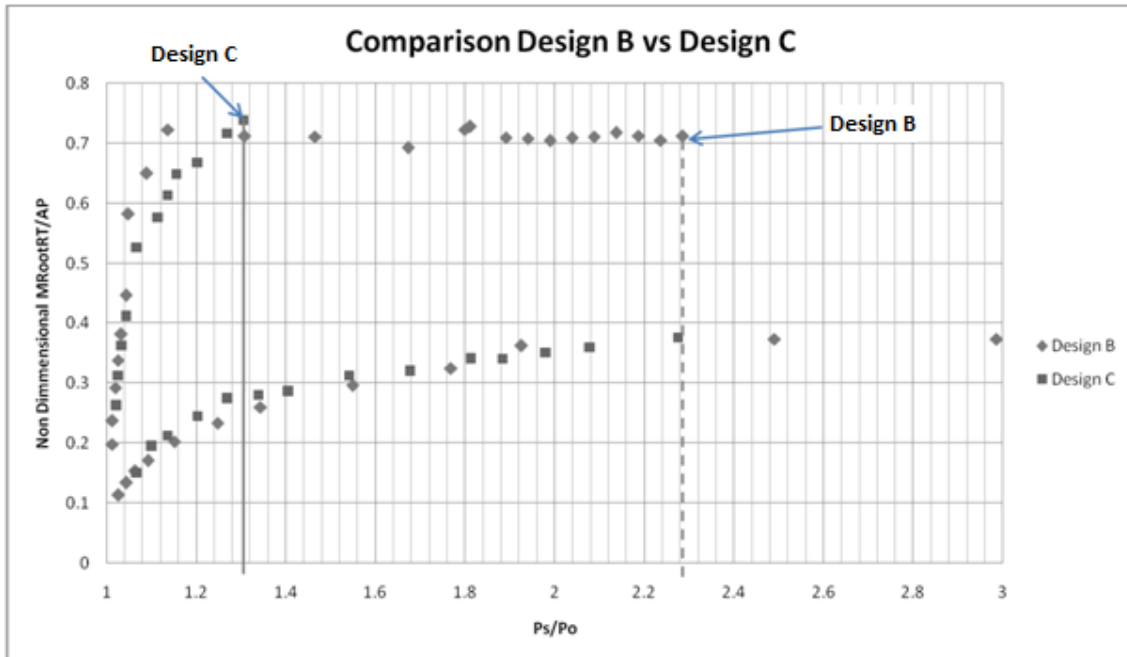


Figure 5.6. - Comparison of Performances between the Design B and the Design C.

From this results one can conclude that given both designs were matched properly the only possible explanation is that a leak could be present in one or even both designs. This could be explained easily given that the device was manufactured by separated plates screwed together, and the control ports were glued to one of these separated plates potentially leaving room for a leak between the faces of the plates or in the joint between the control port and the plate.

A test for leaks was devised, which consists of submerging the device under a volume of water and then supply pressurized air; if there was a leak, bubbles of air would appear.

Following the hydrodynamic test, no leak was found in the DC design, but it was found that a leak on the gluing of the radial control port of the design DB was present and affecting the behaviour of the device.

The leak was acting as if the radial control port was open causing the “increase” in the performance in validating the results for the design DB.

After the leak was fixed, another experiment was made to compare the performance impact of the leak in the previous results. The results are shown in Figure 5.7 which shows the comparison between the performance of the Design B with the leak and without the leak.

These results compared to the design DC’s results shown in Figure 5.3, show that the performance between the DC and the DB designs was matched, but both devices presented really poor and unstable performance in the low resistance state i.e. the device switched unexpectedly from the low resistance state to the high resistance state at very low pressure ratios. The maximum stable point achieved was the same for both designs. This comparison is shown in Figure 5.8.

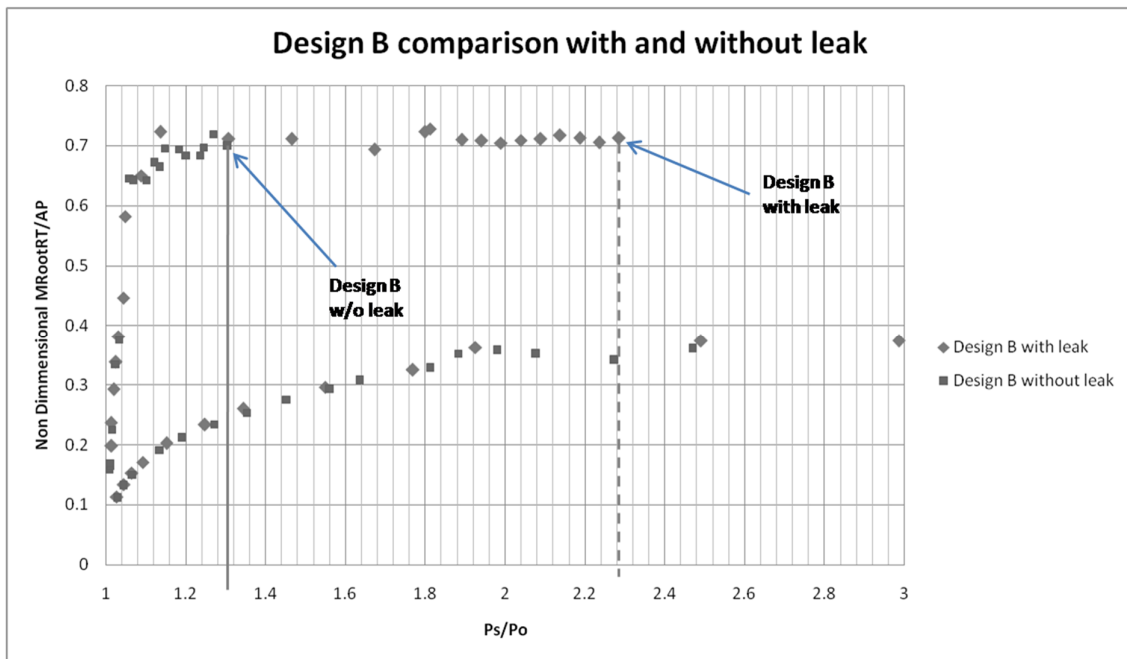


Figure 5.7. - Performance comparison of the Design B with and without the leak.

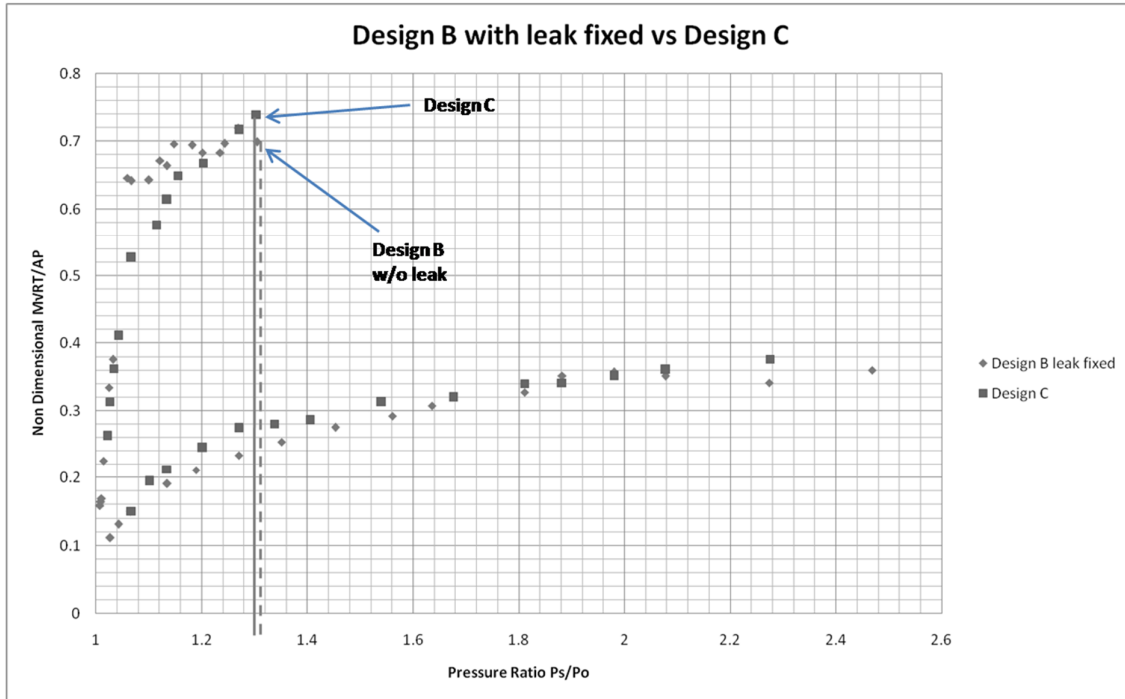


Figure 5.8. - Comparison of the Performance between the Design C and the Design B with the leak fixed.

### 5.3.2 Start up Instabilities and Inlet Nozzle Configuration.

The initial experiments were carried on design DB and the results showed that the Switched Vortex Valve presented an irregular start up; in the normal operation of the SVV, the device would be starting up in the low resistance state, and then switched if required to the high resistance state.

In other words, the device started sometimes in the high resistance state and other times in the low resistance state; once started, the device was set to the low resistance state by manually opening the radial control port to let a small amount of flow leave the device.

This particular problem is related to the symmetry of the device, this is, that given that the device is similar at the diverter part, the flow could easily attach to one or the other channel. In the experiments with incompressible flow, there is no mention of instabilities at the start up but when working with compressible flow the velocities

and the inertia forces are so great that the flow will either attach to one side or the other randomly.

This was not ideal given that, to ensure the start of the device in the low resistance state, a manual induction had to be carried out.

To solve this problem, a simple configuration of inlet angled nozzle was tested, intended to force the inlet air jet to attach to the radial channel maximizing the performance of the device by stabilizing the flow. This inlet angled nozzle is shown in Appendix A.

Figures 5.9 and 5.10 show results for different angles for the inlet nozzle, being 3°, 4°, 5°, and 6°. The differences are subtle, and there were no instabilities at start up in any of the angles tested. Given that no significant difference could be identified from any of the angles, either in the low resistance or the high resistance state, the selected angle for the inlet nozzle was the 5°, this to have some manufactures tolerances. It is also important to consider the flow required to switch to the high resistance state from the low resistance state given that if the angle is too big then it will become harder to switch. Figure 5.9 also shows that with a 5° angled inlet nozzle higher pressure ratios were able to achieve, thus providing insight that the 5° angle could be used instead of the other angles tested.

It is also clear that with an angled nozzle, the device could withstand higher pressure without destabilizing, although it did not switch to the high resistance state due to the fact that the air load was simply more than the system was able to deliver, but when switched manually from the low resistance state to the high resistance state by opening the tangential control port, the device did not present any trouble to adapt rapidly to the high resistance state, which can be an indication that is very probable that if the pressure ratio kept increasing the device would sometime switch by its own.

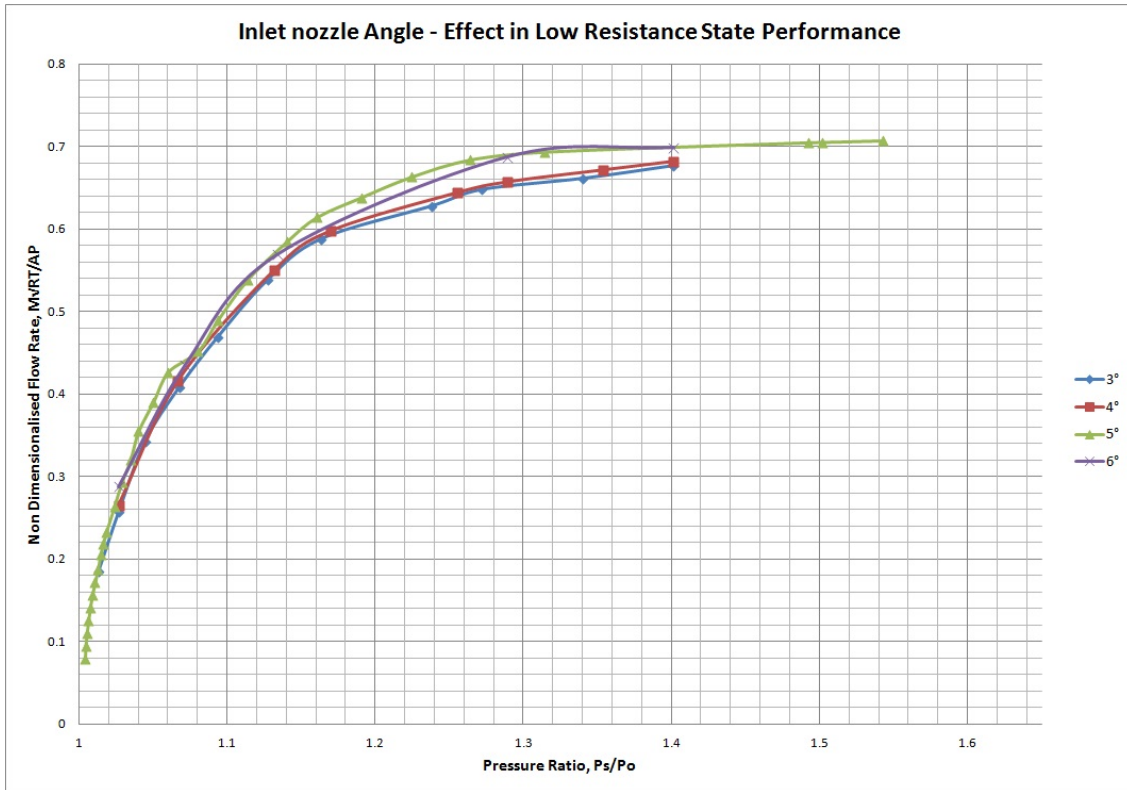


Figure 5.9. - Effect in low resistance state performance with different angles.

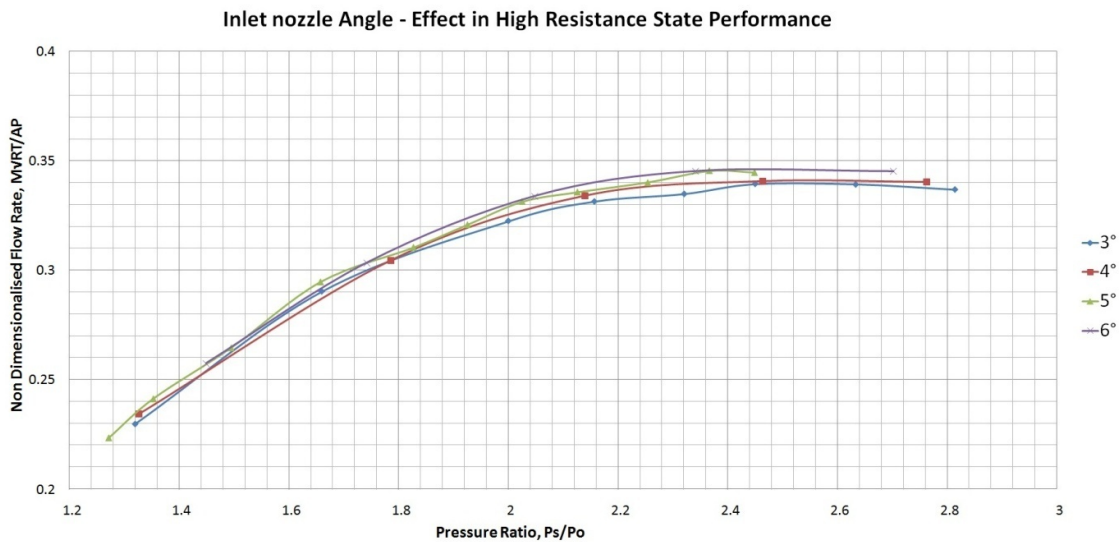


Figure 5.10. - Effect in high resistance state performance with different angles.

The pressure ratios with this configuration were considerably higher than before, achieving pressure ratios of approximately 1.5 and with opening the pressure regulator in order to hold the inlet pressure for a couple of seconds before the pressure reduces due to the fact that the air load was higher than the system delivery capacity, it reached easily pressure ratios of 2.5.

This set of experiments, gave the confidence that the angled nozzle configuration was yielding good performance, although it was not switching by its own to the high resistance state, this is not a problem to final design because the control ports of the device that is going to be manufactured in a ring by Rolls-Royce are going to be connected into a manifold that leads into a solenoid valve. If needed, the solenoid valve would open the tangential control ports and switch the device to the high resistance state until no longer needed and then switch it back to the low resistance state by opening the radial control ports.

### **5.3.3 Control Port Width.**

The control ports are the ones responsible for the switching operation. A bad design could lead to instabilities in the Wall Attachment Diverter, such as oscillations.

In other works one of the control ports has been left open and the other closed, in others connected to each other, but in the case of this particular work, both control ports have been closed and only opened the corresponding one when trying to switch the device from one state to the other.

Figure 5.11 shows results of different widths for the control ports, and it can be seen that there is a zone where the device works without instabilities, this is when the ratio  $a_s/a_{cp}$  is 2, when the ratio becomes higher than this the device becomes unstable.

This instability, i.e. the switching of the device from one state to the other without opening the control port, is shown in Figure 5.12 in which it is seen that an increase in the supply pressure decreases the time that the device stays stable until the point in which the device is no longer stable in the low resistance state. This “stable time”

refers to the time in which the device stays in the low resistance state without inadvertently switching to the high resistance state.

This instability zone can be explained by a pressure build up in the control port (in this case the radial control port), as the pressure supply increases it takes less time for the pressure to build up in that control port zone until the pressure equalize to that of the tangential control port, making the device unstable.

It is not only that the device works without instabilities at an area ratio of 2, but also yields the best performance.

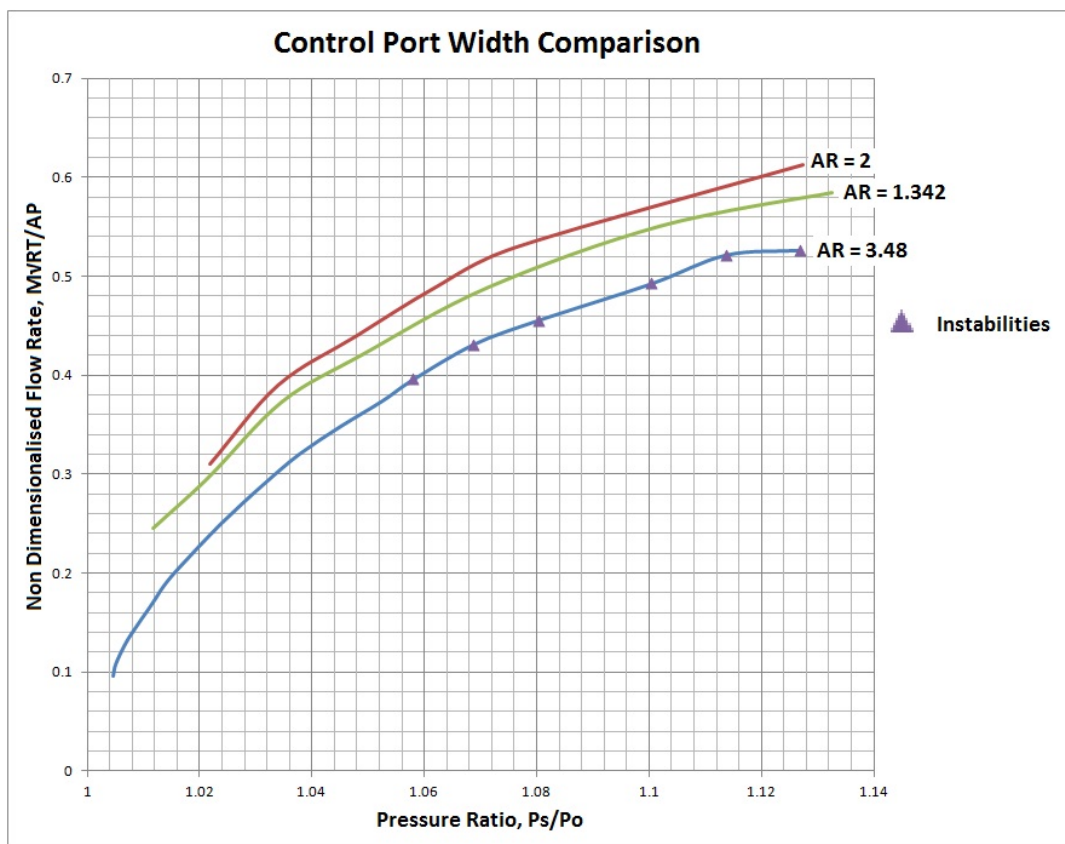


Figure 5.11. - Control Port Width Comparison.

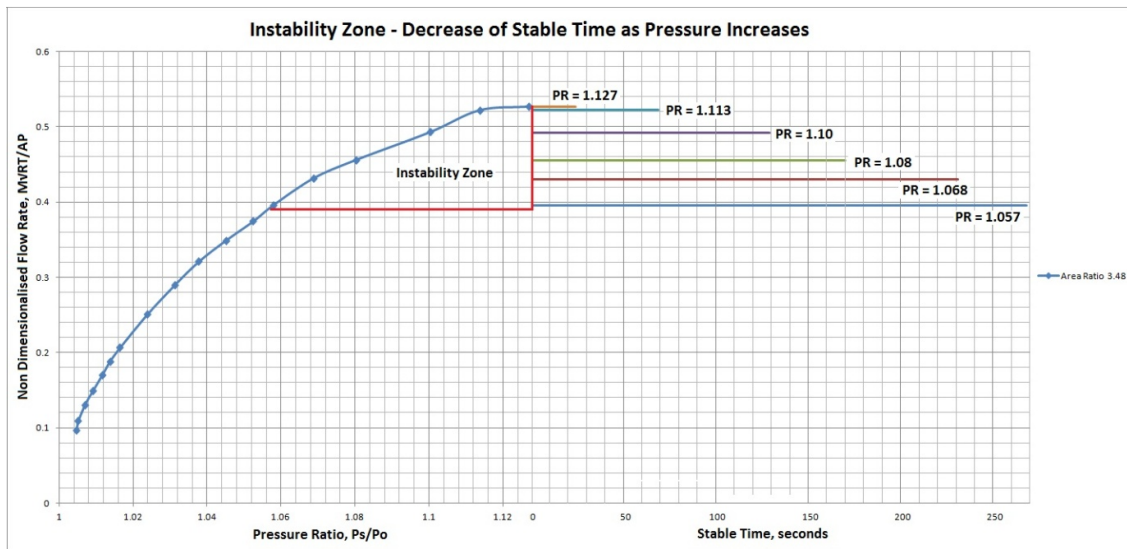


Figure 5.12. - Instability Zone – Decrease of Stable Time as Pressure Increase.

### 5.3.4 Axial Outlet Diameter.

From Priestman [20], it is clear that the vortex chamber diameter and the axial outlet type (bore or diffuser) are of great importance for the performance of the fluidic devices. In this work the axial outlet was a nozzle bore outlet instead of a diffuser given that a diffuser would prove difficult to integrate due to space constraints in the jet engine as well as it increases the complexity of manufacture of the prototype SVV which will be defined in Chapter 7. There is an area ratio range in which the vortex chamber behaves more of a free vortex as seen in Chapter 4. Make it too small and you will have instabilities, make it too big and the performance will drop substantially.

Several area ratios were considered, and as expected the smaller the outlet diameter or the bigger the area ratio would give a better performance of the device. This due to the phenomenon of “making the vortex chamber increase” by a smaller outlet diameter without affecting the velocity of the flow entering the vortex.

Figure 5.13 shows the performance in the low resistance state of the device working with different axial outlet diameters. The area ratio  $a_s/a_o$  will change and as mentioned before, a bigger area ratio improves the performance, although not by a significant amount.

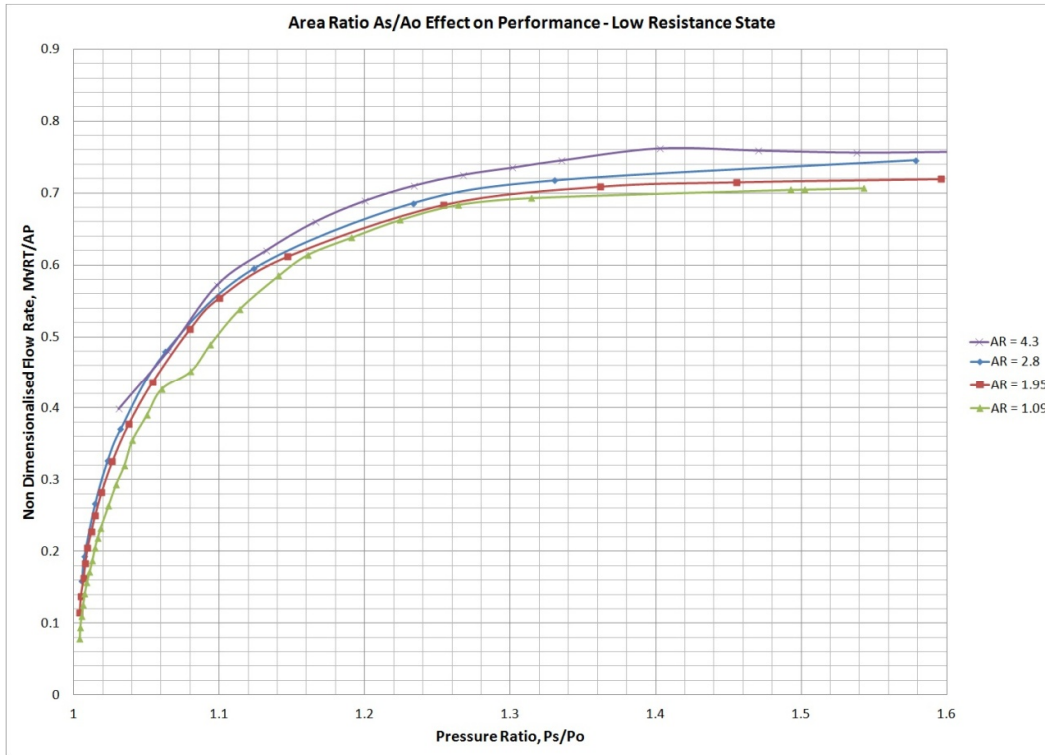


Figure 5.13. - Area Ratio  $A_s/A_o$  Effect on Performance – Low resistance state.

On the contrary as the low resistance state, a smaller area ratio improves the high resistance of the device. Figure 5.14 shows the improvement of the high resistance state with smaller ratios. This difference is even more significant than that shown for the low resistance state. So for design purposes it can be said that the best performance can be achieved by having smaller area ratios, this will have a small impact on the low resistance state, but will have a huge effect in the high resistance state, thus improving the turndown ratio  $T$ , as seen in Figure 5.15, although as decreasing the area ratio, the turndown ratios dipped slightly at very low pressure ratios to later improve as the pressure ratios increase. As mentioned in Chapter 4, low values for the tangential/outlet diameters yield best performance, although in this case the supply area/outlet area ratios are considered.

The turndown ratio curves will tend to be asymptotic once both states, low resistance and high resistance state, reach the critical conditions and become asymptotic as the pressure ratio increases.

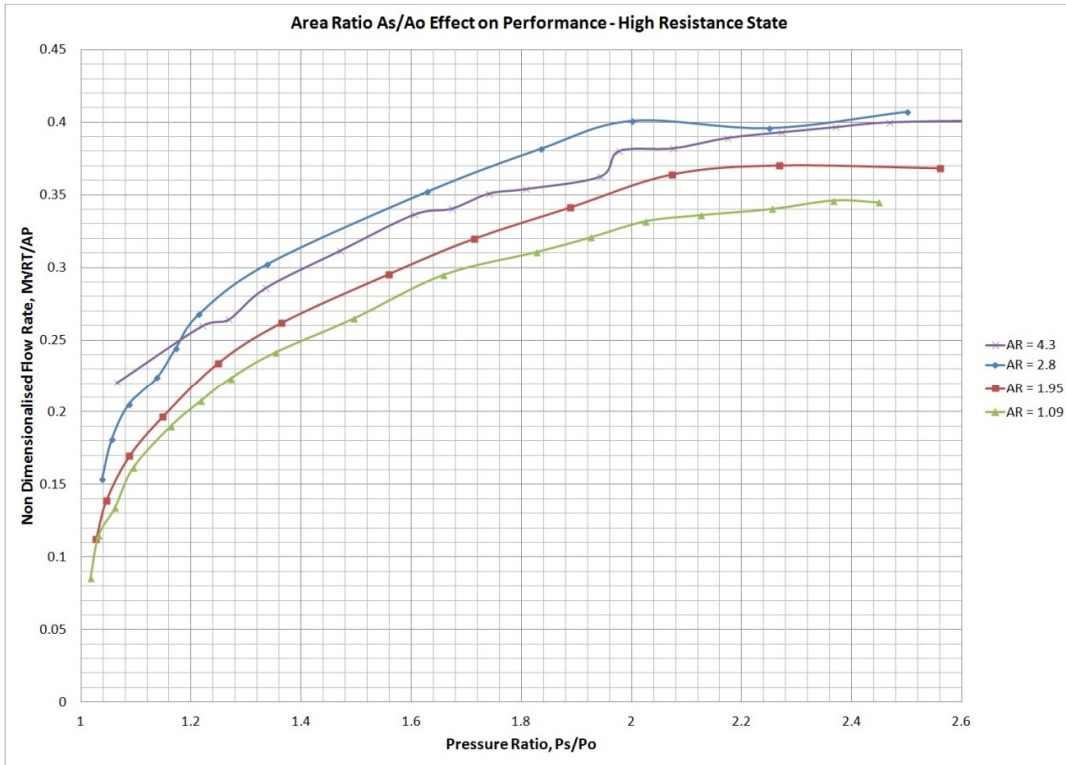


Figure 5.14. - Area Ratio  $A_s/A_o$  Effect on Performance – High resistance state.

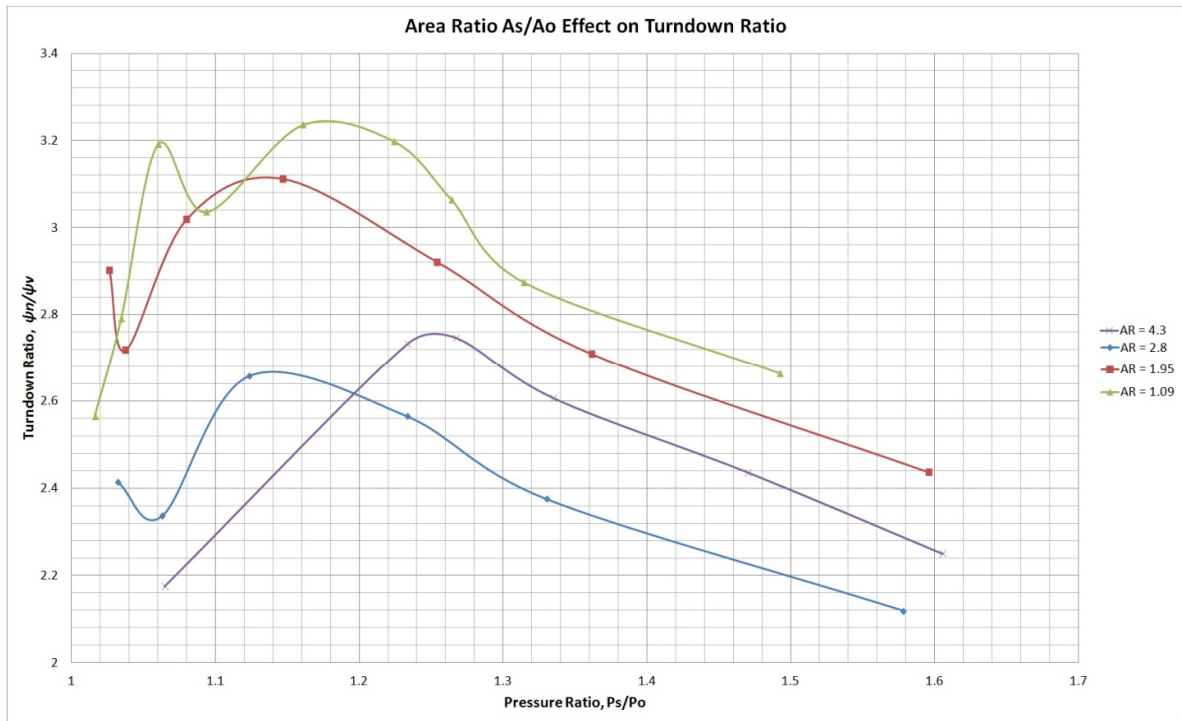


Figure 5.15. - Area Ratio  $A_s/A_o$  Effect on Turndown Ratio.

### 5.3.5 Control Pressures and Flows.

An important function of the Switched Vortex Valve is the capacity to work in two different states, hence, a series of experiments to investigate the amount of flow needed to switch the device from one state to the other were made. These flows, as small as they could be were measured by connecting low range flow rotameters to the outlet of the control ports with a pressure tapping for pressure gauges connections. Given that the pressures in the control ports are quite close to the supply pressures, the pressure gauges for the inlet supply that were not used at the moment of testing, were used to measure these pressures.

Figures 5.16 to 5.19 show the results from the experiments. Figures 5.16 and 5.18 show the percentage of supply flow (supply flow/flow to switch x 100) needed to switch from low state to high state and vice versa, Figures 5.17 and 5.19 show the actual amount of control port flow needed to switch it from low state to high state and vice versa, respectively.

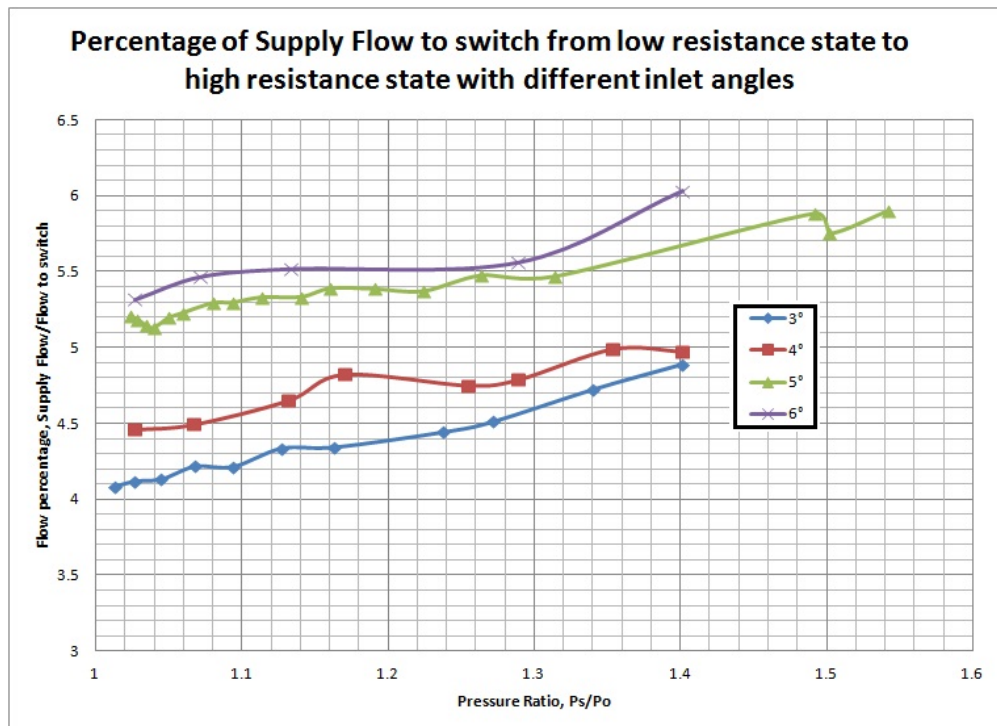


Figure 5.16. - Percentage of supply flow to switch from the low resistance to the high resistance state with different inlet nozzle angles.

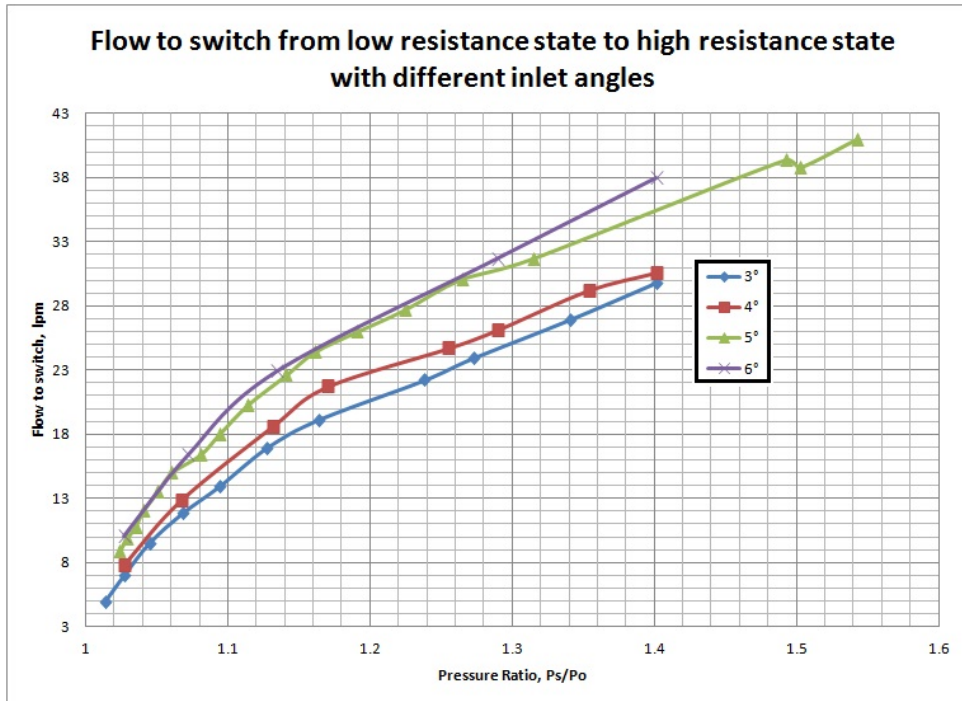


Figure 5.17. - Control port flow needed to switch from the low resistance to the high resistance state with different inlet nozzle angles.

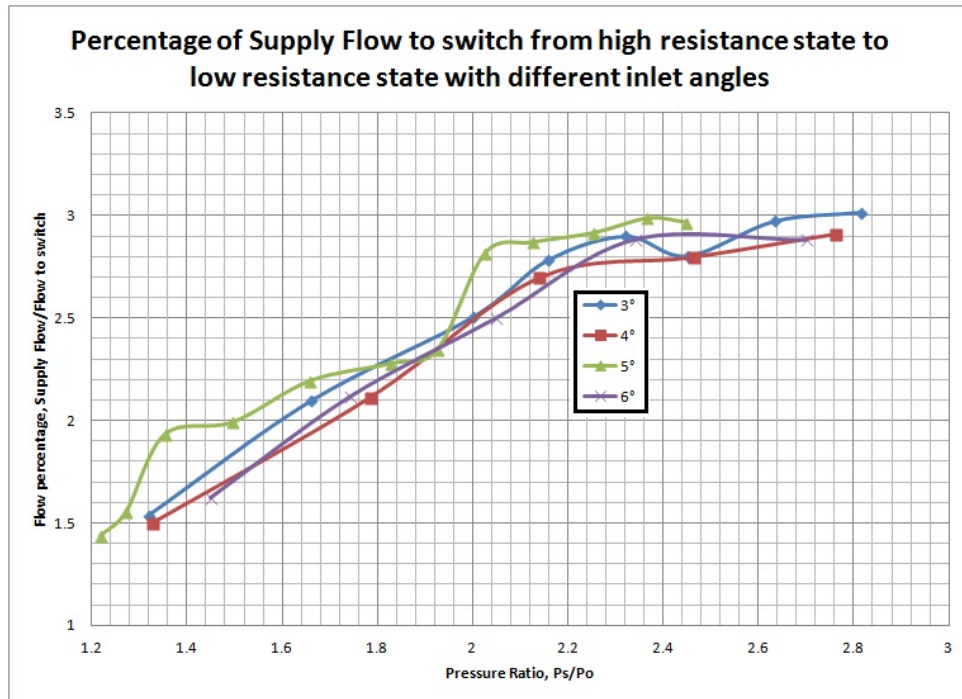


Figure 5.18. - Percentage of supply flow to switch from the high resistance to the low resistance state with different inlet nozzle angles.

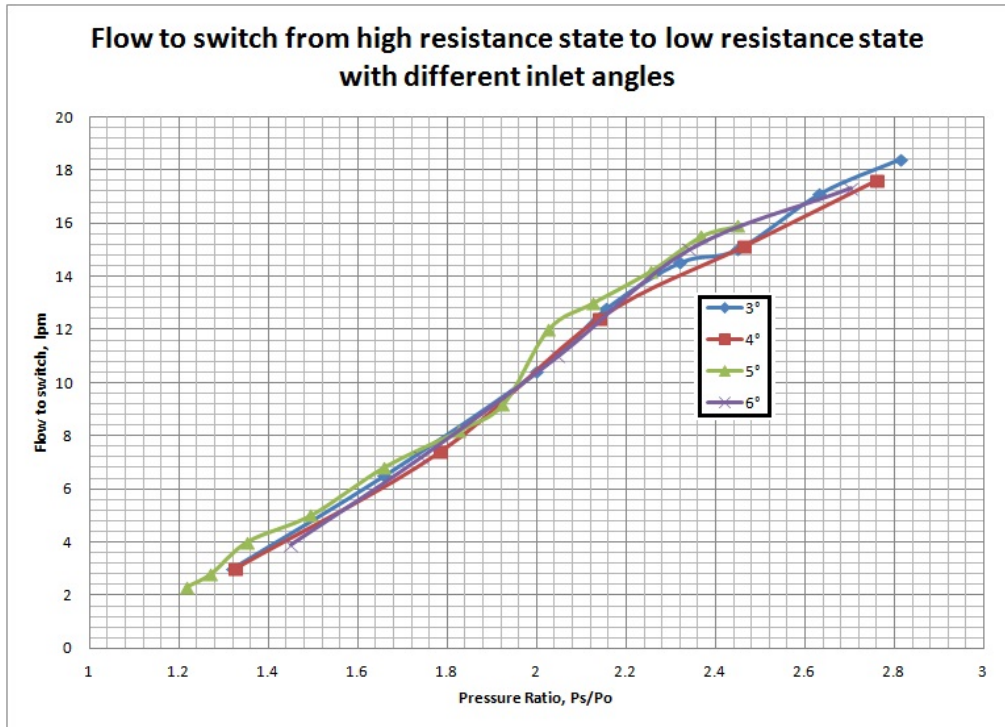


Figure 5.19. - Control Port flow needed to switch from the high resistance to the low resistance state with different inlet nozzle angles.

From Figure 5.16 and Figure 5.17 it is clear that as the angle of the inlet nozzle increases, the amount of flow needed to switch from the low resistance state to the high resistance state is increasing as well, which is mainly due to forcing the incoming air jet to attach to the radial sidewall; increasing the angle will definitely have a greater effect in the amount of flow needed to switch the device, making it more difficult as this increases.

Figure 5.18 and Figure 5.19 show that the percentage of supply needed to switch the device is less than the required to switch it from the low to the high resistance state, which is expected because the angle is again having an effect in inducing the low resistance state, so it needs a slight amount of flow to return to the low resistance state.

It was thought that as the angle of the nozzle increases, the amount of control port flow needed to switch it could be decreasing given that a higher angle increases the attachment effect in the sidewall, however, this is not fully appreciated in the results, or at least not with the significance required to state it conclusively.

### Control Pressure, Outlet flow, and Turndown ratio before and after switching

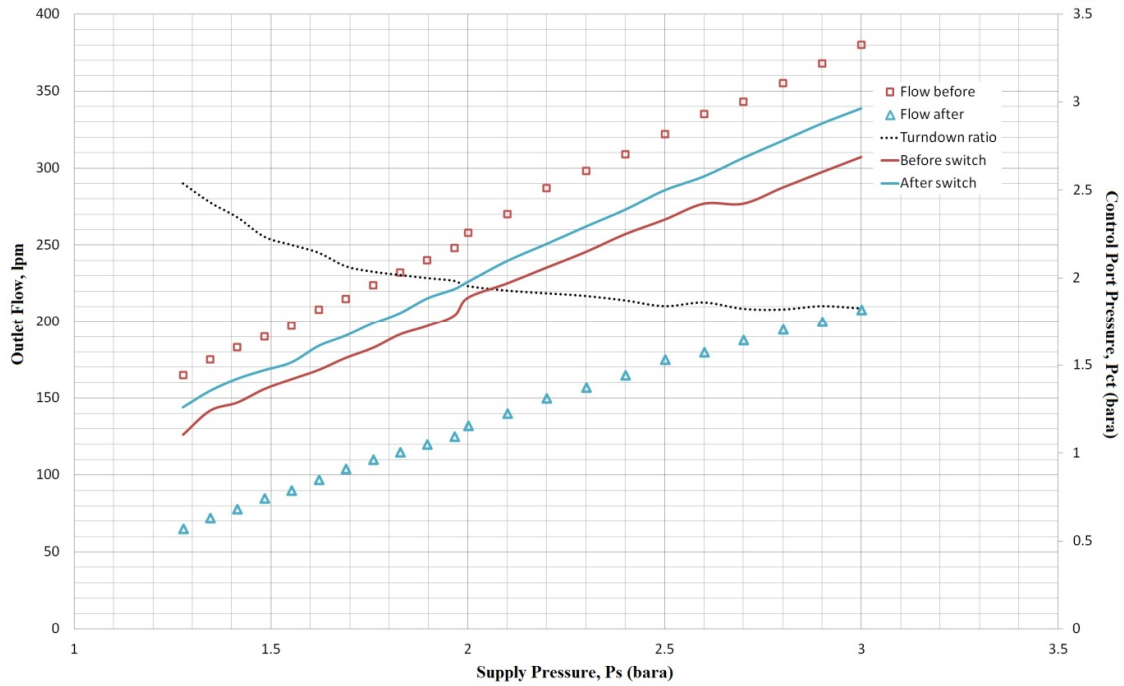


Figure 5.20.- Tangential control port pressure, outlet flow and turndown ratio before and after the switching from low resistance to high resistance state.

Figure 5.20 shows the tangential control port pressure before and after switching from the low resistance to the high resistance state for a 5° inlet nozzle angle. The plot also shows the outlet flow rate before and after the switch and the turndown ratio.

This has great importance as it will be shown in Chapter 7. The flow to control the device is determined by the operating state at which the device is working. If suddenly, as shown in section 5.3.1, there is a leak near the edges of one of the control ports (or both) and the flow leaking is significant then it could inadvertently switch the device from one state to the other or maintaining the device working in the state in which the leak is present i.e. if the leak is in the radial control port, then it could become difficult to switch to the high resistance state or switch it inadvertently from the high resistance state to the low resistance state or vice versa.

### 5.3.6 Splitter Position.

From the different experiments, it is known that the splitter position in the Switched Vortex Valve is an essential part of the device, it can stabilize or destabilize the low resistance state; it has to be positioned in the right position in order for the device to work properly.

Two different experiments were carried out regarding the position of the splitter, the first one involves the rotation of the splitter from its original position, and the second one which involves offsetting the position of the splitter from the original position towards the tangential and the radial channel, as well as increasing and decreasing the parameter  $s$  which is the distance between the inlet nozzle exit and the splitter.

Figure 5.21 shows the rotational experiment geometry, and Figure 5.22 the offsetting experiment.

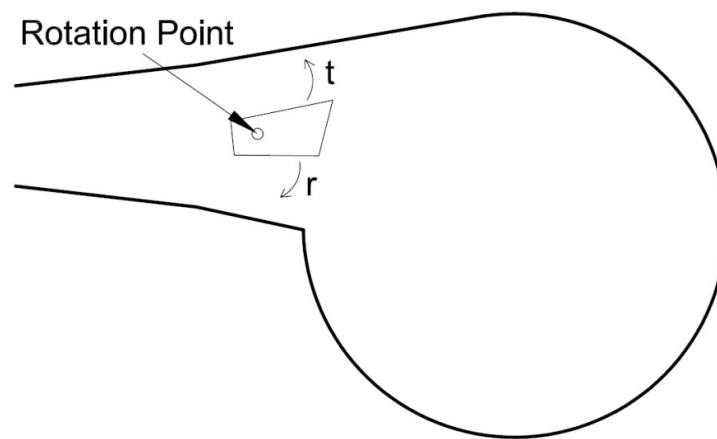


Figure 5.21. - Rotation of the splitter experiment.

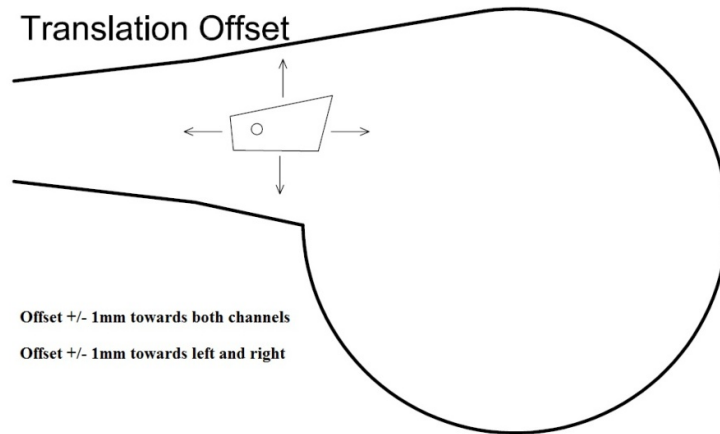


Figure 5.22. - Translation of the splitter experiment.

The device tested was design DC (Appendix A), the experiment consisted on maintaining a fixed inlet supply pressure and rotating the splitter with a screw attached to the pivot or rotation point of the splitter. For the translation of the splitter a fixed inlet pressure was maintained and the middle laminate (with the splitter fixed to it) was translated up/down/left/right. Stability was determined by simply determining if the device was able to maintain the operating state at which it was started up.

The experimental results from the rotation of the splitter determined the original position for the translational experiment. This is determined by the best performance achieved taking into account the change in the width of the tangential channel shown as  $t$  in Figure 5.21. Figure 5.23 shows the outlet flow rate as a function of the tangential channel width  $t$ . The best performance is yielded in the range from 3 to 4 mm, specifically the value of 3.6 mm, which gives a  $a_s/a_t$  ratio value of 0.652 which is close to the value of 0.6 found by Tippetts [34] which is the maximum ratio that is close to the zero entrainment operation point. This range is seen to have the best performance at different inlet pressures. The experiments were only carried out in the low resistance state because the splitter position mostly affects this state, and it is easier to determine whether the device is stable or unstable.

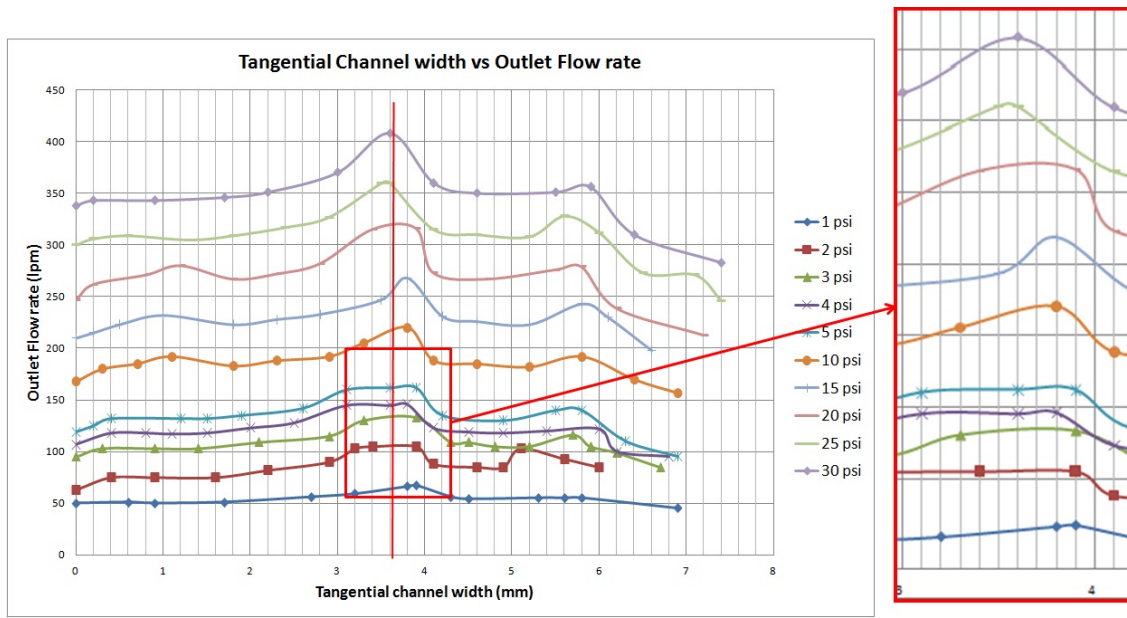


Figure 5.23. - Outlet flow rate as a function of the tangential channel width  $t$ .

Having the value of 3.6 mm for the tangential channel width, the initial position for the translation experiments was decided to be with  $t = 3.6$ mm.

Figure 5.24 and 5.25 show the outlet flow rate as a function of the translation of the splitter (+/-, up/down respectively) in low and high resistance state respectively.

It is shown that in the low resistance state there is no significant effect in the performance as the splitter moves towards the tangential channel, but when the splitter moves toward the radial channel the device starts in the high resistance state but becomes stable once switched to the low resistance state, although with a drop in the performance which is not desirable.

For the high resistance state, Figure 5.25, it is the opposite effect, as the splitter moves toward the tangential channel, the performance drops significantly to the point that the device becomes unstable and switches back to the normal state when the offset is near +0.8 all the way to +1 mm, and stays pretty much unchanged when the splitter moves towards the radial channel.

Both effects are shown throughout a number of inlet pressures, which makes the splitter offset to be insensitive to the pressure.

The flow ratio low/high resistance for the up/down translation of the splitter is shown in Figure 5.26, and it is clear that as the splitter moves towards the tangential channel the flow ratio decreases dramatically from the +0.2 mm value all the way to the +1 mm value. The most stable range is again from -0.2 to +0.2 mm.

Figure 5.27 and 5.28 show the outlet flow rate as a function of the translation of the splitter (+/-, Left/Right respectively) in low and high resistance state respectively. Noise and oscillation at high pressures (20 to 30 psig) can be seen when  $s$  is at its bigger value (-1mm, Left) in the low resistance state; it is also shown that there is no effect in the overall performance of the device when translating the splitter from left to right.

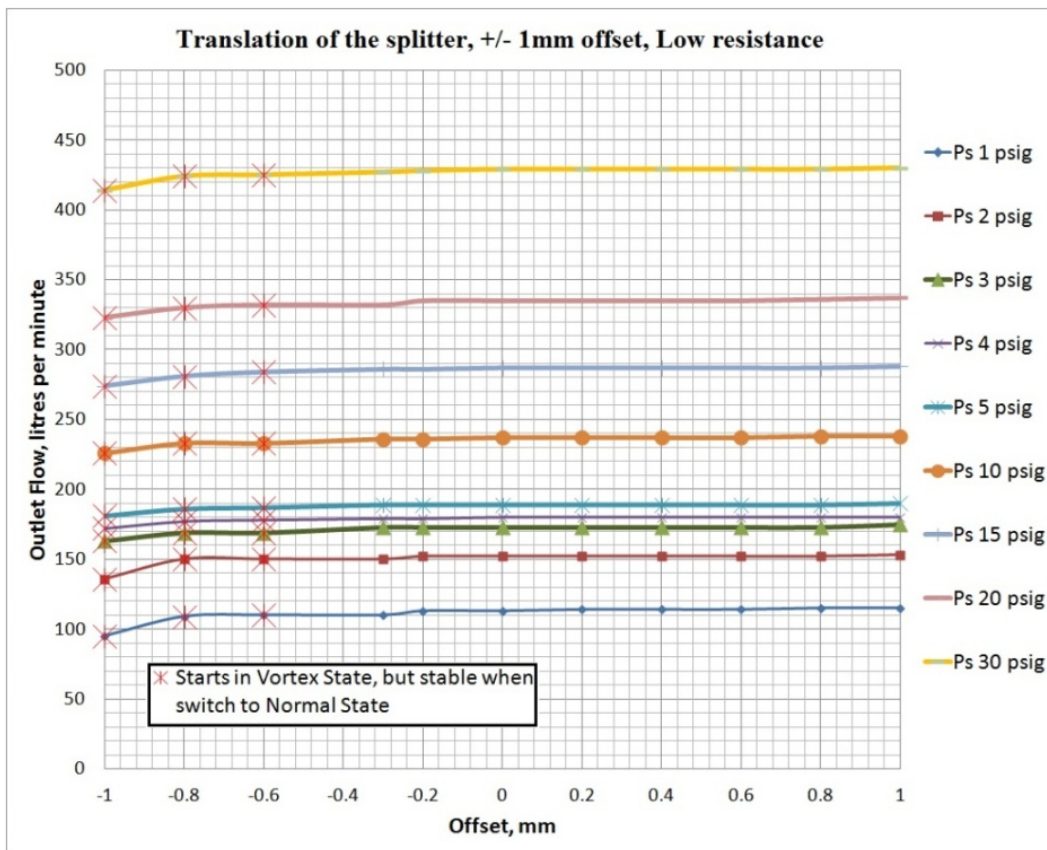


Figure 5.24. - Outlet flow rate as a function of the translation of the splitter up/down in the low resistance state.

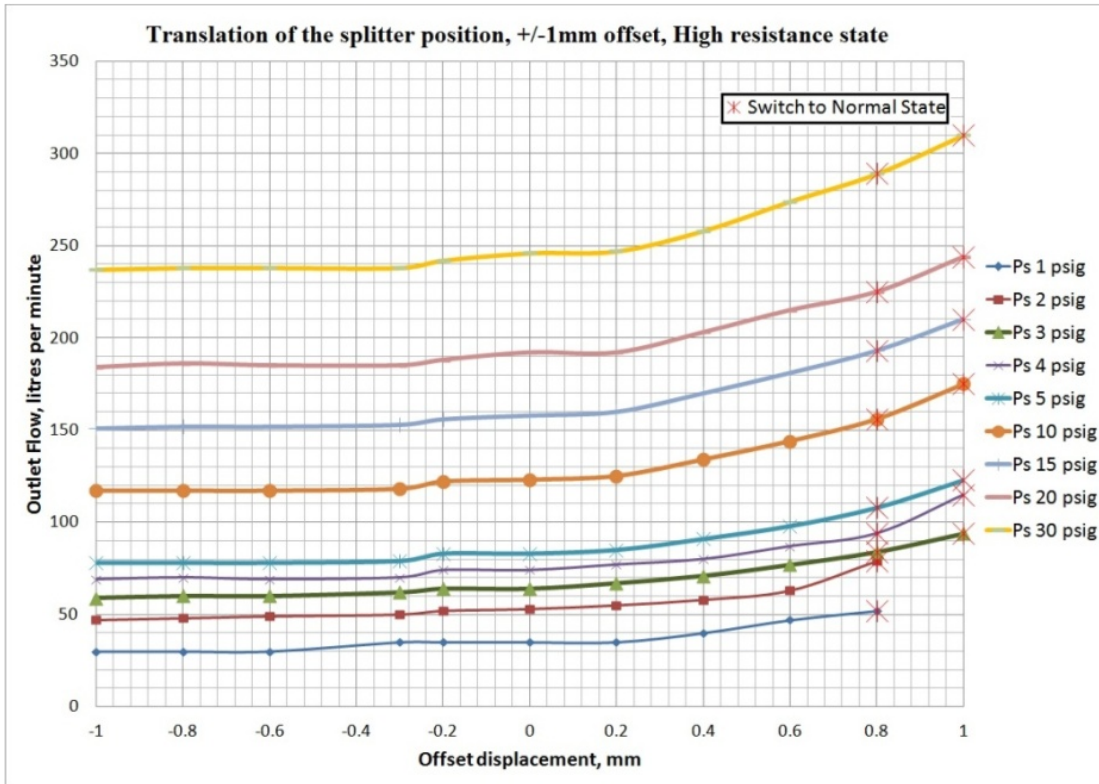


Figure 5.25. - Outlet flow rate as a function of the translation of the splitter up/down in the high resistance state.

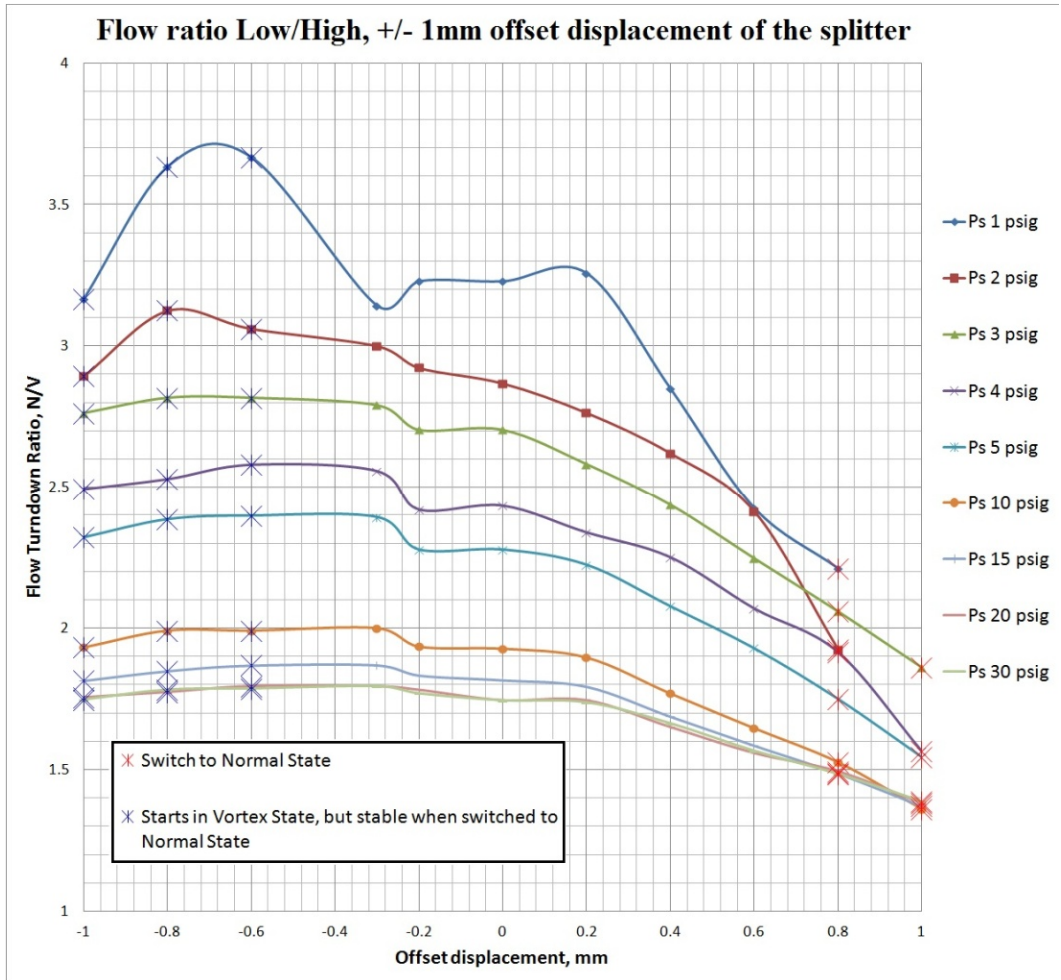


Figure 5.26. - Flow ratio Low/High resistance state as a function of the +/- 1mm offset displacement of the splitter.

**Translation of the splitter position, -1mm (left) to +1mm (right)  
offset displacement, Low resistance state**

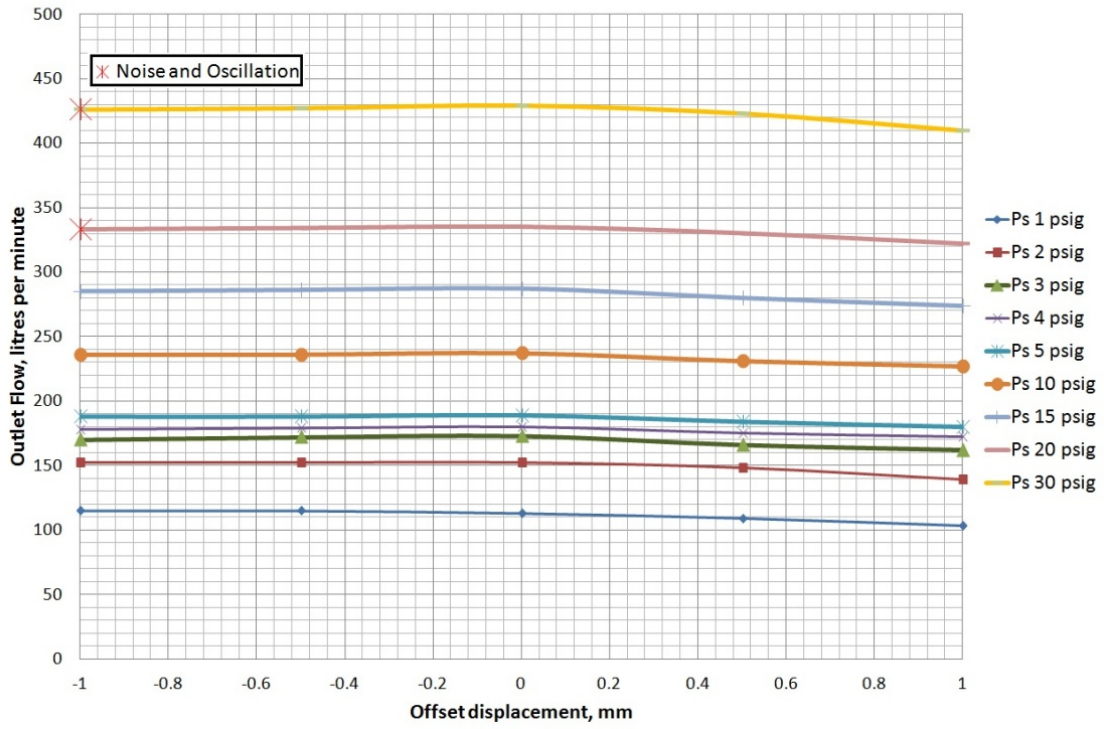


Figure 5.27. - Outlet flow rate as a function of the translation of the splitter left/right in the low resistance state.

**Translation of the splitter position, -1mm (left) to +1mm (right) offset displacement, High resistance state**

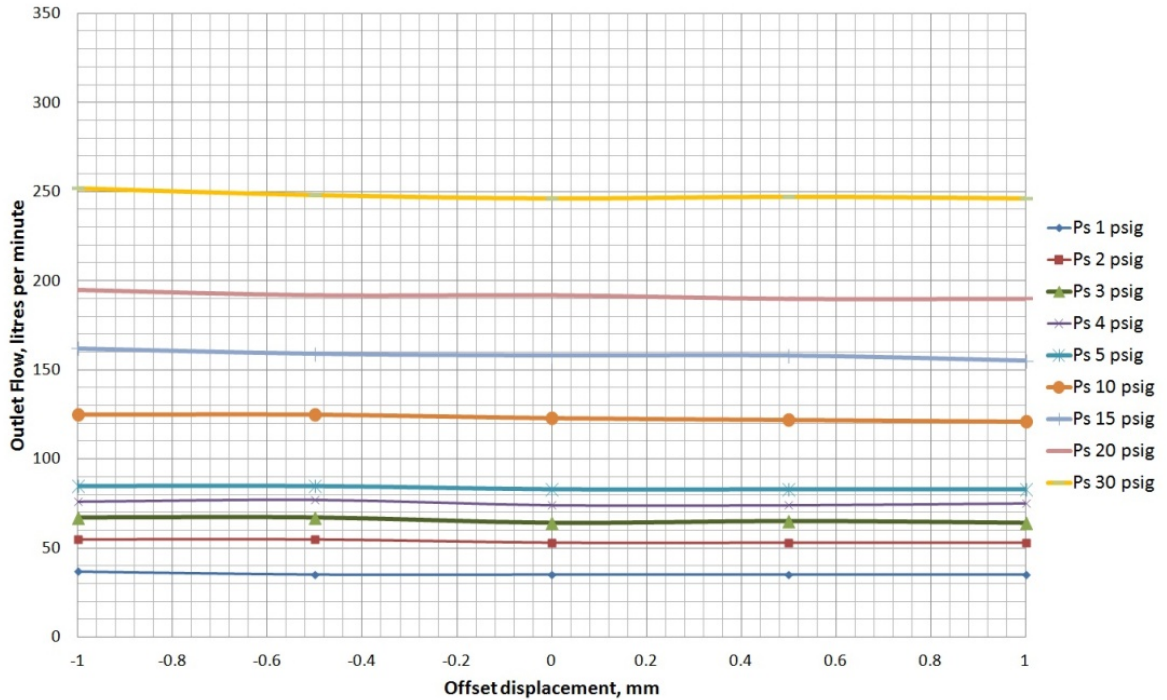


Figure 5.28. - Outlet flow rate as a function of the translation of the splitter left/right in the high resistance state.

The main objective of these tests was to investigate device susceptibility to tolerances of manufacturing i.e. if the manufacture tolerance is within certain range would the device be able to cope with these minuscule but important differences. It could be stated from the results that the device splitter has ample margin to work with. The tolerances in the manufacturing industry are rapidly improving so there would not be a problem to achieve this kind of tolerances.

**5.4 Conclusions.**

Good agreement between the experimental results and the theory has been achieved, there still work to do on this field to fully understand the complexity of these types of devices.

The compressibility effects turns down the previous methodology of analysis of Switched Vortex Valve, specifically when the inlet pressure increases above 1.5 times the outlet pressure, this is when the effects of compressibility starts to become apparent until it reaches the choked point at the critical pressure ratio, and the analysis of the two-holes in series is also of great importance for the study of the Switched Vortex Valves performance, so the isentropic idealisation of a device with a two-hole effective area can be used to analyse the switched vortex valves working with compressible flow in a simple way. It is shown that the experimental data using this type of analysis is very close to the isentropic theory, confirming that the analysis is feasible for these types of devices working with compressible flow.

It is important to state that more studies have to be done regarding leaks within the device, this due to the previously shown instability of the device produced mainly by a leak. This consist of a serious challenge, given the difficulty to measure leaks properly in an experimental rig, so new methods to study the flow allowances due to leaks has to be studied in more detail.

The start-up and the switching point in the low resistance state can be improved by simply forcing the jet to the radial channel as shown in the experiments, this comes with a drawback which was that with the experimental rig, the device was not able to switch to the high resistance state by its own, it had to be switched manually which in some cases can become an issue. From the different inlet angled nozzle (3°, 4°, 5° and 6°) it has been shown that although not significant differences are found between each of the different angles, the angle that proved to have a better performance as well as considering that it did not have a significant effect on the control flow to switch was the 5°.

The control port geometry is again important because further stabilizes or destabilize the device, the value of  $a_c/a_s = 2$  was found to be the value yielding the best performance without showing signs of instabilities, but increasing or decreasing the ratio  $a_c/a_s$  can produce instabilities and a drop in the performance of the device, which is again not ideal. The tangential control port pressure when switching from the low resistance to the high resistance state was measured in order to identify the boundary conditions for a CFD model that is developed at the University of Surrey.

This experiment will help the model to predict the switching pressures in the control port at different inlet pressures and how the model will behave accordingly.

The control switching flow is of great importance in the application given that the device would be dependent of the opening and closing of either control ports. From the experiments no instabilities were detected during the switching, giving the confidence that the switching was actually done by the control port flow.

It could be noted that this switching flow, being intermittent it would be advantageous to other type of devices such as a Vortex Amplifier given that it would only need pulses of air instead of a continuous flow. It was noted as well, that when the device failed independently of reasons, the preferred failure state was the high resistance one. This was shown throughout all the experiments, so this could be a hint to try some monostable devices which only the radial control port exists, this in theory even if the device fails and goes into the high resistance failure mode, the radial control port could be opened to satisfy the cooling needs even in this failure status.

One of the most challenging parts of the device has to be the splitter position, as mentioned before it can completely destabilize the device or affect the performance in both states. Given that the device consists of several plates joined together, it is extremely important to first position the splitter in the preferred position and then run some exploratory experiments to confirm the exact position of the splitter. It is a challenge because a wrong position can affect the results.

From the experiments, the most stable and best performance was achieved near the value of  $t = 3.6 \text{ mm}$ , which corresponded to a value of  $a_s/a_t = 0.652$  which is close to the zero entrainment point. Regarding the translation of the splitter, the allowances can be noted between the values of  $-0.2$  to  $+0.2 \text{ mm}$  in the up/down direction, yielding the better performance and turndown ratio. The turndown ratio does not seem to be greatly affected by the change of splitter position towards the radial channel ( $-$  values) but the start up in the high resistance state does not make it a logical choice given that no significant advantage is provided.

From these experiments it can also be seen that as the tangential width  $t$  becomes shorter, the strength of the vortex in the vortex chamber also decreases.

For the axial outlet geometry and the vortex chamber, a smaller outlet bore will have little impact on the low resistance state but great impact on the high resistance state, so smaller  $a_s/a_o$  ratios will give the best performance and turndown ratios.

The experiments were basically designed for the purpose applications that Rolls-Royce needs; small and compact, stable and able to withstand pressure ratios of a minimum of 2.5 were the principal considerations and the experimental results show that the design can exceedingly cope with the requirements specified.

Overall, the requirements for the application are met. The design DB is compact, stable, yields a good turndown ratio and it operates at the desired pressure ratio without difficulties. The main concern could be the manufacture of the device, given that all the individual components such as inlet geometry, control port width, splitter position have to be within a specific tolerance and the device compactness means that precise manufacture techniques will have to be used.

A better understanding of the effect of the angled type inlet is demonstrated by comparing different angles in order to improve stability and performance. Given that there is little if no information regarding applications of these type of devices working with these type of angled inlets, it could prove useful to further investigate the overall effect of the angled inlet in the Wall Attachment diverter.

Control flow for a bistable device is of great importance. It can be seen that the flow percentages to switch the flow from one state to the other are fairly small, this probably to the fact of the inertia forces inherent of the high pressure air streams. Comparison could be done between the amount of flow needed to switch the same device working with incompressible flow and this work in order to fully appreciate the effects of compressibility in the control ports.

As well as in the control ports, the splitter position has a tremendous effect in the stability and performance of the device. Working with such high pressure compressible streams will have different effects depending on where the splitter is

positioned. For applications in which the device is preferably working in one resistance state, positioning of the splitter could prove useful to achieve such needs.

Dimensions of the vortex chamber and outlet nozzle bore are also discussed here, and as expected from previous compressible work in Vortex throttles mentioned in Chapter 4, it is confirmed that the same geometrical parameters can be applied to these switched vortex valves.

Of particular interest should be to use CFD modelling to first match the model to the experimental data and then as mentioned in Chapter 4 to take the modelling to the high pressures encountered within the jet engine. Such simulations could prove even more useful to fully understand the internal behaviour not only at the same pressure ratios as of the jet engine, but also the same kind of high pressures encountered there.

The Rolls-Royce Switched Vortex Valve design for this specific application is shown in Chapter 7.

## 6

### VORTEX AMPLIFIERS

#### 6.1 Introduction.

The Vortex Amplifier, as mentioned in Chapter 2, is essentially a Vortex Throttle with a radial supply channel. The Vortex Amplifier uses the characteristics of a confined vortex and its effect on the flow into and out of the vortex chamber.

The device operates by varying the strength of a vortex by using a tangential control flow to alter the resistance to a radial supply flow. The main difference between a SVV and a Vortex Amplifier is that the Vortex Amplifier needs a continuous control signal and not a pulse, but it might show better performance than that shown from the vortex throttle.

Applications for this type of devices are from flowmeters for monitoring crude oil production, handling of toxic and corrosive materials and ventilation systems in nuclear plants, and more recently in air control in jet engines [41, 37, 43].

The geometry of the Vortex Amplifier has a significant effect towards its performance. It is critical to identify how geometry will affect the turndown ratio  $T$ , pressure control ratio  $G$ , and the discharge coefficient at the low resistance state  $C_d$ , equations previously described in Chapter 4.

The characteristic curve of a Vortex Amplifier is shown in Figure 6.1 and can be studied by investigating the effect of control flow to the supply flow.

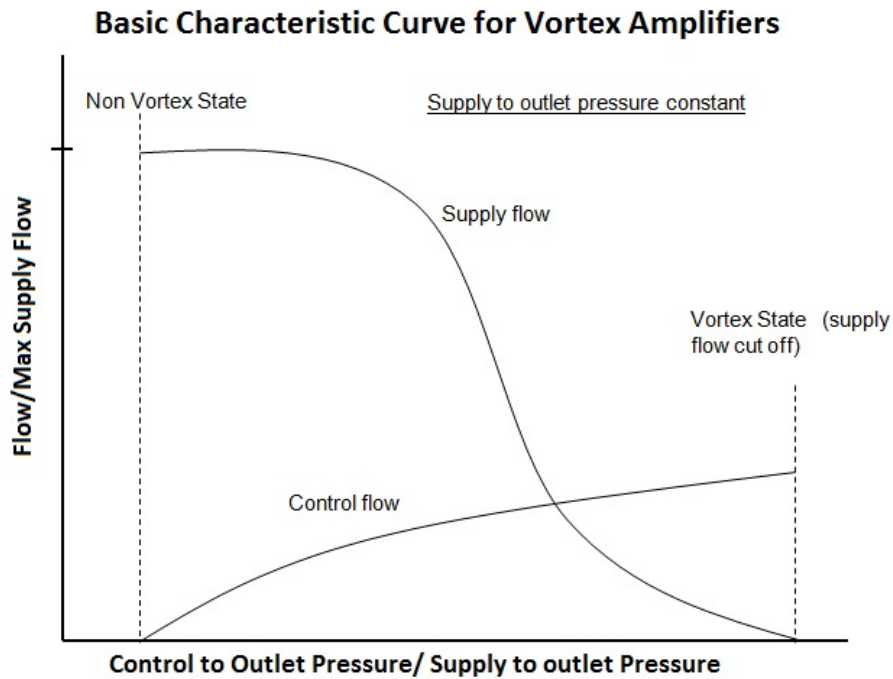


Figure 6.1.- Basic Characteristic Curve for Vortex Amplifiers.

Figure 6.1 indicates that at the low resistance state, no control flow enters the vortex chamber. However, when control flow starts to increase, the supply flow will reduce and at some point, the supply flow is cut off, hence it is called the high resistance state. This is the basic operation and characterization of the Vortex Amplifier, where an increase in control flow will reduce supply flow coming through the device.

From Chapter 5, the switched vortex valve is a laminate device that can be placed in a flat ring. To use the VA for the same application a laminate design is also needed, hence the tests done on this.

The VA can produce similar effects to the SVV by turning down flow but its turndown ratio is much higher than the SVV, so it would need to modulate some of the flow.

For the experiments two different types of geometries were used, the first one is of a laminate design and suited for use in a ring of devices shown here in Figure 6.2, and a second type which has been used more recently for its more compact design which

is shown in Figure 6.3. These type of devices have been devised for applications within the jet engines [33].

This type of geometry has a supply plenum positioned axially to the vortex chamber and this plenum is connected to the vortex chamber with a series of holes, so the air is supplied axially instead of radially to the vortex chamber. The control port remains tangentially connected to the vortex chamber and the outlet remains axially positioned in the vortex chamber. These are useful when supply and outlet are on the same side of the chamber and space constraints are tight.

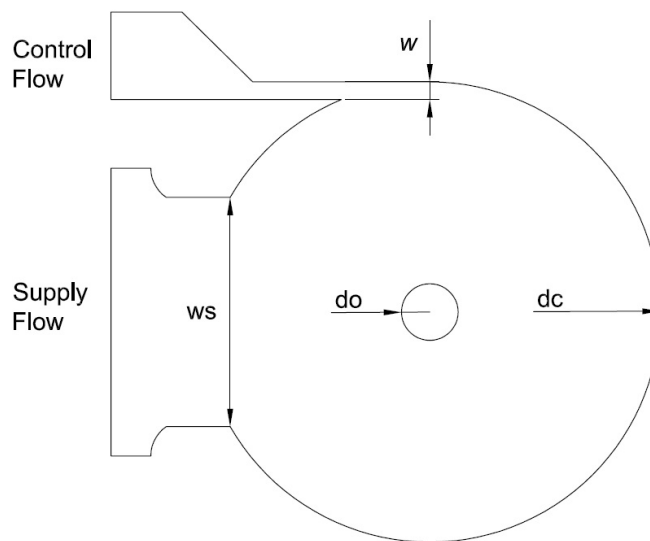


Figure 6.2. - Geometry of generic Vortex Amplifier used.

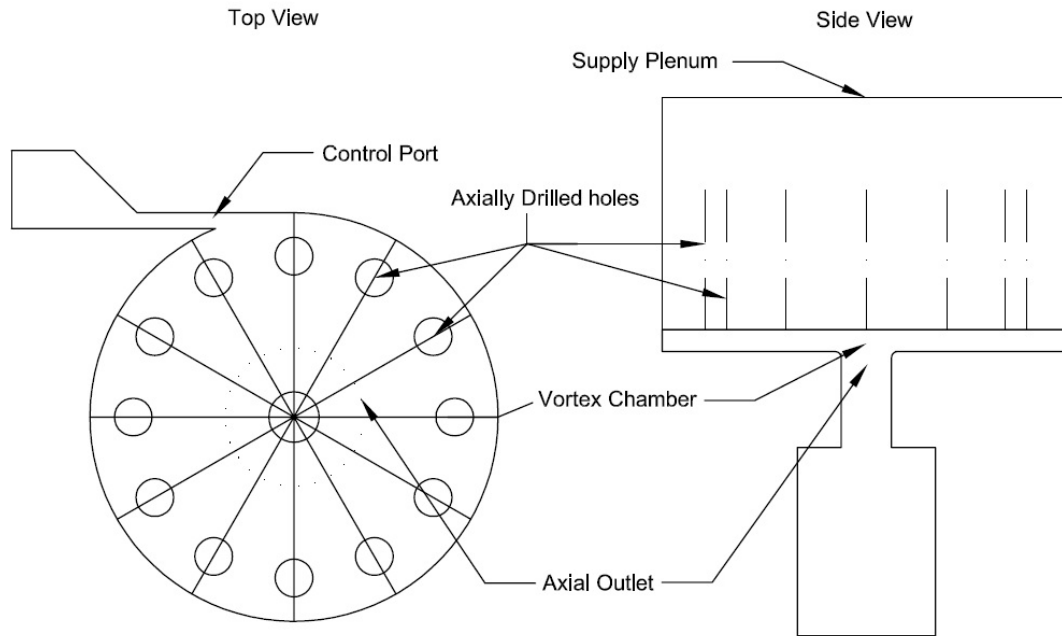


Figure 6.3. - Geometry of Vortex Amplifier compact design.

## 6.2 Experimental Procedure

To test a Vortex Amplifier, the experimental rig consists of two supplies of pressurized air and one inlet, the upstream and downstream part of the Vortex Amplifier respectively.

For the upstream part of the device, one line of pressurized air is connected to the tangential control port, and another line of pressurized air is connected to the inlet supply of the Vortex Amplifier. Both lines with rotameters and pressure gauges to measure flow rates and pressures at any given time.

For the downstream part of the device, the axial outlet is connected to a rotameter and given the small pressures downstream to a manometer.

The same rig can be used for the Vortex Amplifier compact design, just connecting the supply line to the supply plenum of the device.

The rig setup is shown in Figure 6.4.

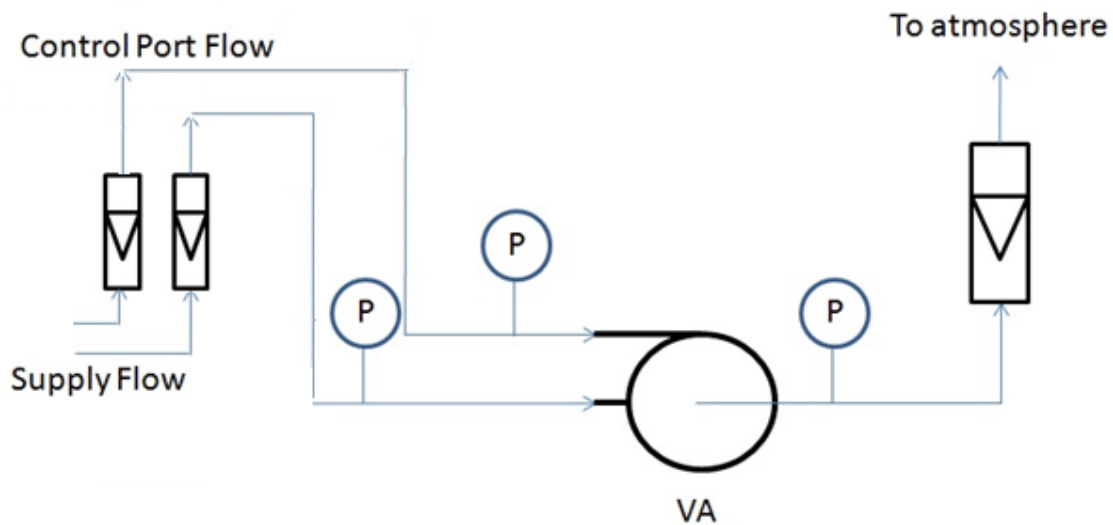


Figure 6.4. - Experimental Rig Setup.

The experiments consisted in using the laminate Vortex Amplifier with constant vortex chamber diameter, and changing the axial outlet diameter and control port width.

Therefore the  $D_{ot}$  and  $D$  parameter will change and it will be easier to identify its effect in the performance parameters  $T$  and  $G$  of the Vortex Amplifier.

Geometry is fully defined in Appendix C.

### 6.3 Experimental Results

From the series of experiments, a systematic increase in the turndown ratio  $T$  is seen as the parameter  $D$  decreases when the experiments were realized at the same supply pressure. This can be seen throughout different supply pressures and different control port widths. Figure 6.5 shows this effect.

This is as expected from the results shown in Chapter 4, in which the turndown ratio is expected to improve as the diameter ratio  $D$  decreases.

From Figure 6.6, a decrease in  $G$  is seen as the  $D_{ot}$  decreases for a particular  $D$ , but  $G$  increases as  $D$  decreases, meaning that the device needs higher control pressures to shutoff the supply flow, so essentially is a trade off between  $D$  and  $G$  and this is further affected by the supply pressure.  $G$  seems to be improved as the supply pressure increases.

The turndown ratio  $T$ , can be said to be affected not as much as the  $G$  parameter, but the supply pressure increase affects the turndown ratio.

There is no much difference between the  $D_{ot}$  values of 5.93 and 2.4 which probably means that the effect of the  $D_{ot}$  parameter would become negligible below these values.

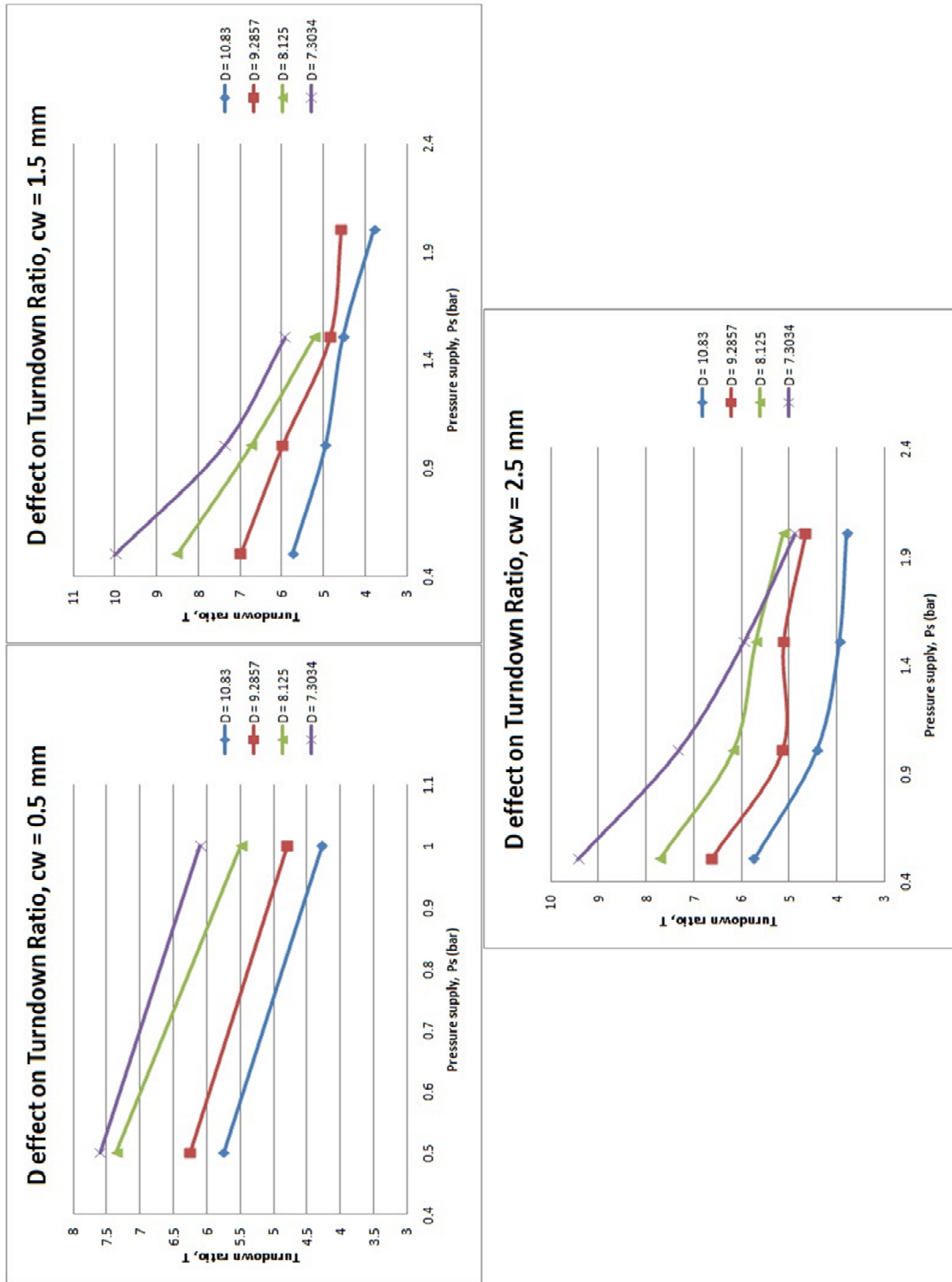


Figure 6.5.- Effect of  $D$  in turndown ratio  $T$  parameter at different supply pressures and different control port widths.

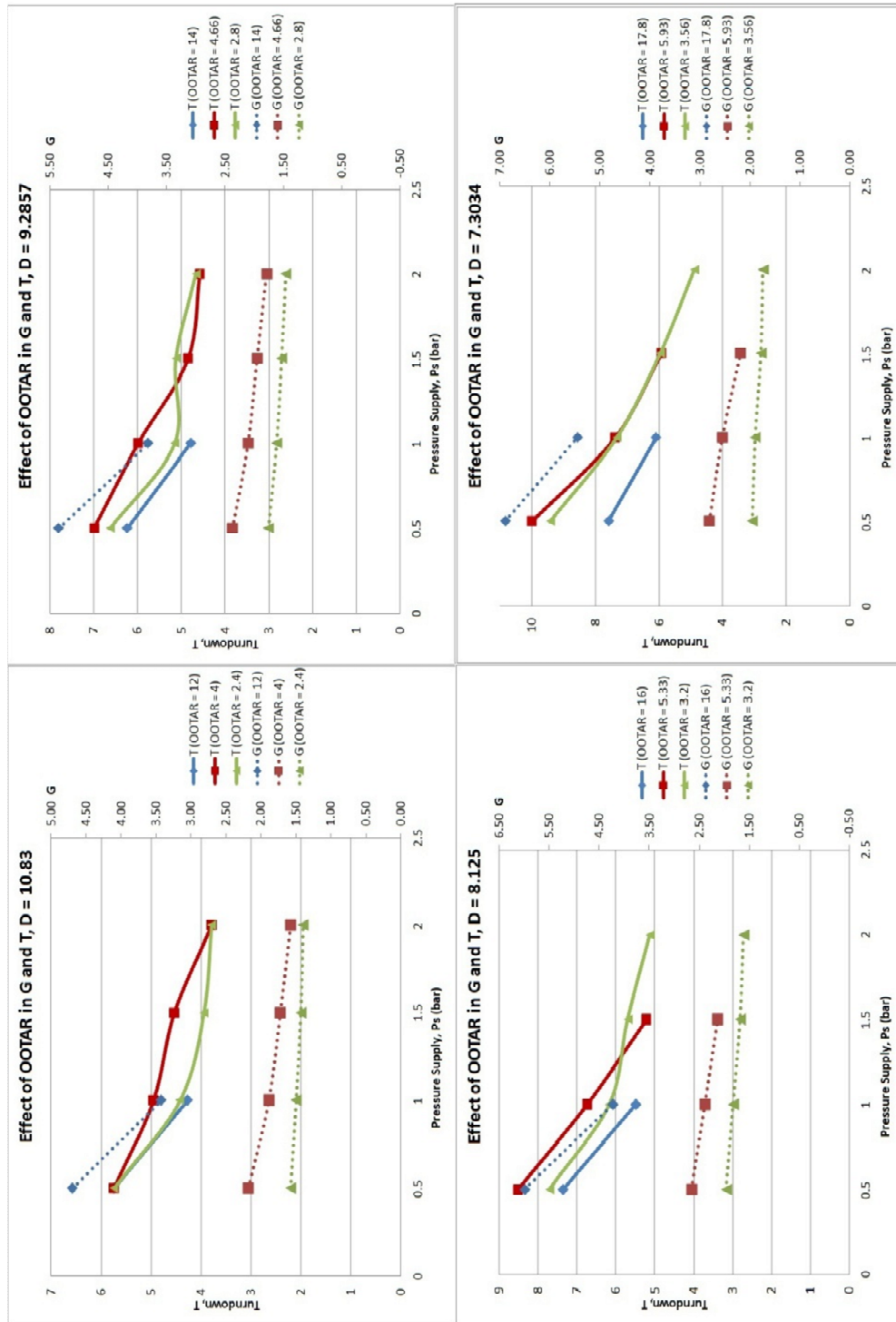


Figure 6.6. - Effect of  $D_{ot}$  in turndown ratio  $T$  and  $G$  parameters at different diameter ratios  $D$ .

## 6.4 Comparison of the Vortex Amplifier with a Vortex Throttle

To be able to properly compare a Vortex Amplifier with a Vortex Throttle, a 5 inch throttle used in the Chapter 4 was converted to a Vortex Amplifier of compact design by adding a supply plenum and a ring of supply feed holes around the periphery of the vortex chamber. Sixteen holes of 0.25 inches were drilled, having an area equivalent to a one inch hole and therefore having an area 3.15 times the largest (14.3 mm) outlet nozzle. As mentioned before this would not affect the resistance in the supply flow path, thus affecting the behaviour. This is shown in Figure 6.7.

From Figure 6.8 there is fairly consistent performance degradation in the high resistance state to a value of 0.83 times the pure throttle (in terms of pressure for the same flow) when comparing the control pressure as a function of the Reynolds number in the tangential control port. More examples are shown in Figure 6.9.

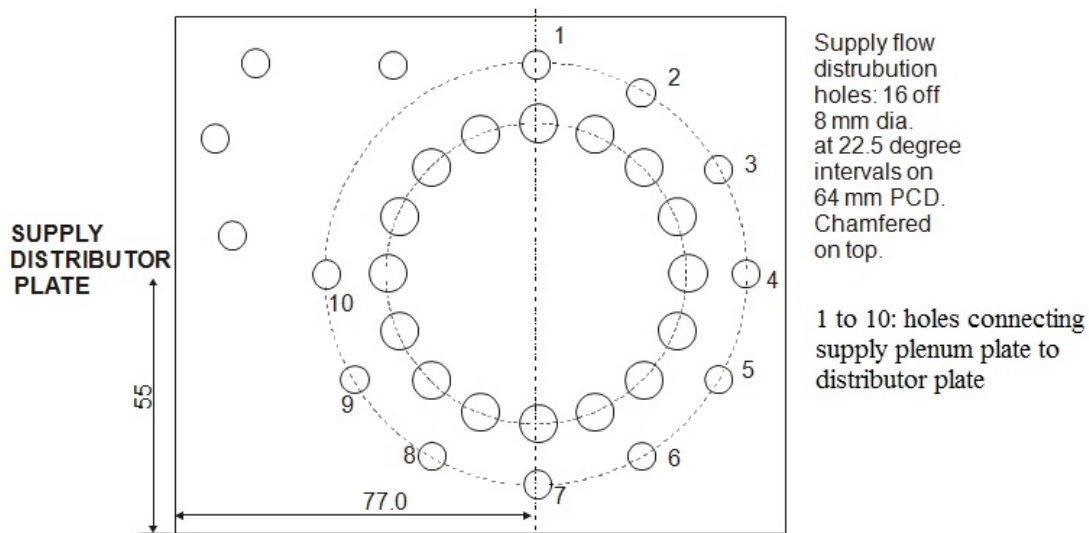


Figure 6.7. - Conversion of a 5 inch Vortex Throttle to a Vortex Amplifier. 16 supply feed holes and 10 connection holes between supply plenum and distributor plate.

Comparison of VT and VA high resistance states, w=18.8mm, outlet bore=14.2875mm

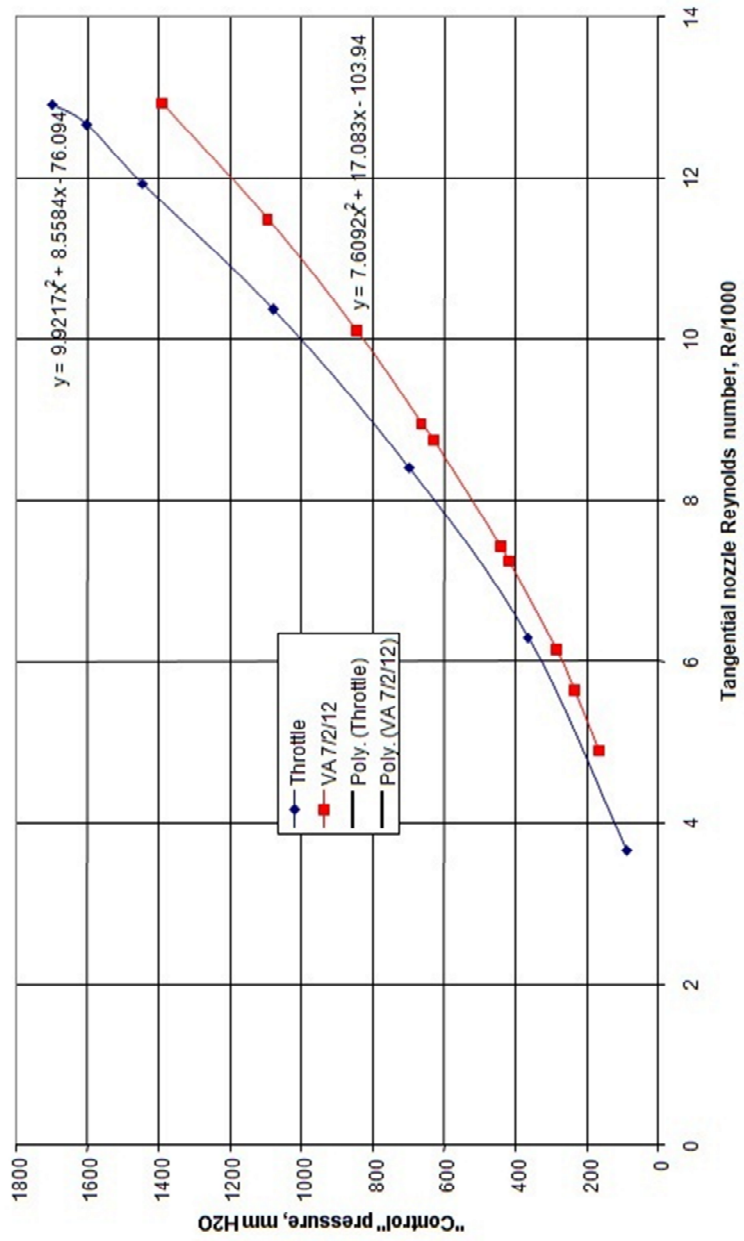


Figure 6.8. - Comparison of Vortex Throttle and Vortex Amplifier high resistance states.

Comparison of VT and VA in high resistance state, w=18.8mm, three outlet bores.

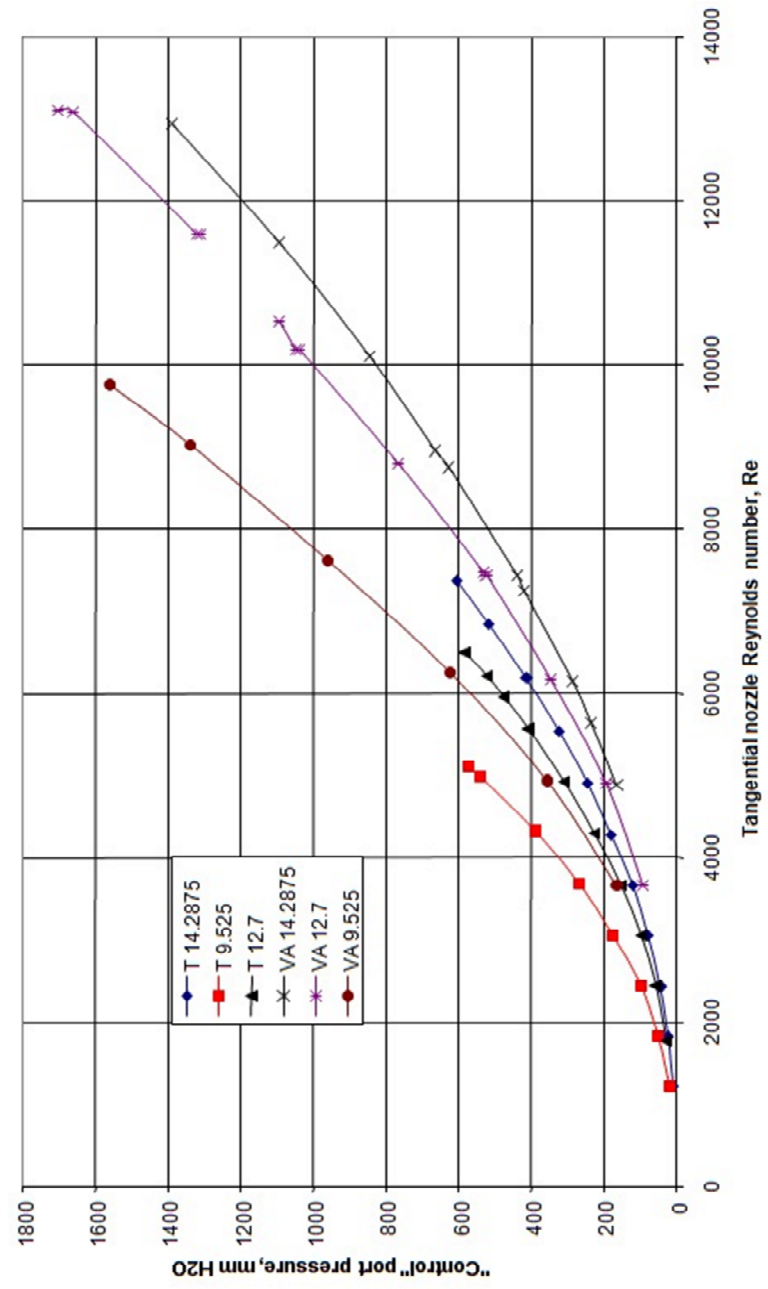


Figure 6.9. - Comparison of Vortex Throttle and Vortex Amplifier high resistance states with three different outlet bores.

## 6.5 Possible Optimization of Vortex Amplifiers with Jet Pumps.

The Jet Pumps are another fluidic device which basic principle is to use the Venturi effect of a converging-diverging nozzle to convert the pressure energy of a motive fluid to kinetic energy in the form of velocity head at the throat of the convergent-divergent nozzle which creates a low pressure zone that draws in and entrains a suction fluid. After passing through the throat of the nozzle, the mixed fluid expands and the velocity is reduced which results in recompressing the mixed fluids by converting the kinetic energy back to pressure energy at the diffuser outlet in accordance to Bernoulli's principle.

### 6.5.1 Circuit Analysis.

A jet pump can be connected to drive the control flow of a vortex amplifier giving useful scope for high turndown ratio but with moderate increases in effective  $G$ . The circuit can be analysed in various degrees of detail and complexity. To simplify the analysis incompressible flow is assumed in non-vortex and vortex states using basic non-dimensional characterising parameters for the Jet Pump and the Vortex Amplifier.

The VA is characterised by  $G$ ,  $T$ , and  $X$  parameters and from these can be defined square-law resistance factors ( $k$ -factors) that represent the normal and vortex states. The  $k$ -factors can be non-dimensionalised by dividing by  $k_o$  the normal state outlet resistance giving three non-dimensional  $k$  factors. These can be regarded as a mathematical gambit to simplify the analysis.

$$G = \frac{(p_c - p_o) \text{ in the high resistance state}}{p_s - p_o}$$

$$T = \frac{q_s \text{ in the low resistance state}}{q_c \text{ in the high resistance state}}$$

$$E_c = \frac{(p_s - p_o)}{(p_c - p_o)} \text{ in the low resistance state}$$

The definitions of  $k_s$ ,  $k_c$ , and  $k_v$  are as follows,

$$K_s = \frac{k_s}{k_o}$$

$$K_c = \frac{k_c}{k_o}$$

$$K_v = \frac{k_v}{k_o}$$

In terms of G, T and X factors,

$$K_s = \frac{1}{X} - 1$$

$$K_s = \frac{T^2}{X}$$

$$K_s = K_v(G - 1)$$

The Jet Pump is defined by  $N$ ,  $M$ ,  $R$  parameters and the analysis can be done in terms of these.

$$N = \frac{(p_o - p_e)}{(p_j - p_o)}$$

$$M = \frac{q_e}{q_j}$$

$$R = \frac{\text{jet pump area}}{\text{jet pump mixing tube area}}$$

where  $p_e$  is the entrainment pressure in the Jet Pump,  $p_j$  is the Jet Pump nozzle pressure,  $q_e$  is the entrained flow and  $q_j$  is the Jet Pump nozzle flow. The Vortex Amplifier, Jet Pump and circuit with relevant variables are shown next,

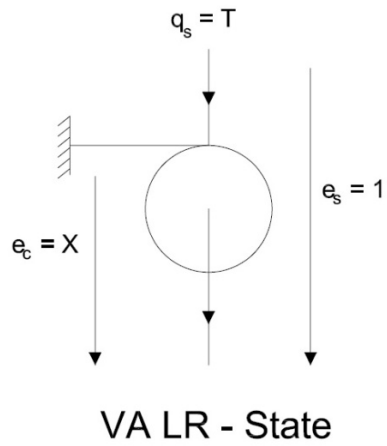


Figure 6.10. - Vortex Amplifier Low resistance state.

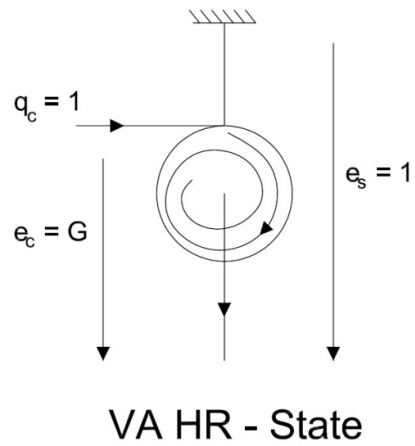
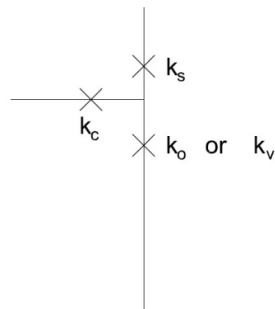
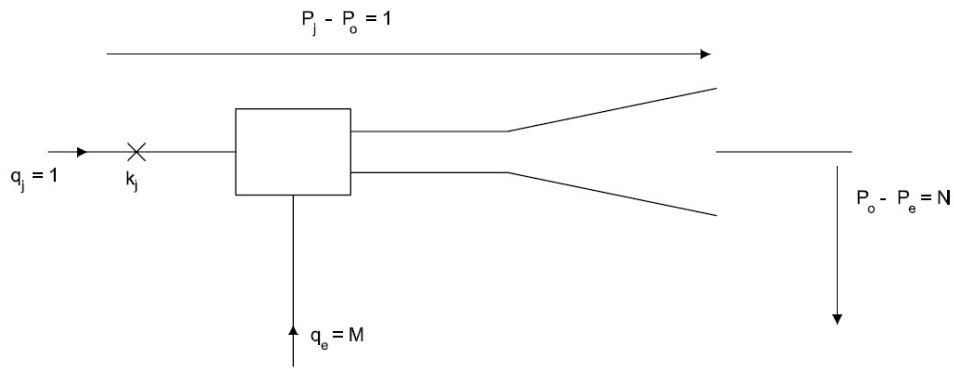


Figure 6.11. - Vortex Amplifier High resistance state.



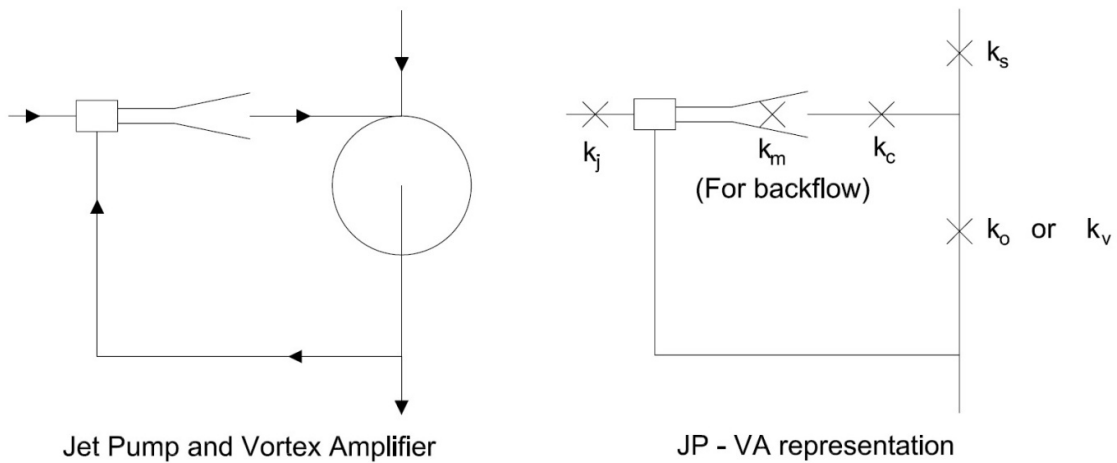
Representation by restrictors

Figure 6.12. - Vortex Amplifier represented by restrictors.



Jet Pump and non-dimensional performance ratios

Figure 6.13. - Jet Pump and non dimensional performance ratios.

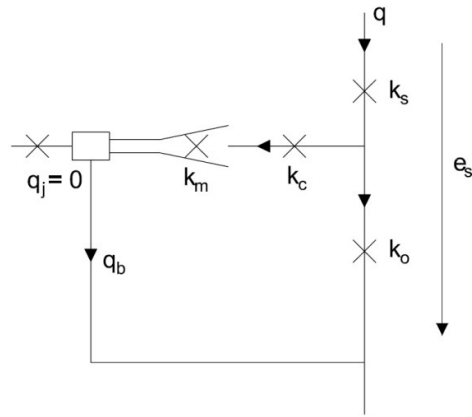


Jet Pump and Vortex Amplifier

JP - VA representation

Figure 6.14. - Jet Pump and Vortex Amplifier.

The resistance  $k_m$  for the Jet Pump is only relevant in the normal state when there is reverse flow through the Jet Pump mixing tube. Basically,  $k_m$  is determined by the bore of the mixing tube. The vortex state outlet resistance of the vortex amplifier is modelled by  $k_v$ , treated mathematically as being completely independent of  $k_c$ , the normal state value.



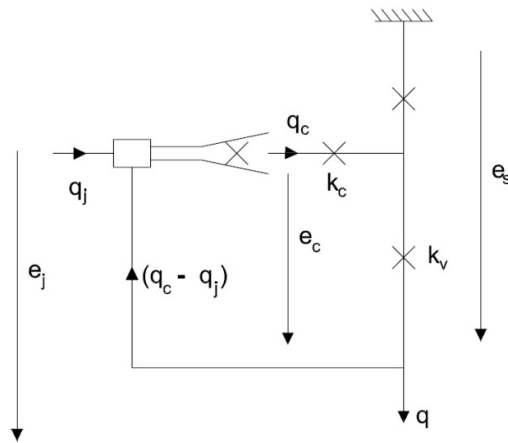
JP - VA LR-state

Figure 6.15. - Jet Pump – Vortex Amplifier in Low resistance state.

From Figure 6.15 two equations can be extracted,

$$e_s = q^2 k_s + q_b^2 (k_m + k_c) \quad \text{Eq. (6.1)}$$

$$q_b^2 (k_m + k_c) = (q - q_b)^2 k_o \quad \text{Eq.(6.2)}$$



JP - VA HR-state

Figure 6.16. - Jet Pump – Vortex Amplifier in High resistance state.

From Figure 6.16, three more equations can be extracted

$$e_s = q_c^2 k_v e_c = G e_s \quad \text{Eq. (6.3)}$$

$$e_c = N(e_j - e_c)(q_c - q_j) = M q_j \quad \text{Eq. (6.4)}$$

$$\therefore q_j = \frac{q_c}{M+1} = \frac{\sqrt{e_s/k_v}}{M+1} \quad \text{Eq. (6.5)}$$

From these equations one can determine the flows, pressures and the Jet Pump sizing as follows.

To find  $T_c$ , which is the circuit turndown ratio

$$T_c = \frac{q}{q_j} \quad \text{Eq. (6.6)}$$

in which  $q_j$  comes from equation 6.5

To find  $q$ , from equation 6.2

$$q - q_b = q_b \sqrt{\frac{k_m + k_c}{k_o}} \quad \text{Eq. (6.7)}$$

$$\therefore q_b = \frac{q}{\left(1 + \sqrt{\frac{k_m + k_c}{k_o}}\right)} \quad \text{Eq. (6.8)}$$

Substituting into equation 6.1 gives,

$$e_s = q^2 k_s + q^2 \frac{1}{\left(1 + \sqrt{\frac{k_m + k_c}{k_o}}\right)^2} (k_m + k_c) \quad \text{Eq. (6.9)}$$

$$\therefore q = \sqrt{\frac{e_s}{\left\{k_s + \frac{(k_m + k_c)}{\left(1 + \sqrt{\frac{k_m + k_c}{k_o}}\right)^2}\right\}}} \quad \text{Eq. (6.10)}$$

$$\therefore T_c = (M + 1) \sqrt{\frac{k_v}{\left\{k_s + \frac{(k_m + k_c)}{\left(1 + \sqrt{\frac{k_m + k_c}{k_o}}\right)^2}\right\}}} \quad \text{Eq. (6.11)}$$

where  $k_m$  depends on Jet Pump size.

The pressures can be obtained from equation 6.4,

$$e_c = N(e_j - e_c)$$

$$e_j = e_c \left( \frac{1}{N} + 1 \right) = e_s G \left( \frac{1}{N} + 1 \right) \quad \text{Eq. (6.12)}$$

therefore  $G$  for circuit

$$G_c = G \left( \frac{1}{N} + 1 \right) \quad \text{Eq. (6.13)}$$

and the Jet Pump sizing by equation 6.12 and 6.5

$$e_j = e_s G \left( \frac{1}{N} + 1 \right)$$

and

$$q_j = \frac{\sqrt{e_s/k_v}}{M + 1}$$

So the Jet Pump nozzle  $k_j$  given by

$$k_j = \frac{e_j}{q_j^2} = \frac{G \left( \frac{1}{N} + 1 \right)}{\left\{ \frac{1}{k_v(M+1)} \right\}} \quad \text{Eq. (6.14)}$$

Simplifying it gives,

$$k_j = k_v G (M + 1) \left( \frac{1}{N} + 1 \right) \quad \text{Eq. (6.15)}$$

From definitions of  $R$  and  $k$ [33],

$$k_m \approx k_j R^2 \quad \text{Eq. (6.16)}$$

So  $k_m$  can be used in equation 5.11 for  $T_c$  or in terms of non dimensional  $K$  coefficients:

$$T_c = (M + 1) \sqrt{\frac{k_v}{k_s + \frac{(k_m + k_c)}{(1 + \sqrt{k_m + k_c})^2}}} \quad \text{Eq. (6.17)}$$

The equations are implemented to calculate the potential  $T_c$  and  $G_c$  values for a properly matched jet pump and vortex amplifier operating in the normal and vortex states. Therefore, given the parameters  $G$ ,  $T$ ,  $X$ ,  $N$ ,  $M$ ,  $R$  and the outlet bore  $d_o$  of the

Vortex Amplifier, one can calculate the bores of the jet nozzle and the mixing tube for the Jet Pump.

### 6.5.2 Design Relationship of the Jet Pump and Vortex Amplifier.

The previous analysis can be used to calculate some examples, using Vortex Amplifier data [33] and characteristics of Jet Pumps[4]. The Vortex Amplifiers used in this analysis are the following:

A:  $d_c = 127 \text{ mm}$ ,  $d_o = 14.2875 \text{ mm}$ ,  $cw = 18.8 \text{ mm}$

B:  $d_c = 127 \text{ mm}$ ,  $d_o = 14.2875 \text{ mm}$ ,  $cw = 7.5 \text{ mm}$

C:  $d_c = 66 \text{ mm}$ ,  $d_o = 8 \text{ mm}$ ,  $cw = 2.5 \text{ mm}$

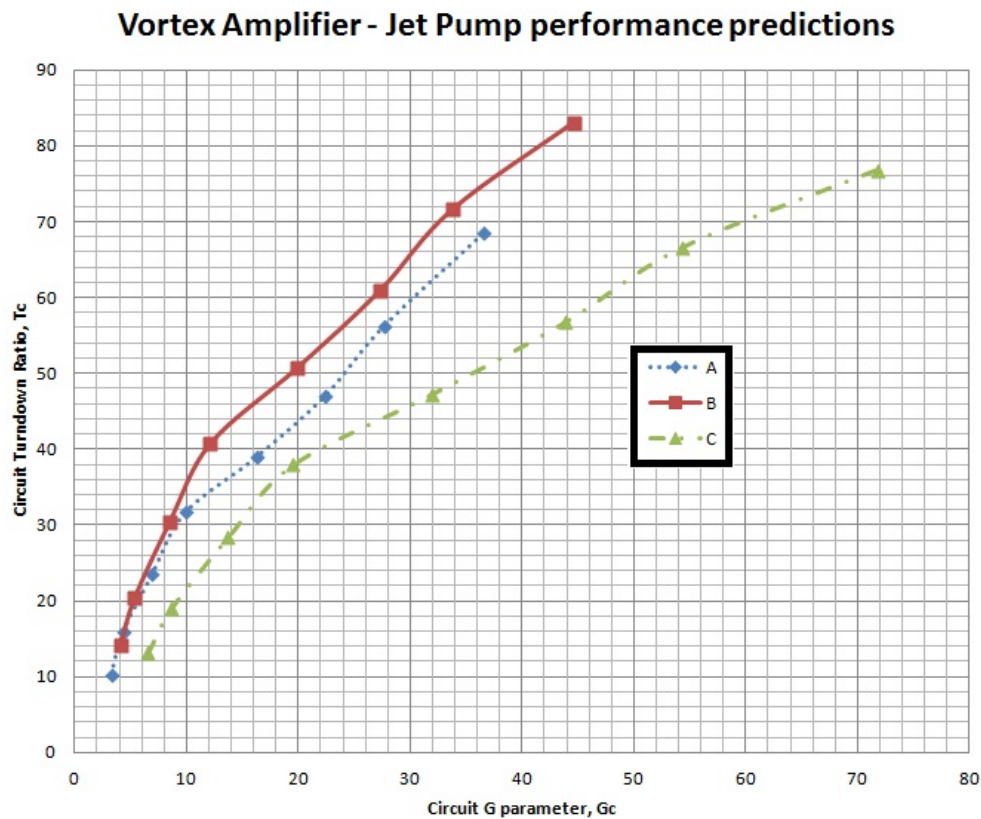


Figure 6.17. - Vortex Amplifier – Jet Pump performance predictions.

Figure 6.17 shows a first approximation to jet pump design to match existing vortex amplifiers.

These results show that a particular choice of Vortex Amplifier, i.e. B, gives better performance for all  $G_c$  values. This choice may not always be the case; other types of Vortex Amplifiers might yield better performance at different  $G_c$  values.

## 6.6 Conclusions.

From the different experiments it was clear that as the pressure of the supply flow increased the parameter  $T$  is affected negatively and as for the parameter  $G$  there is a slight benefit from this. This could be a major issue if to be applied in the engine, given that the changing flight/engine conditions will have a major increase of supply flow in this device, thus a poor turndown ratio would be undesired.

The  $D_{ot}$  value changes is not as paramount as the diameter ratio  $D$  but from the results, a neglect of the  $D_{ot}$  effects where the values drop below 2.4 can be possible.

A constant degradation of 17% between the pure throttle and the Vortex Amplifier can be seen with different outlet bores. This can be explained by the effect of the supply flow from the plenum entering the vortex chamber degrading the vortex created by the control flow.

A possible optimization of the performance of the Vortex Amplifier was analyzed by the use of a Jet Pump in the control port of the Vortex Amplifier, this is intended to increase the effect of the control flow to create a vortex and it will possibly decrease the degradation of the supply flow entering the vortex chamber, thus enhancing the turndown ratio  $T$  and  $G$  performance parameters of the Vortex Amplifier.

The results in this Chapter, match the results from Chapter 4, in which low values of  $D$  can yield better performance.

Overall, it is shown that a Vortex Amplifier could be used for the specified requirements, but it is not clear whether this type of devices would be beneficial to the performance of the engine given its limitations. On the up side, a Vortex Amplifier could be cheaper to build, probably more reliable and easier to manufacture and

install than the Switched Vortex Valve presented on this work, but the performance of the Vortex Amplifier is nowhere near to the capabilities of the SVV: the SVV it is shown to yield the performance needed and its control would only be mere pulses of air from the manifold as in the VA, it is shown that it has a 17% degradation in performance and mainly that as the supply pressure increases the turndown ratio is shown to be decreasing, the SVV does not have that problem given that as the pressure ratio increases the turndown ratio stabilizes becoming an asymptote, theoretically going to even further pressure ratios.

It could be of advantage and it is recommended to do more work relating the Vortex Amplifiers with Jet Pumps. The jet pumps will clearly improve the performance of the VA due to better control supply flow but it is not sure or clear how much big of an improvement the coupling of these two fluidic devices can be.

## ROLLS-ROYCE DESIGN

### 7.1 Introduction.

The final Design DC which will be introduced in the prototype engine for testing will be the shown in Figure 7.1. This device was optimised for the requirements specified by Rolls-Royce and it is expected to go under test for the year of 2013 in which is the prototype engine stage 04.

In this stage, Rolls-Royce will introduce new parts and new technology and one of these new parts will be the Switched Vortex Valve Rim.

This Switched Vortex Valve Rim was designed essentially by Rolls-Royce following the geometry specifications given by the work done in the University of Sheffield. This Rim which is shown in Figure 7.2 is constructed with three individual rim plates which are joined together by a series of threads running around the circumference of the rim plates.

The Rim has 32 individual Switched Vortex Valves; it has two control manifolds, one for the high to low flow resistance and another one for the low to high flow resistance, corresponding to the radial and the tangential control port respectively. The rim uses the 'theory of n' which states that by having smaller devices instead of a bigger one, the device should have the same amount of flow but with a smaller volume. For ' $n \times n$ ' small devices the frontal area is the same as the big one but the volume is only  $1/n$  times that of the big one. This is shown in Figure 7.3.

This Rim will be installed in the turbine IP section as shown in Figure 7.4.

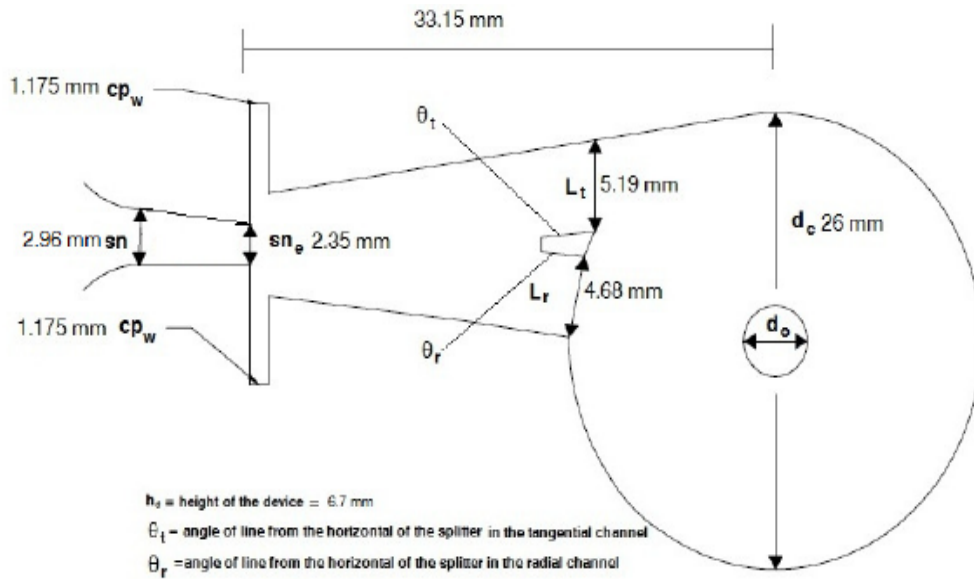


Fig. 7.1. - Final design for testing in the prototype engine. Design C.

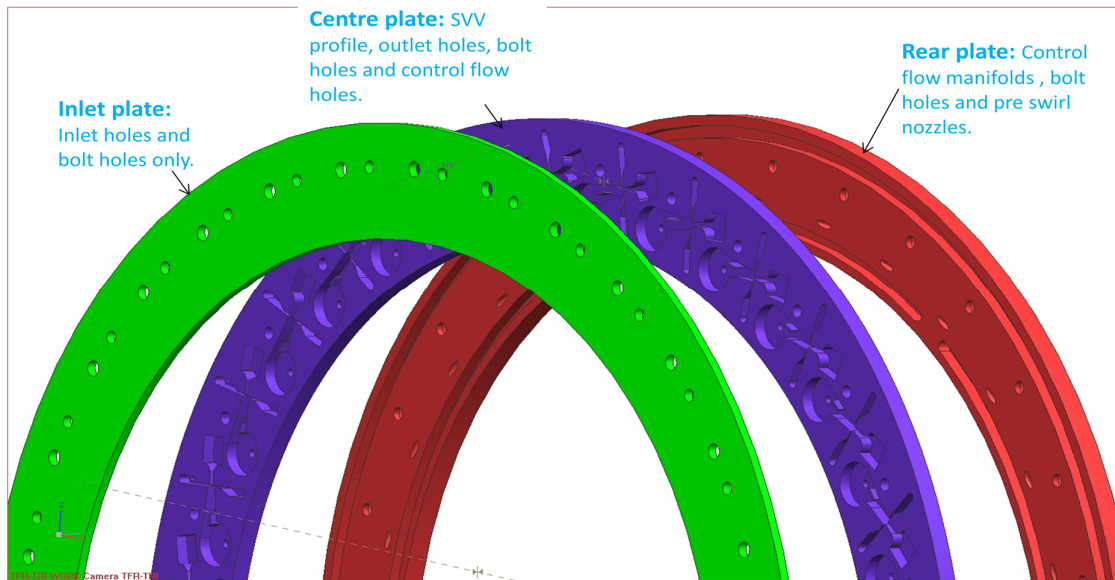


Figure 7.2.- Switched Vortex Valve Rim prototype. Consisting of three separate rim plates.

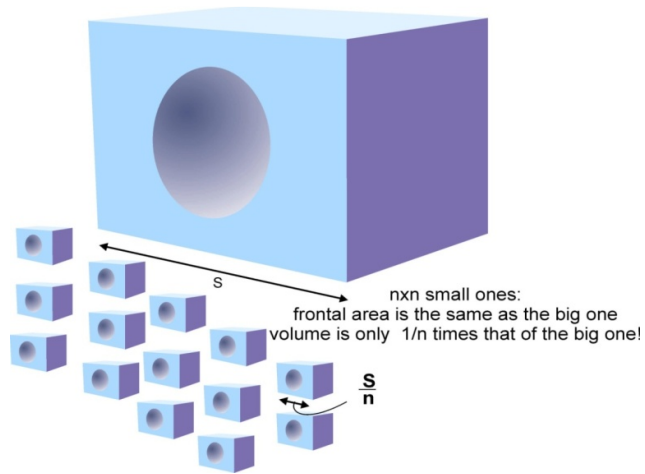


Figure 7.3.- Theory of  $n$  used in the concept of the Switched Vortex Valve Rim.

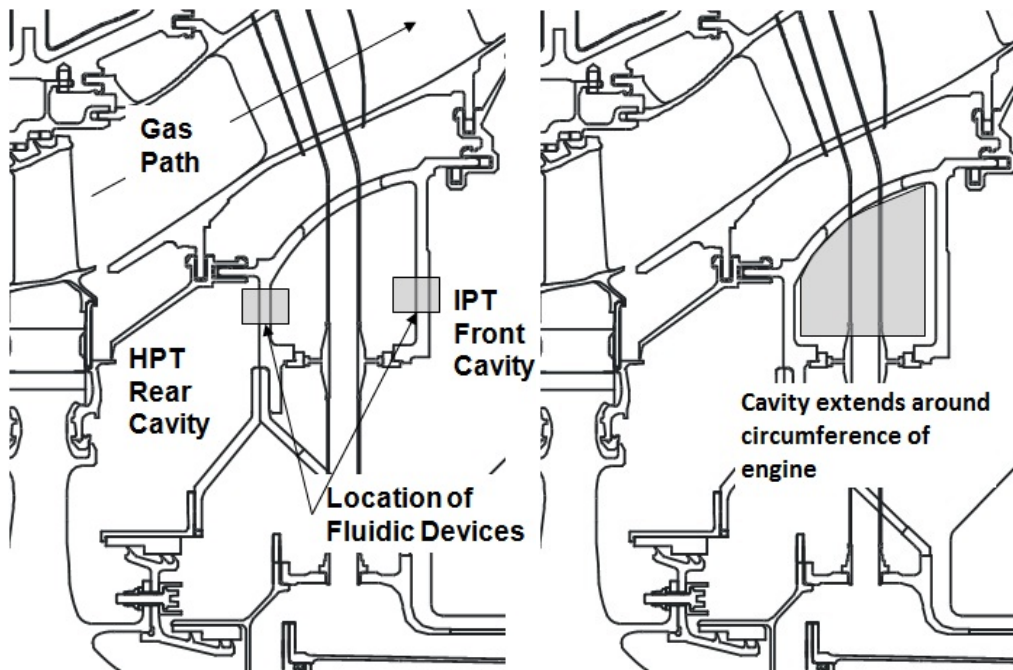


Figure 7.4.- Location of the Switched Vortex Valve Rim. The rim will control the flow of cooling air to the Intermediate Pressure turbine disc and will be mounted on the High Pressure/Intermediate Pressure boundary [43].

## 7.2 Design C – Embedded Device.

As mentioned before, the geometry used for designing the Rim was the Design C with the following geometry specifications:

- $d_{vc}/d_o = 6.5$
- $a_t/a_s = 0.652$
- Coanda throat angle =  $5^\circ$
- $a_s/a_{cp} = 2$

The above mentioned parameters showed the best performance in the experiments. This also means that the device is small and compact, two of the more important requirements for the application of Rim sealing flow, this will ensure that the weight and the space required remains as low as possible but the performance is still as good as expected.

The design was constantly updated according to the experimental results to improve the performance, reduce any instabilities and ensure the correct behaviour of the device under the pressure conditions expected in the jet engine.

## 7.3 Manufacture and Tolerances.

The manufacturing of the Rim will be done by a company outsourced by Rolls-Royce. The technique used was abrasive machining in which material is removed by abrasive particles and the final rim plates were hand polished to ensure that the surface roughness does not affect the overall performance of the device.

The technique used to machine the rim plates, specially the rim plate with the geometry of the Switched Vortex Valve, have to be within less of 1mm of accuracy so there is should not be part of the device that falls outside this tolerance making it viable for the manufacturing.

The tolerances for the splitter position, were given by the experimental results which are shown in Chapter 5. It is important to state that the tolerances are only within the

+/- 1mm, and that any divergence from this tolerances can produce instabilities in the device.

#### **7.4 Switched Vortex Valve Rim.**

The characteristics of the Rim are as follows:

Dimensions of the Rim:

- Inner radius – 257.5 mm
- Outer radius – 342.5 mm
- Thickness – 30 mm

Dimensions of one Switched Vortex Valve (x 32 devices):

- Inlet Diameter – 9 mm
- Outlet Diameter – 4 mm
- Vortex Chamber Diameter – 26 mm
- Device Thickness – 7 mm
- Control Ports Diameter – 9 mm

Figures 7.5 and 7.6 show the Switched Vortex Valve Rim and a close-up of the design layout of the SVV individual component.



Figure 7.5.- SVV Ring Experimental Setup.



Figure 7.6.- SVV Ring Individual components close-up.

## 7.5 Experimental Setup.

The experimental setup was designed in coordination with Rolls-Royce, given that the University of Sheffield will manufacture a rig to run experiments, this had to be done in order to ensure the correct manufacturing and coupling of the experimental rig to the Switched Vortex Valve Rim.

An experimental rig option could involve a rim cap, which could act as a supply manifold, this will ensure that each of the Switched Vortex Valves in the rim, have the same inlet conditions to each other. The control port manifolds can be connected to a similar cap, each experimental cap is connected to a valve this to ensure the ability to run experiments to check for the amount of flow needed to switch the device from one state to the other.

The rim plate containing the outlet will include some experimental probes only in selected outlets, this to monitor the behaviour of the flow and to ensure that no instabilities are present in the whole rim.



Figure 7.7.- SW Ring Experimental Setup.

Further experimental test are encouraged, while the initial test can provide insight to more possible development areas.

## 7.6 Preliminary Experimental Results.

The SW Ring was tested at The University of Sheffield, Buxton's facilities. The tests were conducted to get some preliminary results and to check for overall behaviour and system faults.

The first preliminary test showed that the ring itself presented some leaks. This was expected due to the untested ring design. Overall the results showed fairly good

performance for individual components in the ring. Nonetheless, the overall performance of the ring was poor; this, again, was expected due to lack of significant testing and knowledge about the behaviour of these type of devices working in parallel. It is of importance to state that from the data provided, there is a clear difference between the Non-vortex state and the Vortex state, which indicates promise that the system could work for the required needs.

It is also clear that minor differences in operating conditions affect the behaviour of the individual components in the ring i.e. some individual switched vortex valves do not work the way they are supposed to. These “faulty” behaviours in return, affect the overall performance of the ring.

The data was obtained for each of the 32 devices by measuring outflows in each state for each SVV. One problem was maintaining all the devices switched. The best data to compare with the single SVV would be for the performance of one individual SVV in the ring that switched properly. This is shown in Figure 7.8.

It could be that having multiple devices working in parallel could not be an issue, but the control port manifolds not maintaining their required pressure due to leaks.

As in Chapter 5, the single SVV control port pressures were checked and were at quite high pressures, close to the supply pressure for both states.

In the ring, the control port pressures could not be maintained at the required pressures because air leaked out at the edges. The control port manifolds pressures were checked near the edges of the ring and leaked so the control port manifold pressures dropped below that of a single device leading to the SVV's switching from the Non-vortex state into the vortex state or simply not staying in the vortex state.

Trying to seal the rings with gaskets only tended to make things worse. The poor performance of the ring as a whole was due to not all the individual SVVs being switched correctly.

For the normal state it is shown a difference from the ring to Design C of nearly 25% at a pressure ratio of 1.5, decreasing this difference to 11% for a pressure ratio of 3.

In the vortex state it presents a similar difference from the ring to Design C of almost 22.5% at a pressure ratio of 1.5, decreasing this difference to 9.1% for a pressure ratio of 3.

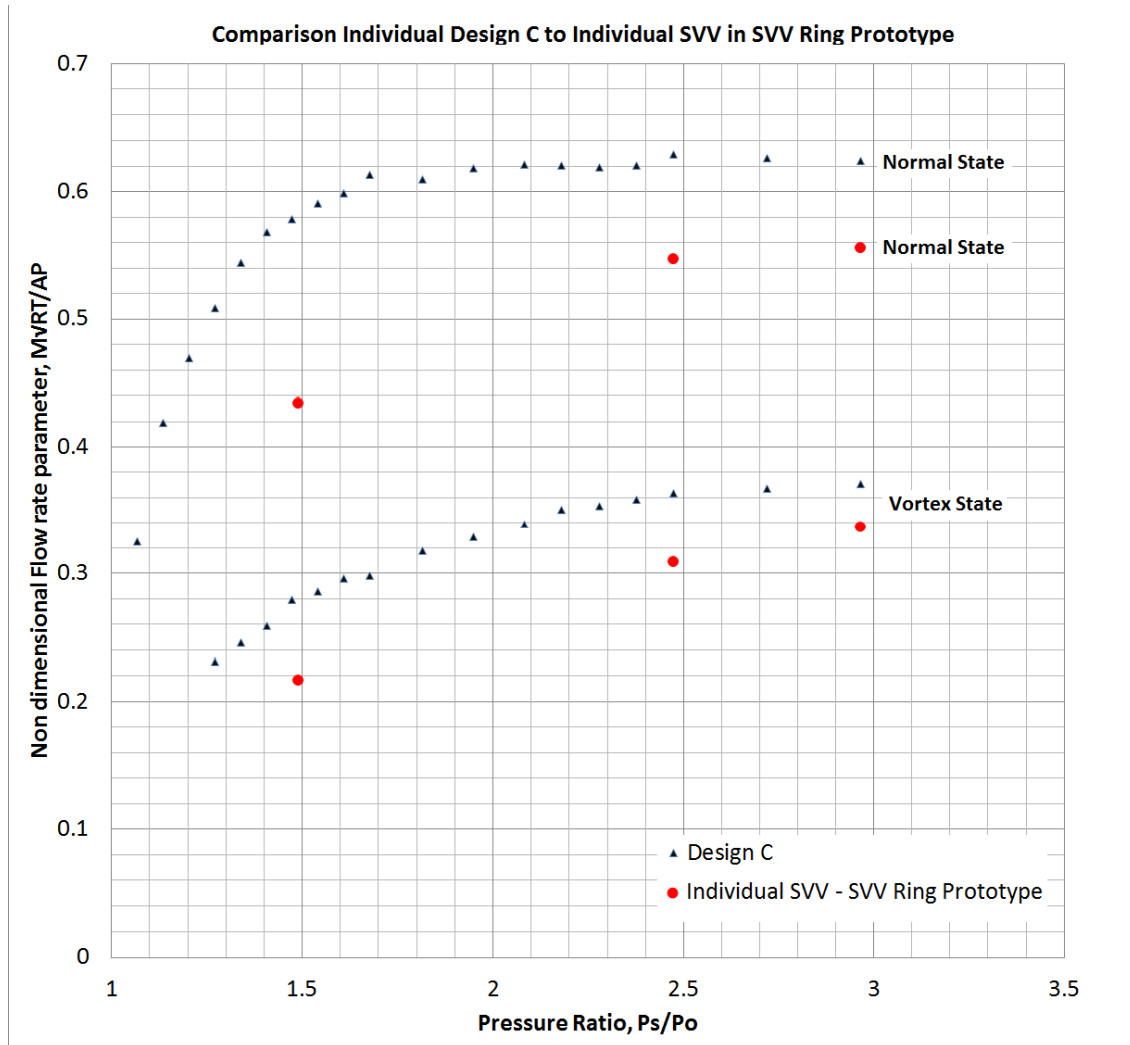


Figure 7.8.- Comparison between the Individual Design C and Individual component (SVV) in the SVV Ring Prototype.

Data from the 32 devices was obtained, not all the devices worked properly. Table 7.1 shows which one of the individual devices presented bad performances in the ring either in the low resistance state or in the high resistance state.

Table 7.1.- 32 devices from SVV Ring – Individual Poor Performance.

Device No.	Poor NS	Poor VS	Device No.	Poor NS	Poor VS	Device No.	Poor NS	Poor VS
1	-	-	11	-	-	21	-	-
2	X	-	12	-	-	22	-	-
3	X	-	13	-	-	23	X	-
4	-	-	14	-	X	24	X	-
5	X	-	15	-	-	25	-	-
6	X	-	16	-	-	26	X	-
7	X	-	17	-	X	27	-	-
8	-	-	18	-	X	28	-	-
9	X	-	19	X	-	29	-	X
10	-	-	20	-	-	30	-	-
31	-	-						
32	-	-						

These poor state performances for some individual components in the SVV ring, relates to the control port pressure issue. Not being able to maintain the required pressure will affect the performance of the device by either making the device to switch from one state to the other at any pressure ratio or not maintaining the required state.

Some of the devices would even switch from the normal to the vortex state and not being able to switch back again to the normal state.

## **7.7 Conclusions.**

The Rim is scheduled to be in the testing bed by mid 2013, this is clearly a great achievement. The experimental results give insight of a good behaviour of the Switched Vortex Valve Rim if the main concerns of maintaining the individual SVVs switched by having a good seal in the control port manifolds and there is no reason to think otherwise but it is of great importance to confirm this by further experiments.

The benefits of introducing this device are, according to Rolls-Royce, to be about 0.13 sfc [24] which in terms of costs represents several million pounds which makes the use of these type of devices to be really appealing and more research funded by Rolls-Royce with the Switched Vortex Valve and other fluidic devices is expected in the following years.

More experiments with the ring will help to identify further areas in which the device could be improved and will show if there is any flaw to the design that was not identified in the current research.

The behaviour of the device has been different when it is used in conjunction with several of the devices, this could also lead to a deeper understanding of the overall behaviour especially in the effect of multiple devices working together as one big device.

The main concern appears to be the control port manifolds pressure. A proper control port flow it is essential for the devices to work in harmony. More tests regarding control port manifolds pressure should be required in order to address this concern.

Furthermore, the results will also be of advantage to the investigation made from the University of Surrey about the computational fluid dynamic simulation of the device, and vice versa. The Rolls-Royce rim prototype could benefit from the results from the CFD research and could be improved even more.

It is important to emphasize that the test could be of great advantage for further research into these types of devices, not only for the Switched Vortex Valves, but also

for the separate devices (Wall-attachment Diverter, Vortex Amplifier) that compose the SVV's.

Overall, close agreement between the individual Design C and the individual SVV component of the ring is shown, especially at higher pressure ratios (3). This could be improved by maintaining the required pressures in the control ports in order to maintain the individual devices of the ring working properly.

The effect of too many individual components working in parallel should be examined further.

## 8

### **CONCLUSIONS AND RECOMMENDATIONS FOR FUTURE WORK**

#### **8.1 Conclusions Overview.**

In this Chapter, conclusions are drawn first from each of the Chapters that compose this thesis and then from a general perspective of the research.

Chapters 1, 2 and 3 are the introduction, literature review and compressible flow theory. Together they give an insight into what a Switched Vortex Valve is, what are the main components of it and how their performance can be obtained and represented properly. Also, it gives some of the history regarding previous experiments.

Chapter 4 explain the basic functionality of the Vortex Throttles and they give an insight into previous experimental data and computational simulation. This chapter provides important parameters that are used in the characterization of the Switched Vortex Valves in the following Chapters. The simulation helps to understand a bit more the behaviour of the fluid within the Vortex Amplifier, the relationship between the angular velocity of the fluid and the pressure drop across the vortex section, and the effect of the axial outlet in the overall performance of the device.

Chapter 5 involves the experimental bulk of this research. Combining the parameters from the previous Chapters to characterize the performance of a series of Switched

Vortex Valves. Different geometries and configurations are tested and implemented into the device. A final device, Device C, complies with the client requirements of space and performance. This Device C, is the one used in the following Chapter 7 for the Rolls-Royce rim prototype.

Chapter 6 combines the Vortex Amplifiers and the Vortex Amplifiers working with Jet Pumps. This chapter also tests some important parameters that are related to characterize the Switched Vortex Valves. Although previous and current experimental data is given for the Vortex Amplifiers, there is no experimental data combining these type of devices with the Jet Pumps. A theoretical analysis of the circuit combining VA's and JP's is given and it shows that good improvement can be achieved by the combination of the two fluidic devices. It could, theoretically, improve the overall performance of the device if properly matched. The Chapter also gives the comparison between the Vortex Amplifiers and the Vortex Throttles. Further research in this area has to be done in order to deepen the behavioural understanding for the device to be implemented in the Switched Vortex Valves or as an independent device working in these type of applications.

Chapter 7 gives a small detailed preview of what the final Switched Vortex Valve Rim will look like. Some of its parameters are drawn out and an experimental setup is explained in order to gather some valuable data for further work and analysis. It also depicts some preliminary experimental results from the ring. These results show that the ring could be working as expected if some concerns are addressed first. The control port manifolds pressure has to be maintained in order for the individual SVVs to work as expected. More tests and experiments are required to first, sort the control port manifold pressure and second to check if the devices working in parallel are also affecting the ring overall behaviour.

## **8.2 Switched Vortex Valves as control devices.**

It is difficult enough to characterize a fluidic device working with incompressible flow. It is a subject that requires further testing and further investigation to fully understand it.

The advances in computer simulation and the different technologies that are always arising, could facilitate the data gathering and most importantly the understanding of the behaviour of the internal flow.

From the point of view of this work, it seems that the Switched Vortex Valve could successfully be applied in these type of applications. Focus on its individual components such as Wall Attachment diverters, Vortex Throttles or Vortex Amplifiers (or even monostable devices) which are simpler devices could be further investigated in order to improve the compressible flow performance of the SVV

By stating the abovementioned, this work has no intention to minimize the important of these type of devices nor the potential applications that it might have in the industrial sector; on the contrary, is to specify that by understanding more about the individual components could improve the overall understanding of the Switched Vortex Valves.

### **8.3 Recommendations for Future Work.**

The current approach for this type of research was more focused in obtaining the results that the client needed than in actually go further and try a 'think-outside-the-box' approach which would be definitely beneficial in the understanding of the Switched Vortex Valves.

Although it is seen that the angled inlet nozzle improves the stability and the overall performance of the device, it also has the drawback of making more difficult the switching from the normal state to the vortex state. More work and special attention to the wall-attachment diverter part of the device is encouraged. Work emphasizing on the control port flows and pressure is also encouraged as these proved to be of high importance during the single SVV testing and the SVV ring as well.

Also, research on monostable devices (one control port) could be useful to further explore the possibilities of these types of devices.

Regarding the Vortex Amplifiers, work related to the addition or pairing of the Vortex Amplifier and the Jet Pumps can be done. If the performance of the Vortex Amplifier can be enhanced by the addition of these small but amazing devices, further improvement in the SW's can be seen in the future.

As said before and mentioned here, the focus on the individual components working with compressible flow would be highly beneficial not only for the applications in which these separate components can be applied, but also from the overall perspective in which the Switched Vortex Valve can be benefitted from the individual focus to its components.

Different applications of control can be experimented not only in the aeronautical industry but nuclear, oil & gas and petrochemical fields can also be benefitted from the particular advantages provided by the different fluidic devices seen in this work. The high-reliability, low (or hardly any) maintenance, low cost, lightness and compactness, are just some of the advantages that these devices offer; advantages that could mean millions of pounds in savings if they are put to good use.

The opportunity could be provided for Masters and PhD students to further develop the current work, expanding it and improving it. Given that the Masters have a tight deadline, they could be handling the individual component research i.e. one Master student doing specific research with bistable or monostable Wall-Attachment diverters working with compressible flow, and other Master student doing specific research with Vortex Amplifiers and Jet Pumps working with compressible flow. Meanwhile, a PhD student could be working hand by hand with the Masters students and gather the data to further develop the Switched Vortex Valves.

# REFERENCES

1. Aljuwayhel, N.F.N., G.F.; Klein, S.A., *Parametric and internal study of the vortex tube using a CFD model*. International Journal of Refrigeration, 2004.
2. ANSYS, *FLUENT Manual*, Sheffield, UK: Flow Europe Ltd.
3. Bartosiewicz, Y.A., Z., *CFD-Experiments Integration in the Evaluation of Six Turbulence Models for Supersonic Ejectors Modeling*, CETC-Varennes: Canada.
4. Bonnington, S.T.K., A.L., *Jet pumps and Ejectors: a state of the art review and bibliography*. 1972: Cranfield, BHRA Fluid Engineering.
5. Boucher, R.T., J.R., *An Investigation Into The Advantages Of Fluidics In Fluid Processing, Part 2, An Inventory Of Power Fluidics*. 1982, Stockholm, Sweden: The Aeronautical Research Institute of Sweden, Aerodynamics Department.
6. Collacott, R.A., *Discharge Coefficients of Chamfered Orifices and Nozzles: An account of a series of experiments carried out in order to determine the effect of chamfer on the variation of discharge coefficient"*. Aircraft Engineering and Aerospace Technology, 1993. **20**(4): p. 112-113.
7. Fisher, M.T., A., *Some Measurements of Liquid Wall Attachment Diverter Valve Characteristics*, in *Paper B.4 3rd. Cranfield Fluidics Conference*. 1968: Turin, Italy.
8. Gibson, M.L., B.E., *Ground Effects on Pressure Fluctuations in the Atmospheric Boundary Layer*. Journal of Fluid Mechanics, 1978(86): p. 491-511.
9. Jawarneh, A.M.S., P.; Vatisas, G.H., *Experimental and Analytical Study of the Pressure Drop Across a Double-Outlet Vortex Chamber*. Journal of Fluids Engineering, 2007. **129**.
10. King, C.f., *Vortex Amplifier Internal Geometry and its Effect on Performance*. International Journal of Heat and Fluid Flow, 1985. **6**(3): p. 160-170.
11. King, C.F.S., N., *Low Control Pressure Ratio Vortex Amplifiers and Their Applications in Nuclear Plants*. Fluidics Quarterly, 1978. **10**(3): p. 29-48.
12. King, D., Inderwildi, O., *Sealing technologies - signed, sealed and delivering emissions savings*. Aviation and the Environment, 04-09: p. 44-48.
13. Launder, B.E.S., D.B., *Lectures in Mathematical Models of Turbulence*. 1972, London, England: Academic Press.
14. Lien, F.S.L., M.A., *Assessment of Turbulent Transport Models Including Nonlinear RNG Eddy-Viscosity Formulation and Second-Moment Closure*. Computer Fluids, 1994. **23**(8): p. 983-1004.
15. Miller, D.S., *Compressible Internal Flow*. BHRA Fluid Engineering Series. Vol. 10. 1984, Cranfield, UK: British Hydromechanics Research Association.
16. Morgan, B.D., K.; Lele, S.K., *Large-Eddy and RANS Simulations of a Normal Shock Train in a Constant-Area Isolator*, in *50th AIAA Aerospace Sciences Meeting*. 2012, American Institute of Aeronautics and Astronautics: Nashville, Tennessee.
17. NATS, *National Aerospace Technology Strategy*. 2010: London, UK.
18. NATS, *Implementation Report*. 2010: London, UK.

19. Pai, S., *Introduction to the Theory of Compressible Flow*. 1959, New York: D. Van Nostrand Company.
20. Priestman, G.H., *A Study of Vortex Throttle Part 1: Experimental & Part 2: Viscid Flow Analysis*. Proc. Instn. Mech. Engrs., 1987. 201(C5).
21. Rolls-Royce, *The Jet Engine*. 2005, London: Rolls-Royce Technical Publications. 288.
22. Rolls-Royce, *Trent 1000*, in *Newsletter*. March 2010, Rolls-Royce.
23. Rolls-Royce, *Trent XWB*, in *Newsletter*. May 2009, Rolls-Royce.
24. Rolls-Royce, *Collaboration Agreement - Application of Fluidic Technology to gas turbine secondary air systems (FLUTE)*. 2007.
25. Rolls-Royce, *Market Outlook 2009, Forecast 2009 - 2028*. 2009: Rolls-Royce plc.
26. Ruh Goh, Y., *Multiphase Flow in the Switched Vortex Valve and Related Devices*, in *Chemical and Process Engineering*. 1996, The University of Sheffield: Sheffield. p. 220.
27. Saunders, D.H., *The Development of a Vortex Valve for Use as a Flow Control Valve*. Proc. Symp. Power Fluidics for Process Control, Instr. Measurement and Control, 1973.
28. Sayma, A., *Computational Fluid Dynamics*. 2009: Ventus Publishing ApS.
29. Shih, T.H.L., W.W.; Shabbir, A.; Yang, Z.; Zhu, J., *A New  $\kappa$ - $\epsilon$  Eddy-Viscosity Model for High Reynolds Number Turbulent Flows - Model Development and Validation*. Computer Fluids, 1995. 24(3): p. 227-238.
30. Syred, N., *A Review of the Performance of Thin Cylindrical Vortex Devices with Reference to Power Fluidics Paper 3, Proc. Symp. Process Control by Power Fluidics, Inst. Measurement and Control*. 1975.
31. Tesar, V., *A Mosaic of Experiments and Results from Development of High-Performance Bistable Flow-Control Elements*, in *Proc. Symp. Process Control by Power Fluidics*. 1975: Inst. Meas. Control, London.
32. Tesar, V., *Fluidic Valve for Reactor Regeneration Flow Switching*. IChemE, 2004(82(A3)): p. 398-408.
33. Tippetts, J.R.P., G.H., *FLUTE 2 Project. Vortex Amplifiers Development*. 2011, Rolls-Royce plc.
34. Tippetts, J.R., *The Characterisation and Uses of Unvented Bistable Fluid Amplifiers*, in *Chemical and Process Engineering*. 1969, The University of Sheffield: Sheffield.
35. Tippetts, J.R., *Developments in Slug Control in Oil Gas Pipelines*. Proc. IChemE, 1991: p. 275-276.
36. Tippetts, J.R., Priestman, G.H., *Application of Fluidics to Burst Duct Protection and Associated Generic Research*. 2008, Rolls-Royce UTC.
37. Tippetts, J.R.R., E.; Higginson, J.; McGuigan, J.A.K., *Vortex Amplifier Controlled Ventilation Systems for Nuclear Reprocessing Plants*. Fluidics Quarterly, 1978. 10(3): p. 67-81.
38. Vatistas, G.H.J., A.M.; Hong, H., *Flow Characteristics in a Vortex Chamber*, Mechanical Engineering Department, Concordia University.: Montreal, Canada.
39. Vatistas, G.H., Jawarneh, A., *Vortex Chamber Flows*, Mechanical Engineering Department, Concordia University.: Montreal, Canada.
40. Von Karman, T., *Aerothermodynamics*. 1947: Department of Physics, Columbia University, New York.

41. Wang, H., *Fluidic Pressure Pulse Transmitting Flowmeters for Remote Metering of Oil Production*, in *Department of Chemical and Process Engineering*. 1997, The University of Sheffield: Sheffield. p. 282.
42. Wilkinson, J., Motamed-Amini, A., Owen, I., *Compressible and confined vortex flow*, *International Journal Heat and Fluid Flow*, Vol. 9, No. 4. 1988. p. 373-380.
43. Wilson, P., *Fluidic Integration (FLUTE) End Of Programme Report*, in *Functional Systems Engineering*. 2009, Rolls-Royce plc.
44. Woolhouse, R.J., Tippets, J.R., Whiteman, M., Young, K.J., Beck, S.B.M., Swithenbank, J., *The Use of Fluidics in Gas Turbine Combustion Design*, in *RTO AVT Symposium "Gas Turbine Engine Combustion, Emissions and Alternative Fuels"*. 1998: Lisbon, Portugal.
45. Wormley, D.N., *A Review of Vortex Diode and Triode Static and Dynamic Design Techniques*. *Fluidic Technology*, Jan. 1976: p. 83-112.
46. Wylie, E.B., Streeter, V.L., *Fluid Mechanics*. 1979, USA: McGraw-Hill.
47. Yang, Z.Y.P., G.H., *Internal Flow Modelling of Vortex Throttles*. *IMechE*, 1991. 205.
48. Wang, J.; P.G.H., *Flow Simulation in a complex fluidics using three turbulence models and unstructured grids*; *International Journal of Numerical Methods for Heat & Fluid Flow*, Vol 19, Nos. 314, 2009, pp 484-500

# NOMENCLATURE

$a_s$	Supply cross sectional area.
$a_t$	Tangential Channel cross sectional area.
$a_o$	Axial outlet cross sectional area.
$A$	Area.
$A_{eff}$	Effective Area.
$A_u$	Inlet nozzle cross sectional area.
$A_d$	Outlet cross sectional area.
$A_o$	SVV inlet nozzle area.
$A_s$	SVV outlet bore area.
$C_d$	Discharge Coefficient.
$cp_w$	Control Port width
$c_p$	Specific heat of a fluid at constant pressure.
$c_v$	Specific heat of a fluid at constant volume.
$d_c$	Diameter of the vortex chamber.
$d_o$	Axial outlet diameter.
$D_{ot}$	Outlet/tangential nozzle area ratio.
$Eu$	Euler number.
$\tilde{f}$	Moody friction factor
$H$	Height ratio of the device.
$h_d$	Height of the device.

$h$	Enthalpy per unit of mass.
$L_t$	Tangential channel width.
$L_r$	Radial channel width.
$M$	Mass flow rate (only in graphs).
$M$	Mach number.
$M$	Vortex strength merit. Indicative of diodicity.
$\dot{m}_{Low}$	Mass flowrate in the Low Resistance State.
$\dot{m}_{High}$	Mass flowrate in the High Resistance State.
$\dot{m}$	Measured Flow.
$\dot{m}_{ideal}$	Ideal flow.
$PR^*$	Pressure Ratio.
$P_s$	Supply pressure.
$P_c$	Control Port Pressure.
$P_o$	Outlet Pressure.
$p$	Static Pressure.
$p_0$	Stagnation Pressure.
$p^*$	Critical Pressure
$Q_o$	Fluid Outlet Flowrate.
$R$	Gas constant.
$Re$	Reynolds number.
$s_n$	Supply nozzle width or inlet nozzle width
$s$	Entropy

$T$	Static Temperature.
$T_o$	Stagnation Temperature.
$T^*$	Critical temperature
$T_f$	Flow Turndown Ratio.
$T$	Turndown ratio.
$u$	Internal energy per unit of mass
$V$	Velocity.
$v$	Volume.
$\gamma$	Ratio of specific heats.
$\mu$	Coefficient of viscosity.
$\rho$	Density.
$\rho^*$	Critical Density.
$\nu$	Coefficient of kinematic viscosity.
$\psi$	Non Dimensional flow rate parameter.
$\psi^*$	Non Dimensional flow rate parameter for choked flow.

# **APPENDICES**

# Appendix A

## SVV Designs

### A1. – Design A (Previously used in different Rolls-Royce applications) - Design laminates and components.



Examples of laser cut profile plates and top and bottom plates.



Accessories: supply and control pipes, splitters and outlet nozzles



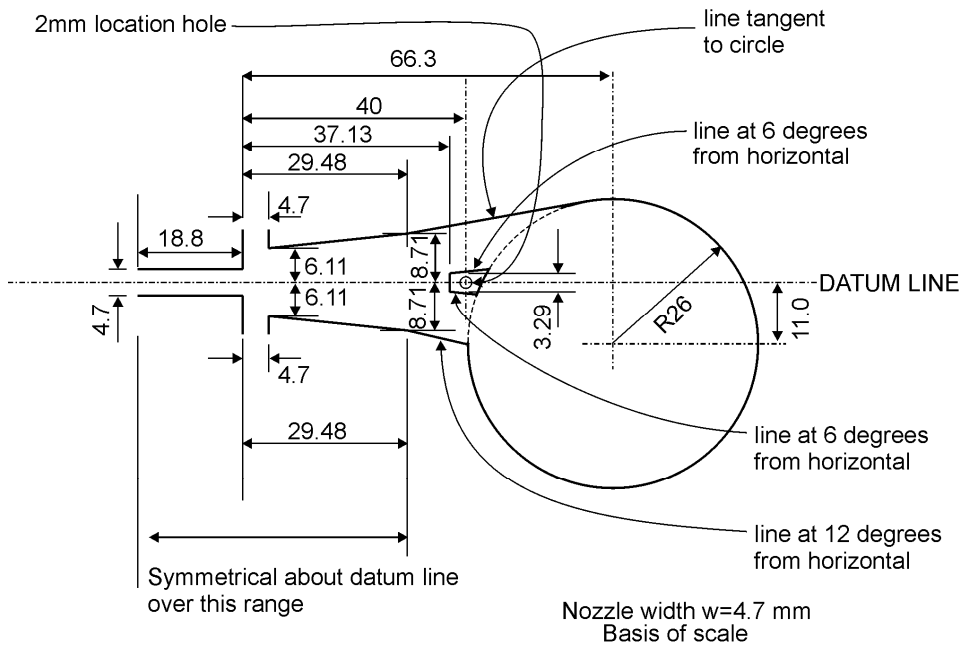
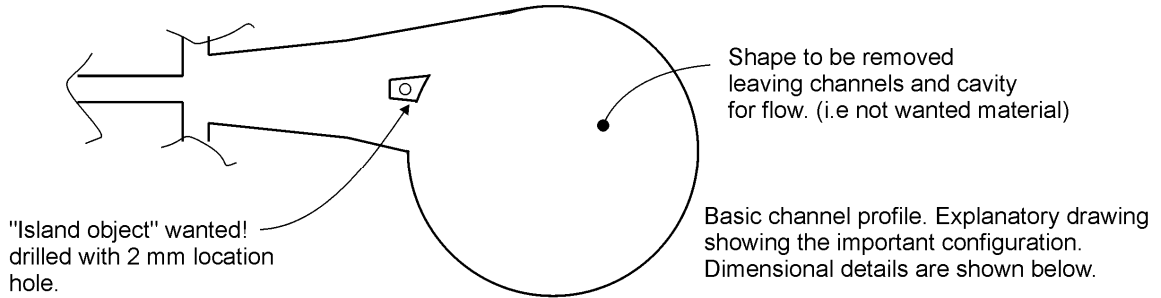
Fully assembled device with single outlet nozzle



Photo showing position of splitter after adjustment to promote stability.

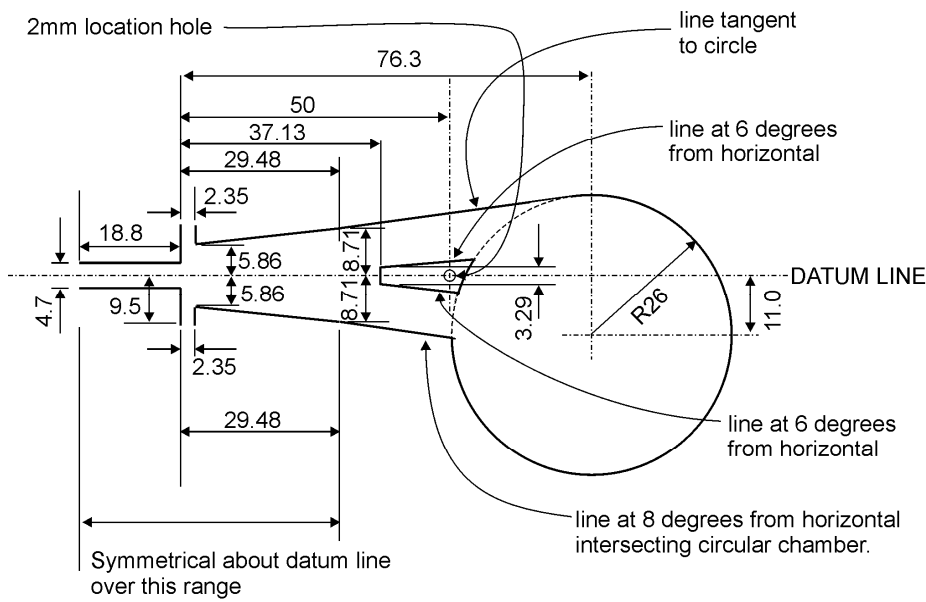
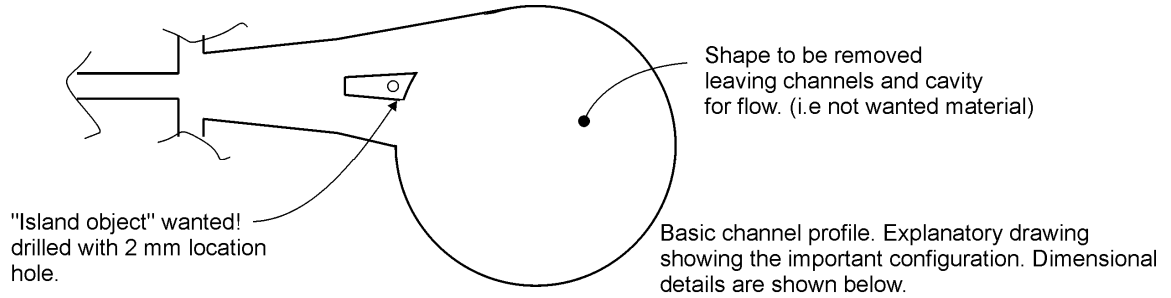
NEWLY MADE SWITCHED VORTEX VALVE SWAug07

## A2. – Design A (Previously used in different Rolls-Royce applications) – Detail of Central Profile



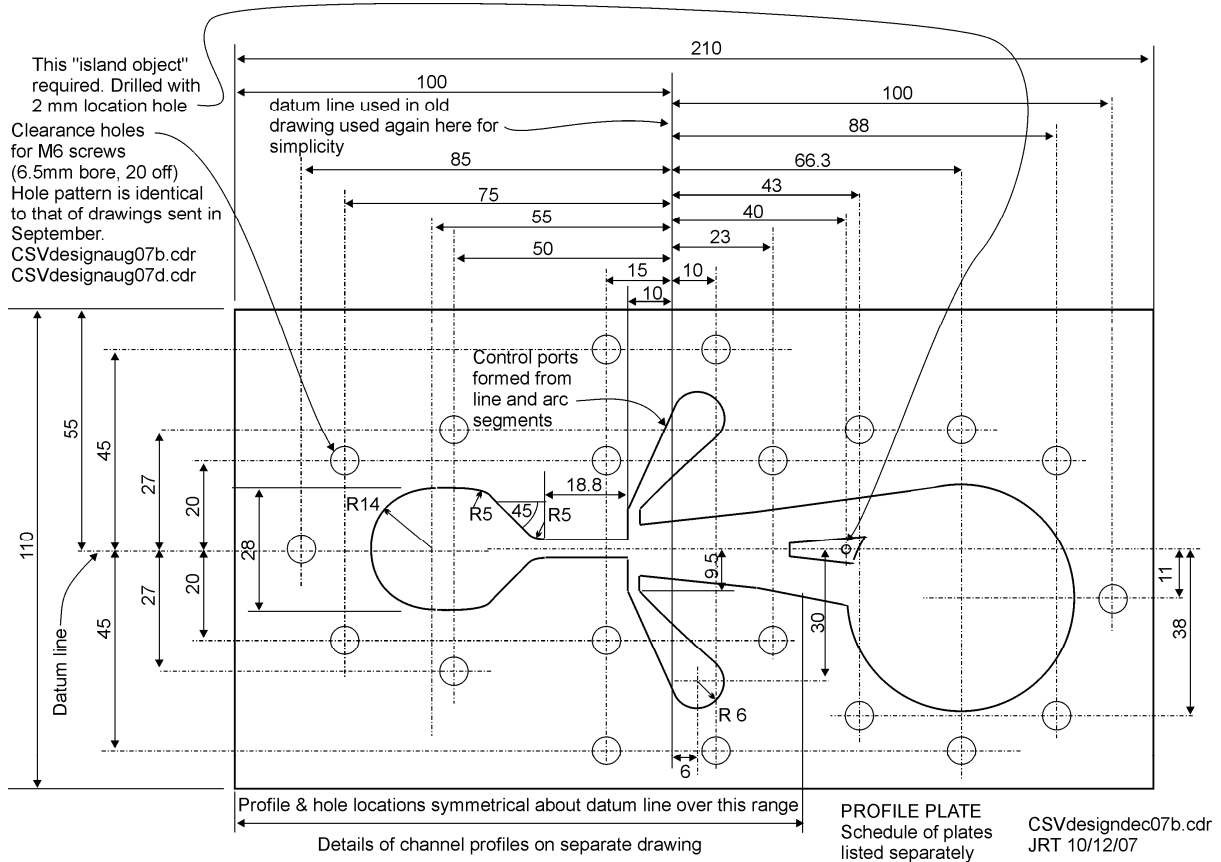
DETAIL OF CENTRAL PROFILE  
 CSVdesignaug07a.cdr  
 JRT 13/09/07  
 Corrected set-backs  
 31/10/07

### A3. – DB Design – Detail of Central Profile.

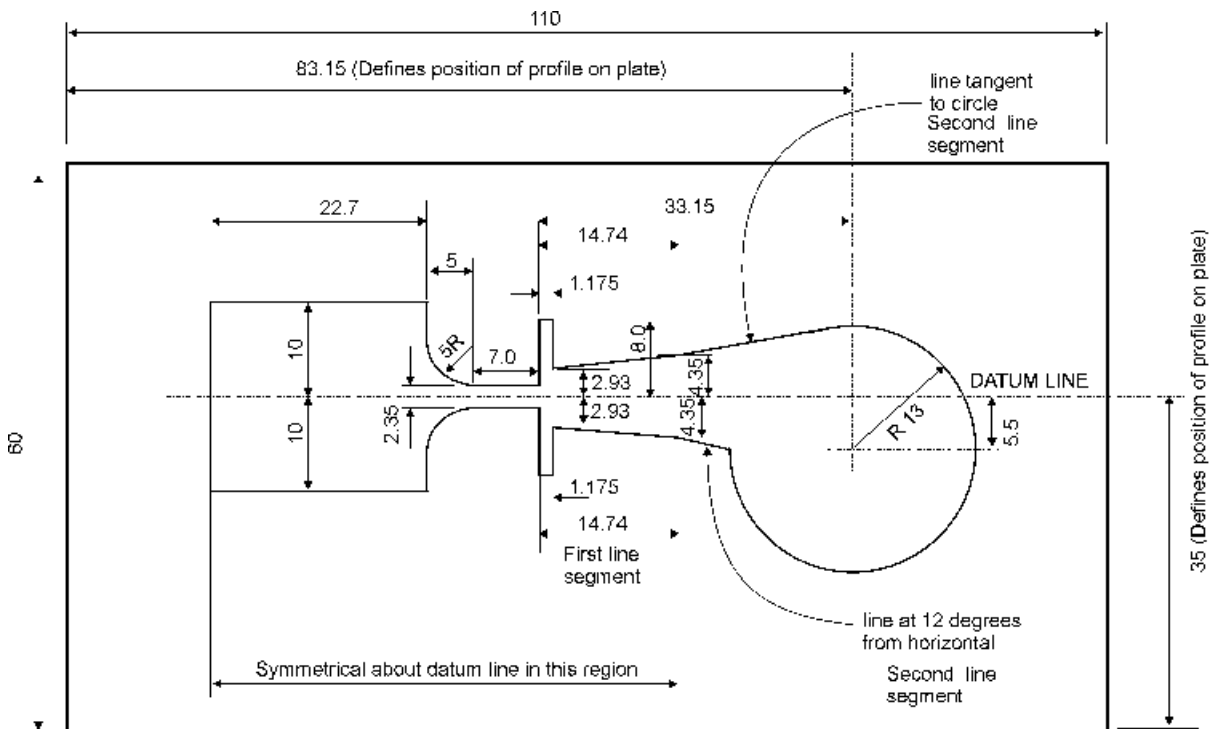


DETAIL OF CENTRAL PROFILE  
 CSVdec07a.cdr  
 JRT 10/12/07

**A4. - Basic Laminate for the DB Design.**



**A5. - Design G Embedded Design - Detail of Central Profile Plate.**



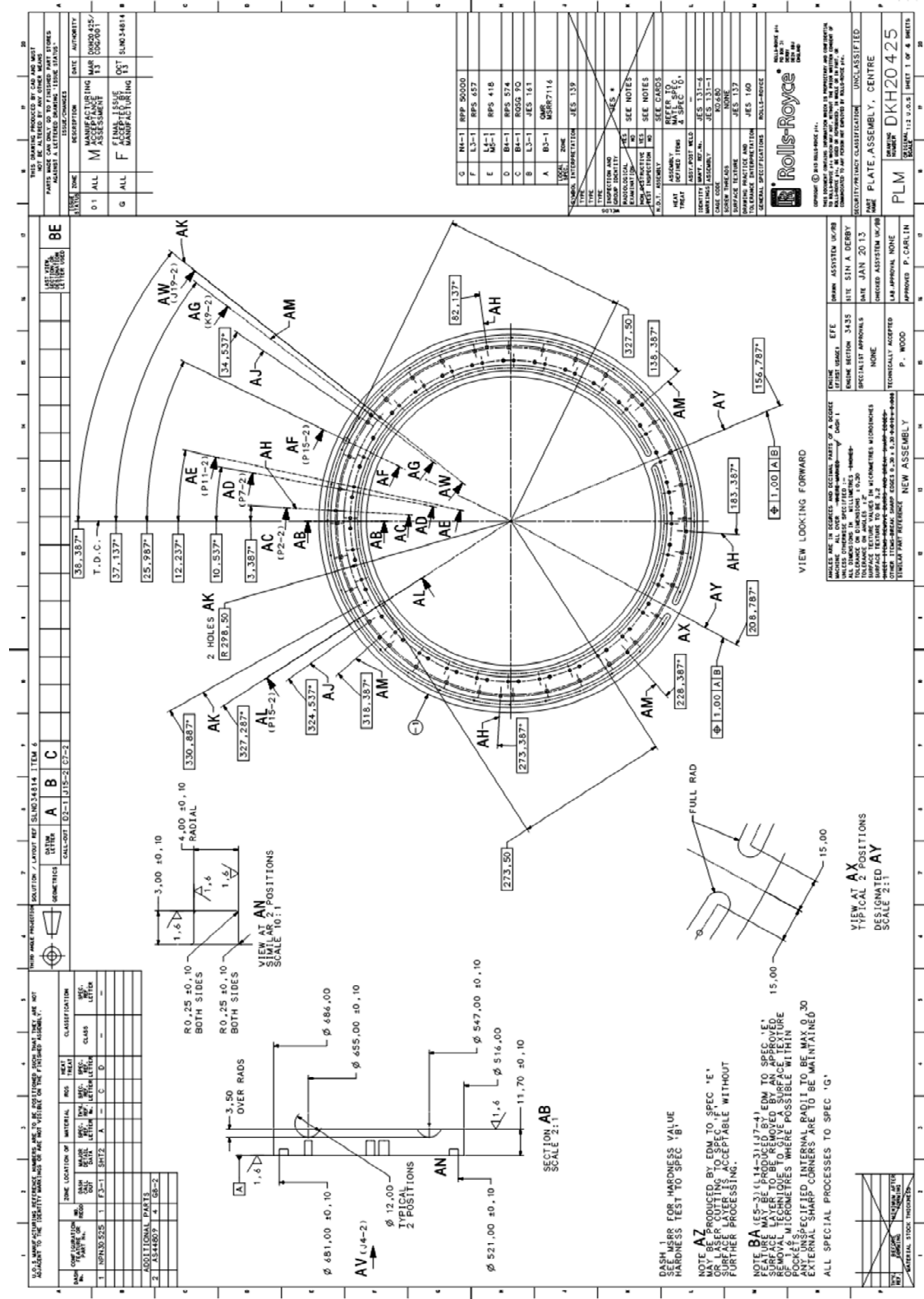
Profile is cut out in sheet (female wanted, male piece scrap)  
 BOLT HOLES SHOWN ON SEPARATE  
 DRAWING "HELICAL939BOLZ". (Embed is same as Helical)

2 off 6 mm thick  
 2 off 3 mm thick  
 2 off 2 mm thick

**"EMBED939" PROFILE PLATE**  
 Embed939a.cdr JRT 09/3/09

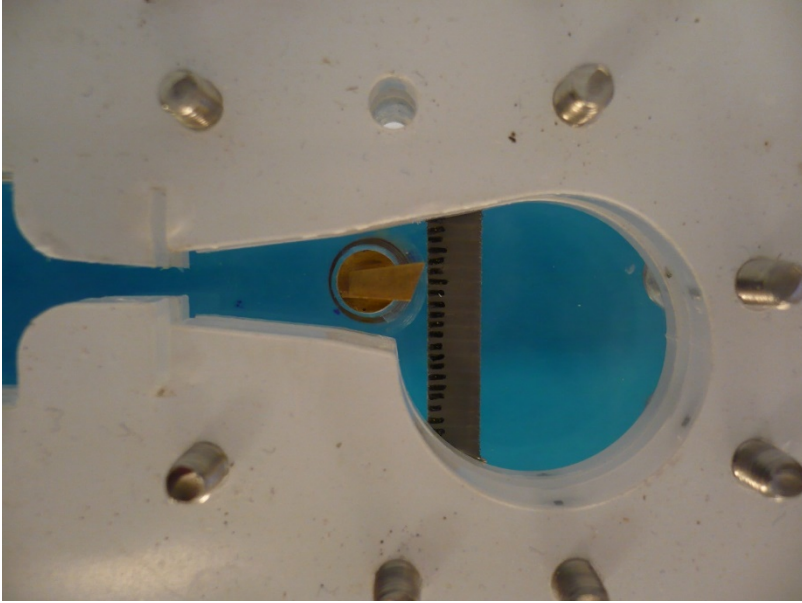
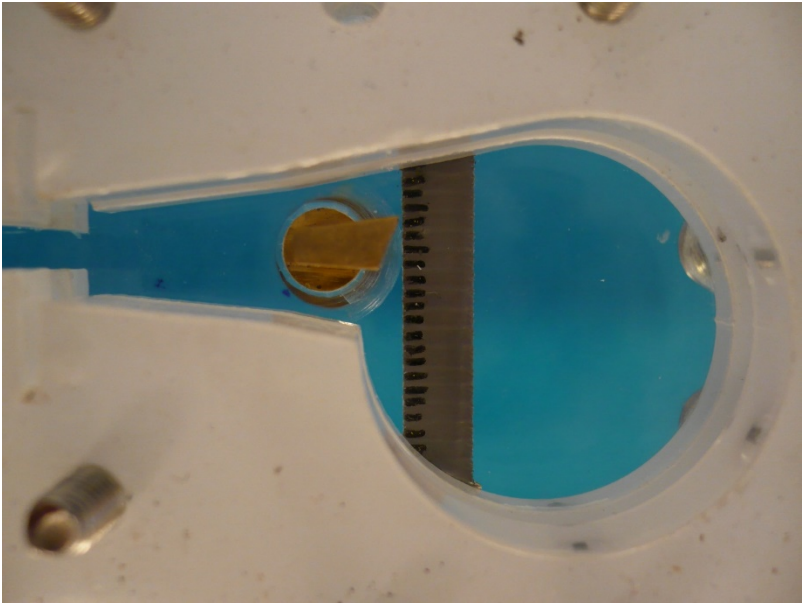
## A6. – Rolls-Royce Rim Design.

# A6. - Rolls-Royce Sloping Outlet Details.





**A7. – Splitter Position Images.**



# Appendix B

## Experimental Data

### B1. – Axial Outlet.

#### Normal State

8mm outlet		5mm outlet		6mm outlet		Design C	
Area Ratio $a_s/a_o = 1.09$		Area Ratio $a_s/a_o = 2.8$		Area Ratio $a_s/a_o = 1.95$		4mm outlet	
$P_s/P_o$	MVRT/AP	$P_s/P_o$	MVRT/AP	$P_s/P_o$	MVRT/AP	$P_s/P_o$	MVRT/AP
1.004	0.078	1.005	0.158	1.004	0.114	1.030	0.398
1.004	0.094	1.007	0.192	1.004	0.137	1.064	0.479
1.005	0.109	1.014	0.266	1.006	0.162	1.098	0.571
1.006	0.125	1.023	0.326	1.007	0.182	1.132	0.62
1.007	0.140	1.032	0.370	1.009	0.205	1.166	0.66
1.008	0.156	1.063	0.478	1.011	0.227	1.199	0.688
1.010	0.171	1.123	0.594	1.014	0.249	1.233	0.71
1.012	0.186	1.233	0.685	1.019	0.282	1.267	0.725
1.014	0.205	1.330	0.717	1.026	0.325	1.301	0.735
1.016	0.218	1.578	0.745	1.037	0.377	1.335	0.745
1.018	0.232			1.054	0.436	1.402	0.761
1.023	0.263			1.079	0.511	1.470	0.758
1.028	0.292			1.099	0.554	1.537	0.755
1.034	0.319			1.146	0.611	1.605	0.756
1.040	0.354			1.254	0.683	1.673	0.754
1.050	0.390			1.361	0.709	1.808	0.753
1.060	0.426			1.455	0.715	1.943	0.752
1.080	0.452			1.595	0.719	1.977	0.768
1.093	0.489					2.075	0.763
1.113	0.538					2.172	0.772
1.140	0.585					2.270	0.775
1.160	0.614					2.368	0.768
1.190	0.638					2.466	0.761
1.224	0.662					2.662	0.758
1.264	0.683					2.858	0.753
1.314	0.693					1.064	0.220
1.492	0.704					1.220	0.259
1.502	0.705					1.267	0.264
1.542	0.706					1.335	0.285
						1.470	0.311

						1.605	0.336
						1.673	0.340
						1.740	0.350
						1.808	0.353
						1.943	0.362
						1.977	0.380
						2.075	0.381
						2.173	0.388
						2.271	0.392
						2.369	0.396
						2.467	0.399
						2.663	0.401
						2.859	0.400

### Vortex State

8mm outlet		5mm outlet		6mm outlet		Design C	
Area Ratio as/ao = 1.09		Area Ratio as/ao = 2.8		Area Ratio as/ao = 1.95		4mm outlet	
Ps/Po	MVRT/AP	Ps/Po	MVRT/AP	Ps/Po	MVRT/AP	Ps/Po	MVRT/AP
1.017	0.085	1.038	0.153	1.027	0.112	1.030	0.398
1.031	0.114	1.055	0.180	1.045	0.138	1.064	0.479
1.061	0.133	1.086	0.205	1.087	0.169	1.098	0.571
1.094	0.161	1.137	0.223	1.147	0.196	1.132	0.62
1.162	0.189	1.172	0.244	1.248	0.234	1.166	0.66
1.216	0.207	1.213	0.267	1.363	0.261	1.199	0.688
1.271	0.223	1.338	0.302	1.558	0.295	1.233	0.71
1.352	0.241	1.627	0.351	1.713	0.319	1.267	0.725
1.495	0.264	1.834	0.381	1.887	0.341	1.301	0.735
1.657	0.294	2.000	0.400	2.072	0.363	1.335	0.745
1.826	0.310	2.250	0.395	2.267	0.370	1.402	0.761
1.925	0.320	2.500	0.407	2.559	0.368	1.470	0.758
2.025	0.331	2.999	0.397			1.537	0.755
2.125	0.335					1.605	0.756
2.254	0.340					1.673	0.754
2.366	0.345					1.808	0.753
2.448	0.344					1.943	0.752
						1.977	0.768
						2.075	0.763
						2.172	0.772
						2.270	0.775
						2.368	0.768

						2.466	0.761
						2.662	0.758
						2.858	0.753
						1.064	0.220
						1.220	0.259
						1.267	0.264
						1.335	0.285
						1.470	0.311
						1.605	0.336
						1.673	0.340
						1.740	0.350
						1.808	0.353
						1.943	0.362
						1.977	0.380
						2.075	0.381
						2.173	0.388
						2.271	0.392
						2.369	0.396
						2.467	0.399
						2.663	0.401
						2.859	0.400

## B2. – Control Flow to Switch.

### Switching from Normal to Vortex

5° angle Device B					
Ps/Po	Q	Qt (Transition)	% of Supply Flow	Actual Qt (Transition)	Actual % of Supply Flow
1.004	50	2.31	4.62	2.3	4.6
1.004	60	2.865	4.775	2.8	4.666
1.005	70	3.489	4.985	3.5	5
1.006	80	4.019	5.024	4	5
1.007	90	4.600	5.112	4.6	5.111
1.008	100	5.033	5.033	5	5
1.010	110	5.706	5.188	5.7	5.181
1.012	120	6.186	5.155	6.2	5.166
1.014	132	6.753	5.116	6.7	5.075
1.016	141	7.410	5.255	7.4	5.248
1.018	150	7.816	5.211	7.8	5.2
1.023	171	8.892	5.200	8.9	5.204
1.028	191	9.931	5.199	9.9	5.183
1.034	210	10.873	5.177	10.8	5.142
1.040	234	12.063	5.155	12	5.128
1.050	260	13.573	5.220	13.5	5.192
1.060	287	14.955	5.211	15	5.226
1.080	310	16.430	5.300	16.4	5.290
1.093	340	18.059	5.311	18	5.294
1.113	381	20.278	5.322	20.3	5.328
1.140	424	22.605	5.331	22.6	5.330
1.160	453	24.466	5.400	24.4	5.386
1.190	483	25.916	5.365	26	5.383
1.224	516	27.784	5.384	27.7	5.368
1.264	550	30.162	5.484	30.1	5.472
1.314	580	31.697	5.465	31.7	5.465
1.492	670	39.442	5.887	39.4	5.880
1.502	675	38.843	5.754	38.8	5.748
1.542	695	41.008	5.900	41	5.899
4° angle Device B					
Ps/Po	Q	Qt (Transition)	% of Supply Flow	Actual Qt (Transition)	Actual % of Supply Flow
1.026	175	7.796	4.455	7.8	4.457
1.066	285	12.856	4.511	12.8	4.491
1.131	400	18.635	4.658	18.6	4.65

1.170	450	21.704	4.823	21.7	4.822
1.255	520	24.723	4.754	24.7	4.75
1.289	545	26.189	4.805	26.1	4.788
1.353	585	29.281	5.005	29.2	4.991
1.401	615	30.686	4.989	30.6	4.975
3° angle Device B					
Ps/Po	Q	Qt (Transition)	% of Supply Flow	Actual Qt (Transition)	Actual % of Supply Flow
1.013	120	4.920	4.100	4.9	4.083
1.027	170	7.064	4.155	7	4.117
1.044	230	9.506	4.133	9.5	4.130
1.067	280	11.818	4.220	11.8	4.214
1.093	330	13.977	4.235	13.9	4.212
1.127	390	16.909	4.335	16.9	4.333
1.163	440	19.174	4.357	19.1	4.340
1.238	500	22.227	4.445	22.2	4.44
1.272	530	23.883	4.506	23.9	4.509
1.340	570	26.944	4.727	26.9	4.719
1.401	610	29.883	4.899	29.8	4.885
6° angle Device B					
Ps/Po	Q	Qt (Transition)	% of Supply Flow	Actual Qt (Transition)	Actual % of Supply Flow
1.026	190	10.127	5.330	10.1	5.315
1.071	300	16.337	5.445	16.4	5.466
1.133	415	22.916	5.522	22.9	5.518
1.289	570	31.682	5.558	31.7	5.561
1.401	630	38.083	6.045	38	6.031

### Switching from Vortex to Normal

5° angle Device B					
Ps/Po	Q	Qt (Transition)	% of Supply Flow	Actual Qt (Transition)	Actual % of Supply Flow
1.017	55	0.651	1.185	0.65	1.181
1.031	75	0.926	1.235	0.93	1.24
1.061	90	1.125	1.25	1.1	1.222
1.094	112	1.366	1.22	1.36	1.214
1.162	140	1.89	1.35	1.89	1.35
1.216	160	2.328	1.455	2.3	1.437
1.271	180	2.79	1.55	2.8	1.555

1.352	207	4.092	1.977	4	1.932
1.495	251	5.030	2.004	5	1.992
1.657	310	6.779	2.187	6.8	2.193
1.826	360	8.203	2.278	8.2	2.277
1.925	392	9.155	2.335	9.2	2.346
2.025	426	11.951	2.805	12	2.816
2.125	453	13.083	2.888	13	2.869
2.254	487	14.233	2.922	14.2	2.915
2.366	519	15.577	3.001	15.5	2.986
2.448	536	15.857	2.958	15.9	2.966
3° angle Device B					
Ps/Po	Q	Qt (Transition)	% of Supply Flow	Actual Qt (Transition)	Actual % of Supply Flow
1.319	195	3.022	1.55	3	1.538
1.660	310	6.51	2.1	6.5	2.096
2.000	415	10.375	2.5	10.4	2.506
2.157	460	12.778	2.778	12.8	2.782
2.320	500	14.495	2.899	14.5	2.9
2.449	535	15.008	2.805	15	2.803
2.633	575	17.117	2.977	17.1	2.973
2.813	610	18.393	3.015	18.4	3.016
4° angle Device B					
Ps/Po	Q	Qt (Transition)	% of Supply Flow	Actual Qt (Transition)	Actual % of Supply Flow
1.326	200	3.000	1.500	3	1.5
1.786	350	7.42	2.12	7.4	2.114
2.140	460	12.363	2.687	12.4	2.695
2.463	540	15.120	2.800	15.1	2.796
2.762	605	17.611	2.911	17.6	2.909
6° angle Device B					
Ps/Po	Q	Qt (Transition)	% of Supply Flow	Actual Qt (Transition)	Actual % of Supply Flow
1.449	240	3.84	1.6	3.9	1.625
1.741	340	7.174	2.11	7.2	2.117
2.048	440	11.22	2.55	11	2.5
2.340	520	14.499	2.788	15	2.884
2.701	600	17.28	2.88	17.3	2.883

**Control Pressure, Outlet Flow and Turndown Ratio before and after switching.**

Switching from Normal to Vortex								
Conditions before switching				Conditions after switching				
Ps (barg)	Ps (bara)	Q	Pct (bara)	Ps (barg)	Ps (bara)	Q	Pct (bara)	Turndown ratio
0.275	1.275	165	1.104	0.344	1.344	65	1.259	2.538
0.344	1.344	175	1.241	0.399	1.399	72	1.353	2.430
0.413	1.413	183	1.287	0.468	1.468	78	1.421	2.346
0.482	1.482	190	1.364	0.544	1.544	85	1.47	2.235
0.551	1.551	197	1.419	0.606	1.606	90	1.515	2.188
0.620	1.620	208	1.472	0.675	1.675	97	1.609	2.144
0.689	1.689	215	1.541	0.754	1.754	104	1.668	2.067
0.758	1.758	224	1.598	0.823	1.823	110	1.739	2.036
0.827	1.827	232	1.675	0.882	1.882	115	1.799	2.017
0.896	1.896	240	1.723	0.951	1.951	120	1.883	2
0.965	1.965	248	1.785	1.027	2.027	125	1.936	1.984
1	2	258	1.887	1.05	2.05	132	1.978	1.954
1.1	2.1	270	1.969	1.16	2.16	140	2.097	1.928
1.2	2.2	287	2.059	1.29	2.29	150	2.194	1.913
1.3	2.3	298	2.148	1.37	2.37	157	2.293	1.898
1.4	2.4	309	2.249	1.46	2.46	165	2.389	1.872
1.5	2.5	322	2.331	1.59	2.59	175	2.499	1.84
1.6	2.6	335	2.422	1.68	2.68	180	2.578	1.861
1.7	2.7	343	2.422	1.76	2.76	188	2.683	1.824
1.8	2.8	355	2.513	1.88	2.88	195	2.781	1.820
1.9	2.9	368	2.601	1.98	2.98	200	2.879	1.84
2	3	380	2.687	2.08	3.08	208	2.965	1.826

**B3.- Splitter Position.**

**Tangential Channel vs Outlet Flow rate.**

1 psi		2 psi		3 psi		4 psi		5 psi	
w	Q	w	Q	w	Q	w	Q	w	Q
0	50	0	63	0	95	0	107	0	119
0.6	51	0.4	75	0.3	103	0.4	118	0.2	125
0.9	50	0.9	75	0.9	103	0.8	118	0.4	132
1.7	51	1.6	75	1.4	103	1.1	117	1.2	132
2.7	56	2.2	82	2.1	109	1.5	118	1.5	132
3.2	59	2.9	90	2.9	115	2	123	1.9	135
3.8	66	3.2	103	3.3	130	2.5	128	2.6	142
3.9	67	3.4	105	3.9	133	3.1	145	3.1	160
4.3	56	3.9	105	4.3	109	3.6	145	3.6	162
4.5	54	4.1	88	4.5	109	3.8	146	3.9	162
5.3	55	4.6	85	4.8	105	4.1	123	4.2	135
5.6	55	4.9	85	5.2	105	4.5	119	4.9	130
5.8	55	5.1	103	5.7	116	4.9	118	5.5	140
6.9	45	5.6	93	5.9	105	5.4	120	5.8	140
		6	85	6.2	99	6	122	6.3	110
				6.7	85	6.2	100	6.9	95
						6.8	95		
10 psi		15 psi		20 psi		25 psi		30 psi	
w	Q	w	Q	w	Q	w	Q	w	Q
0	168	0	210	0	247	0	300	0	338
0.3	180	0.2	215	0.2	262	0.2	306	0.2	343
0.7	185	0.5	223	0.8	271	0.6	309	0.9	343
1.1	192	1	232	1.2	280	1.3	305	1.7	346
1.8	183	1.8	223	1.8	267	1.8	309	2.2	351
2.3	188	2.3	228	2.3	272	2.4	317	3	370
2.9	192	2.8	233	2.8	282	2.9	327	3.6	408
3.3	205	3.5	247	3.4	315	3.5	360	4.1	360
3.8	220	3.8	268	3.9	316	3.6	360	4.6	350
4.1	188	4.2	231	4.1	273	4.1	315	5.5	351
4.6	185	4.6	226	4.7	267	4.6	310	5.9	356
5.2	182	5.2	223	5.5	276	5.2	308	6.4	310
5.8	192	5.8	243	5.8	279	5.6	328	7.4	283
6.4	170	6.1	230	6.2	239	6	312		
6.9	157	6.6	198	7.2	213	6.5	273		
						7.1	271		
						7.4	246		

### Translation of the Splitter.

Ps 1				Ps 10		
Offset	Qo Normal	Qo Vortex		Offset	Qo Normal	Qo Vortex
-1	95	30		-1	226	117
-0.8	109	30		-0.8	233	117
-0.6	110	30		-0.6	233	117
-0.3	110	35		-0.3	236	118
-0.2	113	35		-0.2	236	122
0	113	35		0	237	123
0.2	114	35		0.2	237	125
0.4	114	40		0.4	237	134
0.6	114	47		0.6	237	144
0.8	115	52		0.8	238	156
1	115	-		1	238	175
Ps 2				Ps 15		
Offset	Qo Normal	Qo Vortex		Offset	Qo Normal	Qo Vortex
-1	136	47		-1	274	151
-0.8	150	48		-0.8	281	152
-0.6	150	49		-0.6	284	152
-0.3	150	50		-0.3	286	153
-0.2	152	52		-0.2	286	156
0	152	53		0	287	158
0.2	152	55		0.2	287	160
0.4	152	58		0.4	287	170
0.6	152	63		0.6	287	181
0.8	152	79		0.8	287	193
1	153	-		1	288	210
Ps 3				Ps 20		
Offset	Qo Normal	Qo Vortex		Offset	Qo Normal	Qo Vortex
-1	163	59		-1	323	184
-0.8	169	60		-0.8	330	186
-0.6	169	60		-0.6	332	185
-0.3	173	62		-0.3	332	185
-0.2	173	64		-0.2	335	188
0	173	64		0	335	192
0.2	173	67		0.2	335	192
0.4	173	71		0.4	335	203

0.6	173	77		0.6	335	215
0.8	173	84		0.8	336	225
1	175	94		1	337	244
Ps 4				Ps 30		
Offset	Qo Normal	Qo Vortex		Offset	Qo Normal	Qo Vortex
-1	172	69		-1	414	237
-0.8	177	70		-0.8	424	238
-0.6	178	69		-0.6	425	238
-0.3	179	70		-0.3	427	238
-0.2	179	74		-0.2	428	242
0	180	74		0	429	246
0.2	180	77		0.2	429	247
0.4	180	80		0.4	429	258
0.6	180	87		0.6	429	274
0.8	180	94		0.8	429	289
1	180	115		1	430	310
Ps 5						
Offset	Qo Normal	Qo Vortex				
-1	181	78				
-0.8	186	78				
-0.6	187	78				
-0.3	189	79				
-0.2	189	83				
0	189	83				
0.2	189	85				
0.4	189	91				
0.6	189	98				
0.8	189	108				
1	190	123				

**Flow ratio Normal/Vortex as a function of offset displacement of the splitter.**

Ps 1 psi		Ps 2 psi		Ps 3 psi		Ps 4 psi	
Offset		Offset		Offset		Offset	
-1	3.166	-1	2.893	-1	2.762	-1	2.492
-0.8	3.633	-0.8	3.125	-0.8	2.816	-0.8	2.528
-0.6	3.666	-0.6	3.061	-0.6	2.816	-0.6	2.579
-0.3	3.142	-0.3	3	-0.3	2.790	-0.3	2.557
-0.2	3.228	-0.2	2.923	-0.2	2.703	-0.2	2.418
0	3.228	0	2.867	0	2.703	0	2.432
0.2	3.257	0.2	2.763	0.2	2.582	0.2	2.337
0.4	2.85	0.4	2.620	0.4	2.436	0.4	2.25
0.6	2.425	0.6	2.412	0.6	2.246	0.6	2.068
0.8	2.211	0.8	1.924	0.8	2.059	0.8	1.914
1	NA	1	NA	1	1.861	1	1.565
Ps 5 psi		Ps 10 psi		Ps 15 psi		Ps 20 psi	
Offset		Offset		Offset		Offset	
-1	2.320	-1	1.931	-1	1.814	-1	1.755
-0.8	2.384	-0.8	1.991	-0.8	1.848	-0.8	1.774
-0.6	2.397	-0.6	1.991	-0.6	1.868	-0.6	1.794
-0.3	2.392	-0.3	2	-0.3	1.869	-0.3	1.794
-0.2	2.277	-0.2	1.934	-0.2	1.833	-0.2	1.781
0	2.277	0	1.926	0	1.816	0	1.744
0.2	2.223	0.2	1.896	0.2	1.793	0.2	1.744
0.4	2.076	0.4	1.768	0.4	1.688	0.4	1.650
0.6	1.928	0.6	1.645	0.6	1.585	0.6	1.558
0.8	1.75	0.8	1.525	0.8	1.487	0.8	1.493
1	1.544	1	1.36	1	1.371	1	1.381
Ps 30 psi							
Offset							
-1	1.746						
-0.8	1.781						
-0.6	1.785						
-0.3	1.794						
-0.2	1.768						
0	1.743						
0.2	1.736						
0.4	1.662						
0.6	1.565						
0.8	1.484						

1	1.387
---	-------

**Translation of the splitter L to R.**

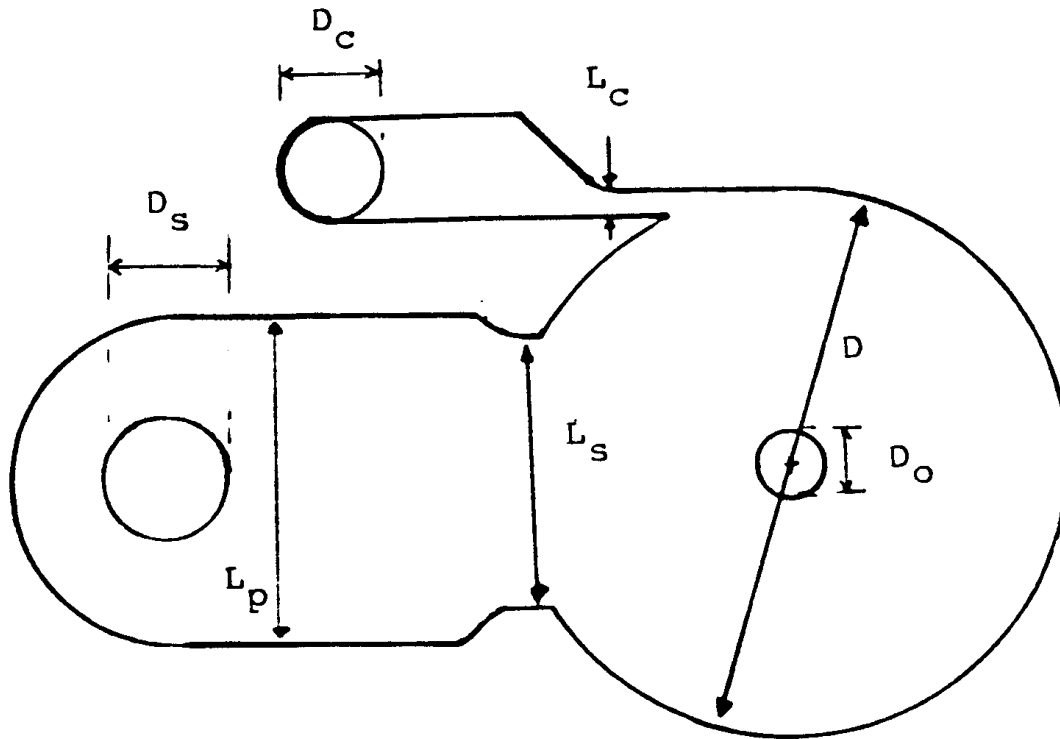
Ps 1 psig				Ps 10 psig		
Offset	Qo Normal	Qo Vortex		Offset	Qo Normal	Qo Vortex
-1	115	37		-1	236	125
-0.5	115	35		-0.5	236	125
0	113	35		0	237	123
0.5	109	35		0.5	231	122
1	103	35		1	227	121
Ps 2 psig				Ps 15 psig		
Offset	Qo Normal	Qo Vortex	Offset	Qo Normal	Qo Vortex	
-1	152	55		-1	285	162
-0.5	152	55		-0.5	286	159
0	152	53		0	287	158
0.5	148	53		0.5	280	158
1	139	53		1	274	155
Ps 3 psig				Ps 20 psig		
Offset	Qo Normal	Qo Vortex		Offset	Qo Normal	Qo Vortex
-1	170	67		-1	333	195
-0.5	172	67		-0.5	334	192
0	173	64		0	335	192
0.5	166	65		0.5	330	190
1	162	64		1	322	190
Ps 4 psig				Ps 30 psig		
Offset	Qo Normal	Qo Vortex	Offset	Qo Normal	Qo Vortex	
-1	178	76		-1	426	252
-0.5	179	77		-0.5	427	248
0	180	74		0	429	246
0.5	175	74		0.5	423	247
1	172	75		1	410	246
Ps 5 psig						

Offset	Qo Normal	Qo Vortex				
-1	188	85				
-0.5	188	85				
0	189	83				
0.5	184	83				
1	180	83				

# Appendix C

## Vortex Amplifier Design

C1. – Laminate Type Vortex Amplifier.



Laminate thickness	$h = 6.25 \text{ mm}$
Main Chamber diameter	$D = 115 \text{ mm}$
Control Port width	$L_c = 5.6 \text{ mm}$
Control Inlet Pipe diameter	$D_c = 16 \text{ mm}$
Supply Port width	$L_s = 69 \text{ mm}$
Supply Entry width	$L_s^p = 92 \text{ mm}$
Supply Inlet Pipe diameter	$D_s^p = 28 \text{ mm}$